Kabuki syndrome: Reversing Intellectual Disability by Promoting Open Chromatin

By

Joel Samuel Benjamin

A dissertation submitted to Johns Hopkins University in conformity with the requirements for the degree of Doctor of Philosophy

Baltimore, Maryland

November, 2015

Abstract

Kabuki syndrome (KS) is a rare intellectual disability syndrome caused by mutations in two genes (*KMT2D* and *KDM6A*) both involved in promoting open chromatin. If an imbalance between open and closed chromatin states is central to the pathogenesis of KS, we hypothesized that agents that promote chromatin opening might have therapeutic potential. To test this hypothesis, we have characterized a novel mouse model of KS with a heterozygous deletion in the mouse *Kmt2d* gene ($Kmt2d^{+/\beta Geo}$), leading to a loss of function of methyltransferase function from one allele. Novel *in vitro* reporter alleles demonstrate a reduction in histone 4 acetylation and histone 3 lysine 4 trimethylation (H3K4me3) activity in mouse embryonic fibroblasts from $Kmt2d^{+/\beta Geo}$ mice, which responds to AR-42, a histone deacetylase inhibitor. *In vivo*, deficiency of H3K4me3 in the dentate gyrus granule cell (DG GCL) layer of $Kmt2d^{+/\beta Geo}$ mice correlates with reduced neurogenesis and volume as well as hippocampal memory defects. These abnormalities improve upon postnatal treatment with two weeks of AR-42. Additionally we report that treatment with a ketogenic diet elevates beta-hydroxybutyrate (BHB), an endogenous histone deacetylase inhibitor (HDACi). Ketogenic diet treatment is also able to modulate H3Ac and H3K4me3 in the DG GCL, with concomitant rescue of both the neurogenesis defect and hippocampal memory abnormalities seen in $Kmt2d^{+/\beta Geo}$ mice. We were also observed similar effects in the rescue of neurogenesis upon exogenous administration of BHB. Furthermore, $Kmt2d^{+/\beta Geo}$ mice appear to have a NADH/NAD^+ ratio abnormality that predisposes them to have increased elevation of BHB on a ketogenic diet, suggesting that this dietary treatment may be especially productive for Kabuki syndrome. Overall, our work suggests that a reversible deficiency of postnatal

neurogenesis underlies intellectual disability in KS, and that both pharmacological and dietary agents that promote open chromatin appear to be viable strategies for potential treatment strategy for the intellectual disability seen in Kabuki syndrome and related disorders.

Readers:

Thesis Advisor: Hans T. Bjornsson, M.D./Ph.D.

Hilary J. Vernon M.D./Ph.D.

Thesis Committee:

Roger Reeves Ph.D. (chair)

Andrew S. McCallion Ph.D.

Hilary J. Vernon M.D./Ph.D.

Kaspar D. Hansen Ph.D.

Preface

Acknowledgements

First and foremost I would like to thank my Ph.D. advisor Hans Bjornsson. After my previous advisor left the IGM and I was left without a home, Hans took a chance on me to accept me in to his lab (which didn't even exist yet), without the need of a rotation and I will always be grateful for that. Through my time in the Bjornsson lab I have learned a lot about what it takes to be a good scientist and a good mentor, and these skills will stay with me as I carry out the rest of my scientific carrier. I would also like to thank the other members of the lab including the lab manager Li Zhang who was instrumental to both my own, as well as, the success of the lab. And also the other graduate students, Giovanni Carosso and Genay Pilarowski, who became an important peer group in my final stage of grad school and gave me the opportunity to become a mentor.

I would also like to thank the previous labs that I rotated in, the labs of Randy Reed, Aravinda Chakravarti, and Ronni Cohn. While I did not finish my graduate training in their labs, each rotation was instrumental in my growth as a laboratory scientist. I would like to especially thank Ronni Cohn for initially accepting me into his lab for my thesis work. Even though I was unable to finish my graduate career there, I very much enjoyed my time with Ronni and my first real experience as life as a graduate student.

I would like to thank the members of my thesis committee, Roger Reeves, Andy McCallion, Hilary Vernon, and Kaspar Hansen for helping me develop and flesh out my ideas into a thesis project that I am proud to call my own.

I would like to thank members of other labs who have helped me in my research along the way. These include Yi-Chun Chen, Sara Cooke, Liz Gerber, Stefani Fontana, Elena Gallo, Juan Calderon, and Shira Ziegler from the Dietz lab, Michelle Potter and Josh Crawford from the Pletnikov lab, Kaspar Hansen from the Hansen lab, Hilary Vernon and Kaitlin Victor from the Vernon lab, and David Huso from the Huso Lab.

I would further like to thank the Human Genetics program for the chance to earn my doctorate at Johns Hopkins. Thank you to Dave Valle, Kirby Smith, and Sandy Muscelli for their many years of guidance and direction as I made my way through my graduate career.

Thank you to my classmates who came into the program with me and stayed my friends throughout this long journey (Cory Smith, , Shannon Ellis, Foram Ashar, Nicole Eckart, Tara Doucet, and Melissa Lee). You have always pushed me to do better, and I'm so lucky to have had you all as colleagues. Also thank you to other classmates (Ben Bell, Jevon Cutler) who both provided great friendships and sources of advice throughout our time together.

Finally I would also like to extend my deepest thanks to my family and loved ones, who have always had my back and been my biggest supporters. Thank you to my best friend and fiancée Anna Moes who has given me love and support through my time in grad school, shared in my triumphs and successes, and been a shoulder to lean on when I needed it most. You truly have been my better half since we've been together. Thank you to my parents Tammi and Ilan Benjamin and my brother Daniel Benjamin for your constant support and encouragement for any and every endeavor I've chosen in life. All

of you have always made me feel unconditionally loved, and given me the believe that I can accomplish any dream that I set my mind to.

Table of Contents

Tables

Chapter 2

Chapter 3

Figures

Chapter 2

Chapter 1: Introduction

Introduction

Since the inception of the field of medical genetics, case examples of genetic disorders have always been at the forefront. Because of the limitations of early genetics, some of the best-characterized disorders were those that followed a Mendelian inheritance pattern. Disorders were classified by clinical phenotype and inheritance pattern, and by large-scale genomic rearrangements that could be seen through karyotype banding (Rimoin and Hirschhorn, 2004).

Recently, because of advances in technology including whole genome and exome sequencing, as well as a bridge between the fields of molecular biology and genetics, a new subgroup of Mendelian disorders has come to light based on a shared molecular mechanism of disease; the Mendelian disorders of the epigenetic machinery (Fahrner and Bjornsson, 2014). As the name suggests, these disorders are caused by mutations in genes that maintain epigenetic marks, and are therefore likely to lead to downstream epigenetic abnormalities when these factors are not working properly. There are four main groups of genes that currently are thought to form components of the epigenetic machinery, these include writers, readers, erasers, and remodelers. Writers are proteins that add modifications to histones (such as methylation or acetylation), erasers remove histone modifications, readers interact with histone marks and recruit proteins that change chromatin states, and remodelers actively move nucleosomes to different areas of DNA to change the underlying sequence accessibility (Hargreaves and Crabtree, 2011). Disorders of these type include Kabuki syndrome and Rubinstein Taybi syndrome

(mutations in histone writers; Ng et al., 2010; Petrij et al., 1995), BDMR syndrome (histone eraser; Williams et al., 2010), Börjeson-Forssman-Lehmann syndrome (histone reader; Lower et al., 2002), and ATRX syndrome (remodeler; Gibbons et al., 1992), among others.

What is particularly interesting about this subgroup of Mendelian disorders, is despite a wide variety in gene functions (with genes that can promote opposite chromatin states), there are many overlapping phenotypes. These include growth abnormalities (short stature, obesity), limb abnormalities, and hypotonia (Bjornsson, 2015). Additionally, many of these disorders also have overlapping dysmorphic facial features (broad, flattened face) as well as cardiac malformations, which may indicate shared epigenetic abnormalities (Fahrner and Bjornsson, 2014). Despite the fact that a large fraction of these disorders are caused by mutations in enzymes, nearly all of these disorders are inherited in either an autosomal dominant or x-linked manner. This is of interest because nearly 80% of Mendelian enzyme disorders are inherited in a recessive manner (Jimenez-Sanchez et al., 2001). This may suggest that these disorders are caused by the dosage imbalance of a tightly regulated system in which losing a single copy of a gene can cause disease (Bjornsson, 2015). Because of the function of many of the genes involved (that both promote open and closed chromatin), it seems likely that the underlying hallmark for this class of disorders is a disruption of the balance of normal chromatin states.

The most unifying phenotype seen in these disorders (and potentially the most devastating) is intellectual disability. Intellectual disability is defined as the impairment of the normal development of cognitive skills and functions, and currently it is estimated

that the worldwide prevalence of intellectual disability is between 1-3% (Maulik et al., 2011), highlighting the prevalence of this affliction. However, despite the relatively high prevalence, there currently is no known medical cure or treatment for intellectual disability (Bhaumik et al., 2011).

Because intellectual disability is such a cardinal feature of the Mendelian disorders of the epigenetic machinery, we hypothesized that an imbalance in chromatin states (the shared molecular phenotype of these disorders) is responsible for this phenotype. As a proof of principle for this hypothesis, we investigated Kabuki syndrome. Along with the aforementioned intellectual disability, Kabuki syndrome is also marked by a characteristic facial gestalt, cardiac defects, postnatal growth deficiencies, and immune deficiencies of currently unknown ideology (Bogershausen and Wollnik, 2013). Kabuki syndrome is inherited either in an autosomal dominant or X-linked manner because it can be caused by mutations in two separate genes, the autosomal *KMT2D* (Ng et al., 2010), and the X chromsome gene *KDM6A* (Lederer et al., 2012). As a disease of the epigenetic machinery, both KMT2D and KDM6A have roles in modifying histone marks. KMT2D is a methyl-transferase (writer) that adds H3K4me3 (a mark associated with open chromatin; ENCODE, 2007) as well as mono- and di-methylation to the same residue (Lee et al., 2013), while KDM6A is demethylase (eraser) that removes H3K27me3 (a mark associated with closed chromatin; ENCODE, 2007; Sengoku, 2011). Furthermore, as both KMT2D and KDM6A are part of the same open chromatin promoting SET1 complex (Goo et al., 2003), Kabuki syndrome may be caused by disruption of the normal function of this complex. In support of this hypothesis, mutations in another gene that is

part of this complex, *CHD7,* lead to a disorder (CHARGE syndrome) that has phenotypic overlap to Kabuki syndrome (Schulz et al., 2014).

The basis for this thesis was the hypothesis that Kabuki syndrome 1 (mutations in *KMT2D*) would be marked by decreased H3K4me3 (and consequently closed chromatin) of downstream target genes of *KMT2D*. Because histone marks can be changed reversibly in a way that impacts gene expression (Xu and Andreassi, 2011), the possibility might exist for postnatal rescue of some of the disease phenotypes by normalizing the potentially imbalanced chromatin state. To test this hypothesis, we characterized a mouse model of Kabuki syndrome ($Kmt2d^{+/\beta Geo}$) to see if both an imbalance of chromatin states could be detected *in vivo*, and if a disease relevant cell type that might be followed during therapeutic trials could be identified. (Bjornsson et al., 2014). This work uncovered defects of H3K4me3 in the granule cell layer of the dentate gyrus, as well as decreased adult neurogenesis in this structure, and hippocampal memory defects (Chapter 2; Bjornsson et al., 2014).

One possible therapeutic approach would involve restoring the normal chromatin balance in Kabuki syndrome by promoting open chromatin *in vivo,* through the action of a pharmacological agent. For pharmacological treatment (chapter 2), we chose to treat with the histone deacetylase inhibitor (HDACi) AR-42. Classically, HDAC inhibitors were identified as compounds that inhibited lysine deacetylases (HDACs) that removed acetylation from histones (Bose et al., 2014). Because histone acetylation is widely accepted as a mark of open chromatin (Gorisch et al., 2005) and because many HDACis also are known to increase other marks of open chromatin (Huang et al., 2011), HDACis

can be broadly viewed as agents that promote open chromatin states. HDACis are defined based on which classes of mammalian HDACs (3 total classes) they inhibit. These classes are based on which yeast HDAC they share homology with (Dokmanovic et al., 2007). As epigenetic dysfunction has been shown to play a greater role in human disease, investigators have started investigating HDACis as possible therapeutic agents. These include treatment for cancer (Azad et al., 2013; Yang et al., 2010), epilepsy (Rosetti et al., 2012),Alzheimer's disease (Sung et al., 2013), and even as agents that could improve cognitive function (Graff and Tsai, 2013). The rationale for the use of AR-42 as HDACi for treatment was due to its ability to also increase H3K4me3 (Huang et al., 2011). The treatment strategy we chose closely mirrors work done in a model of Rubinstein-Taybi syndrome, *Crebbp*$^{+/-}$ (Alarcon et al., 2004), but expands on several key areas pertinent to understanding the mechanism of the disease as well as future clinical application of treatment. This previous work reported that mice with a heterozygous loss of function allele of Crebbp (writer of histone acetylation), showed growth defects and hippocampal memory defects. Furthermore, after a two-week treatment with the HDACi SAHA, they reported a rescue of the hippocampal memory defect (through an increase of histone acetylation in the hippocampus). However, despite their discovery of hippocampal memory defects that recovered with treatment, this work did not lead to a mechanistic insight (or suggest a specific cell population of the hippocampus) into how promoting open chromatin might rescue the disease phenotype. Treatment with AR-42 as opposed to SAHA further provides more translational insights, as AR-42 is provided orally while SAHA was injected. In summary, the aims in chapter 2 are to further explore the phenotypes, cell populations affected, and mechanism of disease in *Kmt2d*$^{+/\beta Geo}$, but also

to explore the effect treatment with AR-42 would have on these defined markers of the disease.

While in chapter 2 we explore the ability of a pharmacological treatment to promote open chromatin, there are several barriers that may prevent immediate clinical implementation of this treatment strategy. These include potential toxicity of a chemotherapy agent (as well as the concern from the use of such a drug for a non-lethal disease), determining appropriate human dosing, as well as the length of a clinical trial. The next aim of this thesis (chapter 3) then was to see if an alternative path towards treatment might exist that could bypass these barriers. Recently, increasing amounts of evidence has come to light that suggests that dietary manipulation can affect the epigenome. For example, treatment with many vitamins including biotin and niacin are known to cause changes to histone modifications, and other dietary compounds such as curcumin and reseravtol have been shown to inhibit HDACs and histone acetyl transferases respectively (Choi and Freso, 2010). Furthermore, a large number of food items thought to decrease the risk of cancers (Remely et al., 2015) have been shown to have an effect on the epigenome. Taken together, these findings suggest that one could take advantage of a known ability of dietary treatments to modify the epigenome for a desired therapeutic outcome. Recent evidence suggests that the endogenously produced ketone body, beta-hydroxybutyrate (BHB) has HDACi properties (Shimazu et al., 2012). During times of low dietary glucose intake, fatty-acids are preferentially broken down in the liver through beta-oxidation to produce acetyl-CoA for the TCA cycle, which also results in the production of the ketone bodies (of which BHB is one; Fukako et al., 2014). Such a diet that decreases glucose levels to preferentially promote the production of ketone bodies is known as a ketogenic

diet (Baranano et al., 2008). Consequently, we hypothesized that treatment with a ketogenic diet (which produces the HDACi BHB) might have a similar therapeutic effect on Kabuki syndrome outcomes as a pharmacological HDACi. Chapter 3 of this thesis explores what effect treatment of *Kmt2d*$^{+/\beta Geo}$ with a ketogenic diet would have on the known pathologies.

During ketogenic diet treatment, our work also uncovered an intrinsic redox abnormality ($NADH/NAD^+$ ratio increase) in *Kmt2d*$^{+/\beta Geo}$ mice, which resulted in increased production of BHB while treated on a ketogenic diet (Chapter 3). While it is unclear exactly what the underlying cause of this metabolic alternation, it may be due to shifts towards the increase in metabolic processes that increase NADH levels, which include glycolosis and beta-oxidation of fatty acids. The mechanism not withstanding, if this exaggerated BHB elevation holds true in patients with Kabuki syndrome, this may make the ketogenic diet a particularly effective treatment strategy for this patient population, as they would be provided with higher levels of HDACi than your average individual and perhaps a less stringent diet could be used but still achieve therapeutic effects.

While these two projects lay a proof of principle groundwork for the treatment of Kabuki syndrome and potentially other Mendelian disorders of the histone machinery, there may be other therapeutic options that could be implemented. As previously mentioned, there are many others HDACis that have shown therapeutic potential (Azad et al., 2013; Yang et al., 2010; Rosetti et al., 2012), and may also have beneficial effects for *Kmt2d*$^{+/\beta Geo}$ similar to AR-42 and ketogenic diet treatment. As a follow-up to ketogenic diet therapy, there are several other ways to bring about increased BHB. These include direct

injection/treatment with exogenous BHB, increasing exercise (Matoulek et al., 2014), fasting (Nakamura et al., 2014), and treatment with oral ketone esters (Hashim 2014). Furthermore, when the gene networks disrupted in Kabuki syndrome have been delineated, taking an approach to modulate these down stream pathways (Das et al., 2013) may provide a more specific rescue with less risk of adverse side effects. However, while there may be many potential routes towards a rescue, the fact as of now two separate disorders of histone machinery (Alarcon et al., 2004; Bjornsson et al., 2014) show recovery through treatment based on modifying chromatin states, suggests that this therapeutic strategy may have relevance for other disorders in this group.

In summary, the purpose of our research was three fold: to test the hypothesis in a mouse model that Kabuki syndrome's intellectual disability is a manifestation of an imbalance in chromatin states, to see if these phenotypes can be rescued *in vivo* by pharmacologically promoting open chromatin, and to also see if a dietary treatment can have a similar response. While these data serve primarily as a proof of principle for the treatment of this class of disorder, and although these interventions will later need to be refined for length and appropriate window of treatment, they provide a potential option for a class of disorders that currently have few choices for medical intervention.

Chapter 2: *Kmt2d*$^{+/\beta Geo}$ characterization and HDACi treatment

Introduction

Kabuki syndrome is an autosomal dominant condition caused by heterozygous loss-of-function mutations in either of two genes (Ng et al., 2010;Lederer et al., 2012; Miyake et al., 2013) with complementary functions, lysine-specific methyltransferase 2D (*KMT2D*) on human chromosome 12 or lysine-specific demethylase 6A (*KDM6A*) on human chromosome X. KMT2D is a methyltransferase that adds a trimethylation mark to H3K4 (H3K4me3, an open chromatin mark), whereas KDM6A is a demethylase that removes trimethylation from histone 3 lysine 27 (H3K27me3, a closed chromatin mark). Both genes facilitate the opening of chromatin and promote gene expression (Ng et al., 2010;Lederer et al., 2012; Miyake et al., 2013). It is therefore likely that the observed gene dosage sensitivity in Kabuki syndrome, despite the apparent redundancy of the H3K4 trimethylation machinery, involves a relative imbalance between open and closed chromatin states for critical target genes. If this is the case, it may be possible to restore this balance with drugs that promote open chromatin states, such as histone deacetylase inhibitors (HDACi). To test this hypothesis, we have characterized a mouse model of Kabuki syndrome with a heterozygous mutation in *Kmt2d* that results in replacement of the SET (Suvar, Enhancer of Zeste, Trithorax) methyltransferase domain ($Kmt2d^{+/\beta Geo}$) by a β-Geo cassette. $Kmt2d^{+/\beta Geo}$ mice have hippocampal memory defects that correlate with multiple abnormalities in the granule cell layer of the dentate gyrus, a prominent site of adult neurogenesis (Brus et al., 2013;Altman 1962). Guided by the results of *in vitro* analyses using reporter alleles that monitored histone 4 (H4) acetylation and H3K4 trimethylation in cells derived from Kabuki syndrome mice, we find that oral administration of the HDACi AR-42 to either young (1-2 month-old) or adult (5-6

month-old) *Kmt2d*$^{+/\beta Geo}$ mice normalized both structural and functional deficits in the dentate gyrus in association with restoration of H3K4 trimethylation.

Results

KMT2D is a member of the mixed lineage leukemia (MLL) family of *Drosophila* Trithorax orthologs that is encoded on human chromosome 12 and mouse chromosome 15. An alternative name for *KMT2D* is mixed lineage leukemia 2 (*MLL2*). All members of this family contain a SET domain, which confers the H3K4 methyltransferase activity, as well as other domains (Hunter et al., 2012) that delineate individual functions (Fig. 2.1A). A mouse model harboring a loss-of-function allele for *Kmt2b*, encoded on human chromosome 19 and mouse chromosome 7, has been characterized previously (Kerimoglu et al., 2013), demonstrating hippocampal memory defects. This gene has been alternatively designated *Mll4* or *Mll2*, leading to confusion in the literature regarding nomenclature for this particular gene family, as discussed in a recent publication by Bögerhausen *et al* (Bögershausen et al., 2013). To specifically assess the underlying pathogenesis of Kabuki syndrome, we have characterized a mouse model with insertion of an expression cassette encoding a β-galactosidase neomycin resistance fusion protein (β-Geo) into intron 50 of *Kmt2d* (*Mll2*) on mouse chromosome 15. Inclusion of a splice acceptor sequence and a 3'-end cleavage and polyadenylation signal at the 5' and 3' ends of the β-Geo cassette, respectively, is predicted to generate a truncated KMT2D protein with peptide sequence corresponding to the first 50 exons of *Kmt2d* fused to β-Geo, but lacking the SET domain and therefore methyltransferase activity (Fig. 2.1B, Sup fig

2.1A). As predicted from this targeting event, quantitative real-time polymerase chain reaction analysis of *Kmt2d* messenger RNA in *Kmt2d*$^{+/\beta Geo}$ mice demonstrated normal abundance of sequence corresponding to exon 20 but a 50% reduction for exon 52, when compared to *Kmt2d*$^{+/+}$ littermates (Fig. 2.1C). Expression of a KMT2D-β-galactosidase fusion protein in *Kmt2d*$^{+/\beta Geo}$ animals demonstrated transcription and translation of the targeted allele (Sup fig. 2.1B). Furthermore, chromatin immunoprecipitation followed by next generation sequencing (ChIP-seq) on splenic cells from *Kmt2d*$^{+/\beta Geo}$ mice and *Kmt2d*$^{+/+}$ littermates using an antibody against H3K4me3 revealed an overall genome-wide decrease in H3K4me3 in *Kmt2d*$^{+/\beta Geo}$ mice (Fig. 2.1D), supporting the predicted functional consequences of the mutant allele. Finally, *Kmt2d*$^{+/\beta Geo}$ mice demonstrated facial features that are consistent with Kabuki syndrome including flattened snout (Sup fig. 2.2A) and downward rotation of the ear canal (Sup fig. 2.2B). Blinded analysis of X-rays of *Kmt2d*$^{+/\beta Geo}$ mice revealed a significantly shorter maxilla ($P < 0.005$) when compared to *Kmt2d*$^{+/+}$ littermates (Sup fig. 2.2B-C), as judged by the extent of protrusion beyond the mandible (Sup fig. 2.2C).

Disruption of several histone modifying enzyme genes has been shown to lead to hippocampal memory defects in mice, illustrating a critical role for epigenetic homeostasis in memory acquisition (Guan et al., 2002; Gupta et al., 2010; Cohen-Armon et al., 2004). *Kmt2d*$^{+/\beta Geo}$ mice showed significant deficits in novel object recognition ($P < 0.05$, Fig. 2.1E), Morris water maze probe trial ($P < 0.005$, Fig. 2.1F) and contextual fear conditioning ($P < 0.05$, Sup fig. 2.3) when compared to *Kmt2d*$^{+/+}$ littermates, all consistent with hippocampal memory dysfunction. When performed before the hidden platform stage of training, the flag-training phase of the Morris water maze did not reveal

significant differences between *Kmt2d*$^{+/\beta Geo}$ and *Kmt2d*$^{+/+}$ littermates (Sup fig. 2.4). Importantly, *Kmt2d*$^{+/\beta Geo}$ mice did not show decreased activity (Sup fig. 2.5A), reduced grip strength (Sup fig. 2.5B) or slower swim speeds (Sup fig. 2.5C), any of which would be indicative of a more generalized limitation of performance potential in these assays. There were no significant differences in the time that it took *Kmt2d*$^{+/\beta Geo}$ mice to identify the platform (escape latency) compared to *Kmt2d*$^{+/+}$ mice during the training phase (Sup fig. 2.6).

Immunofluorescence analyses revealed particularly high levels of expression of KMT2D protein in the dentate gyrus granule cell layer of the hippocampus in *Kmt2d*$^{+/+}$ mice (Fig. 2.2A) and a striking deficiency of H3K4me3 in the dentate gyrus granule cell layer of *Kmt2d*$^{+/\beta Geo}$ mice compared *to Kmt2d*$^{+/+}$ littermates ($P < 0.05$, Fig. 2.2, B and C). We also saw a similar deficiency of H3K4me3 in the pyramidal layer of the hippocampus ($P < 0.01$, Sup fig. 2.7). The amount of H3K4me3 showed substantial cell-to-cell variability in *Kmt2d*$^{+/\beta Geo}$ animals (Fig. 2.2B), suggesting that variation in cell state or identity within the granule cell layer or dentate gyrus may influence vulnerability to the consequences of heterozygous *Kmt2d* disruption. *Kmt2d*$^{+/\beta Geo}$ mice showed a significant decrease in body weight but not brain weight ($P < 0.05$, Sup fig. 2.8), and had reduced dentate gyrus granule cell layer volume when standardized to brain weight ($P < 0.05$, Fig. 2.2D, E). This correlated with reduced neurogenesis in the granule cell layer of *Kmt2d*$^{+/\beta Geo}$ mice, as evidenced by significantly reduced expression of both doublecortin (DCX; Rao et al., 2004) ($P < 0.001$, Fig. 2.2F, G) and 5-ethynyl-2'-deoxyuridine (EdU) staining, a marker

of both neurogenesis in the granule cell layer and a marker of neuronal survival when monitored 30 days after labeling ($P < 0.01$, Sup fig. 2.9). Confocal microscopy revealed an apparent decrease in dendritic branching complexity of DCX positive cells (DCX+) in the granule cell layer of *Kmt2d*$^{+/\beta Geo}$ mice (Sup fig. 2.10). However, given the decreased amounts of DCX+ cells in these mice, further work is needed to determine if this is a true or primary manifestation of Kmt2d deficiency. Staining with an antibody against activated caspase 3 did not reveal evidence for enhanced cell death in the dentate gyrus in heterozygous-targeted animals (Sup fig. 2.11). To explore whether there are hippocampal memory defects in patients with Kabuki syndrome, we analyzed comprehensive neuropsychological testing performed on three patients with known disease causing mutations in *KMT2D* (Table 2.1). Although, not all deficiencies observed can be explained by hippocampal dysfunction, patients consistently had abnormalities in tasks known to be associated with dentate gyrus function (Kesner et al., 2013; Morris et al., 2013; Epp et al., 2011). Other functions linked to other regions of the hippocampus (Brickman et al., 2011) were also abnormal in some patients as were some tasks not linked to hippocampus indicating that other cell populations in the central nervous system may also play a role. These data support the hypothesis that observations in *Kmt2d*$^{+/\beta Geo}$ mice are, at least in part, reminiscent of findings in Kabuki syndrome in human patients.

We created epigenetic reporter systems that monitored either H4 acetylation or H3K4 trimethylation machinery activity in an effort to determine whether there was an ongoing activity deficiency in cells from *Kmt2d*$^{+/\beta Geo}$ mice (Fig. 2.3A). Both reporter alleles

encode halves of green fluorescent protein separated by a flexible linker region (Baird et al., 1999) with a histone tail and a histone reader at the N- and C- termini, respectively. When the histone tail corresponding to either H4 or H3 is modified by acetylation or methylation, respectively, GFP structure and function are reconstituted, as detected by a fluorescent readout (Fig. 2.3B). The acetyl reporter protein quantifies the activity of the acetylation machinery (acetylation of H4 specifically at sites K5, K8, K12, and K16) and comprises an H4 tail (residues 1-30) on one end and a TATA binding protein (TBP)-associated factor II (TAFII) bromodomain on the other end (Fig. 2.3A). The TAFII bromodomain only recognizes and binds to the acetylated H4 tail. This acetylation-dependent reporter protein demonstrated a linear fluorescence response when quantified by fluorescence-activated cell sorting (FACS) in the presence of increasing amounts of suberoylanilide hydroxamic acid (SAHA), an HDACi, in culture systems (Fig. 2.3C and D). Saturation of this response correlated well with immunoblot data using antibodies to the modified H4 tail (Munshi et al., 2006). This response was attenuated by co-transfection with a construct encoding a histone deacetylase (Sup fig. 2.12) and absent upon mutagenesis of all potential acetylation sites (Fig. 2.3E), attesting to its specificity. The H3K4 trimethylation reporter allele encodes the H3 tail (residues 1-40) on one end and the TBP-associated factor III (TAF3) plant homeodomain (PHD) on the other end, which binds to trimethylated K4 on H3 (Fig. 2.3A). The H3K4 trimethylation reporter also demonstrated a dose response with increasing amounts of the HDACi AR-42 (Fig. 2.3F), in keeping with prior work suggesting that AR-42 can also influence the methylation status of H3K4 through inhibition of demethylases (Huang et al., 2011). Activity was greatly attenuated upon mutagenesis of critical residues (M882A,

D890A/W891A, *20, 21*) in the TAF3 reader domain (Fig. 2.3G) or with mutation of K4 (H3K4Q) in the H3 tail (Fig. 2.3G). Both reporter alleles showed decreased activity when stably introduced into embryonic fibroblasts derived from *Kmt2d*$^{+/\beta Geo}$ mice, when compared to *Kmt2d*$^{+/+}$ littermates (Sup fig. 2.13). H3K4 trimethylation activity was enhanced upon treatment of *Kmt2d*$^{+/\beta Geo}$ cells with HDAC inhibitors AR-42 or MS275 (Fig. 2.3H, Sup fig. 2.14A). An analysis of transfection efficacy in cells with both genotypes indicated comparable transfection efficacy (Sup fig. 2.14B).

Because of the ability of HDACis to increase H3K4 trimethylation *in vitro* in *Kmt2d*$^{+/\beta Geo}$ cells, we next asked whether the H3K4 trimethylation deficiency seen in the dentate gyrus granule cell layer of *Kmt2d*$^{+/\beta Geo}$ mice could be attenuated or reversed upon *in vivo* postnatal treatment with an HDACi. Previously, the HDAC inhibitors AR-42 and MS275 have both been shown to increase H3K4 trimethylation and histone acetylation (Huang et al., 2011). AR-42 appeared to have the strongest effect on H3K4me3 (Huang et al., 2011) and was shown to be well tolerated in mice in a long-term preclinical trial (Jacob et al., 2012); it was therefore chosen for *in vivo* studies. We started at an AR-42 dose of 25mg/kg/day, previously used in mouse models of prostate cancer (Huang et al., 2011), commencing at 20 weeks of age and continuing for two weeks. This dose increased H3K4 trimethylation in the granule cell layer in *Kmt2d*$^{+/\beta Geo}$ mice, compared to untreated mutant littermates (Sup fig. 2.15A, B), to a level that was indistinguishable from treated *Kmt2d*$^{+/+}$ animals. Unexpectedly, however, this dose of AR-42 was associated with decreased DCX expression in the granule cell layer in both young (1-2 month-old) and

old (5-6 month-old) *Kmt2d*$^{+/+}$ and *Kmt2d*$^{+/\beta Geo}$ mice (Sup fig. 2.15C,D). Given the known cytotoxic potential of AR-42 (Huang et al., 2011, Zhang et al., 2011*)* we next tested 5 and 10 mg/kg/day doses, and observed a dose-dependent increase in H3K4me3 and preservation or restoration of DCX expression in *Kmt2d*$^{+/+}$ or *Kmt2d*$^{+/\beta Geo}$ animals in both age groups, respectively (Fig. 2.4A-D and Sup fig. 2.15D). This dose also led to a genome-wide increase in H3K4me3 in spleen cells from *Kmt2d*$^{+/\beta Geo}$ mice, when compared to *Kmt2d*$^{+/+}$ littermates on vehicle (Fig. 2.4E) in association with normalization of expression of *Klf10* (Sup fig. 2.16), a known Kmt2d target gene (Guo et al., 2012). In fact, this dose appeared to overcorrect the deficiency (Fig. 2.4E), which can be observed when representing data as MA plots (the relationship between log ratios and mean averages, Sup fig. 2.17) or visualizing the shifts in balance among the two states (Sup fig. 2.18). We also compared other state combinations with the same representations, showing a relative normalization of genome-wide H3K4me3 in *Kmt2d*$^{+/\beta Geo}$ mice treated with AR-42, when compared to *Kmt2d*$^{+/+}$ littermates that did (Sup fig. 2.17E) or did not (Sup fig. 2.17B) receive drug. The bigger effect at lower intensity Log2 counts per million (CPM) fits with data from ablation of the Rubinstein-Taybi gene encoding CREB-binding protein (CBP), which has dose-dependent effects on gene expression thought to depend on the strength of recruitment for a particular site (Kasper et al., 2010).

In keeping with the hypothesis that abnormal granule cell layer neurogenesis contributes to functional deficits, we found that performance in hippocampal memory testing correlated with AR-42 dose-dependent effects on DCX expression. Specifically, both

Kmt2d$^{+/+}$ and *Kmt2d*$^{+/\beta Geo}$ mice showed improved performance on Morris water maze platform crossing during probe trial (Garthe et al., 2013) in response to 10mg/kg/day of AR-42 ($P < 0.001$), with a greater response in *Kmt2d*$^{+/\beta Geo}$ animals and no significant difference between genotypes in the treatment group ($P = 0.27$, Fig. 2.4F).

Discussion

Prior studies have associated structural abnormalities of the dentate gyrus with impaired neurogenesis and hippocampal memory defects (Ansorg et al., 2012; Denis-Donini et al., 2008). In accordance with the previously observed phenotype in *Kmt2b*-targeted mice (Kerimoglu et al., 2013), we found that heterozygosity for a loss-of-function *Kmt2d* allele associates a deficiency of H3K4me3 in the dentate gyrus granule cell layer with hippocampal memory defects in a mouse model of KS. Support for a causal relationship is now increased by our observation that memory deficits in a mouse model of Kabuki syndrome can be prevented or even reversed through systemic delivery of drugs that directly influence the histone modification events that favor chromatin opening.

Our data support the hypothesis that the neurodevelopmental deficiency in Kabuki syndrome is maintained by an impairment of adult neurogenesis due to an imbalance between open and closed chromatin states for critical target genes. In this light, other Mendelian disorders involving the histone modification machinery, now numbering over 40 (Berdasco et al., 2013), might be amenable to therapeutic intervention with HDAC inhibitors (Dash et al., 2009; Vecsey et al., 2007, Graff et al., 2013). In keeping with this concept, neurological phenotypes in mouse models of Rubinstein-Taybi syndrome with

haploinsufficiency for the gene encoding the histone acetyl transferase CREB-binding protein (*Crebp*) respond to intracerebroventricular or intraperitoneal administration of the histone deacetylase inhibitors SAHA or trichostatin A, respectively (Korzus et al., 2004; Alarcon et al., 2004); however, no cellular mechanism was described. The specific correlation between H3K4me3 and neurogenesis within the dentate gyrus of Kabuki syndrome mice offers a potential unifying mechanism for hippocampal memory defects seen in inherited defects of the histone modification machinery (Gupta et al., 2010, Cohen-Armon et al., 2004 ;Korzus et al., 2004; Alarcon et al., 2004). The further positive correlation of these events with functional outcome supports the hypothesis that the fate of the granule cell layer in the dentate gyrus is a critical determinant of both disease pathogenesis and treatment. More work is needed to determine the relative contribution of precursor cell recruitment, differentiation, proliferation and survival (Yang et al., 2012; Lubitz et al., 2007*)*. Future studies using lineage-specific *Kmt2d* targeting will help to elucidate the contribution of individual cell populations (granule cell layer, pyramidal layer, molecular layer of the cerebellum) to specific neurodevelopmental phenotypes.

Although there is an overall decrease in H3K4me3 in the dentate gyrus granule cell layer of $Kmt2d^{+/\beta Geo}$ mice, we note substantial cell-to-cell variation. This might reflect redundancy of enzymes capable of adding the H3K4 trimethylation mark (Kerimoglu et al., 2013) that could vary in their expression (and therefore compensation capacity) in a cell type-dependent (e.g. differentiation state) or cell state-dependent (e.g. electrochemical environment) manner. Alternatively, this could indicate that stochastic events thought to contribute to epigenetic individuality (Bjornsson et al., 2004) play a role.

There is precedent that HDACi not only increases histone acetylation, but also H3K4 trimethylation (Huang et al., 2011). Our indicators nicely illustrate coupling between H4 acetylation and H3K4 trimethylation, with *Kmt2d*$^{+/\beta Geo}$ mice having defects in both systems. Although AR-42 was used here for this proof of principle study, such a generalized HDACi may have an unacceptable toxicity profile in patients. The reporter alleles described here have the potential for application in small molecule screens to identify drugs with greater potency, specificity and tolerance. There are also many FDA-approved medications, some that have had longstanding clinical use, that influence epigenetic modifications in addition to their originally established functions. An example is the anti-epileptic agent valproic acid, which was recently shown to be a potent HDACi (Phiel et al., 2001). Several widely-used supplements or dietary substances, such as folic acid, genestein, and curcumin, are known to influence epigenetic modifications (Meeran et al., 2010). A recent publication suggests that ketosis, as achieved in a ketogenic diet, might favor chromatin opening through beta-hydroxybutyrate, an endogenous HDACi (Shimazu et al., 2013). This indicates the potential that dietary manipulations, such as a ketogenic diet, might have as another therapeutic avenue for treatment in disorders with a deficiency of open chromatin, such as Kabuki syndrome. These observations may inform the question of potential toxicity of interventions that have broad effects on pervasive epigenetic events. The apparent tolerance to chronic use of such agents during postnatal life likely reflects, at least in part, the complex context within which gene transcription and ultimate function is achieved. Contributing factors include DNA modifications, a repertoire of both positive and negative effectors of transcription, and feedback mechanisms that titrate both gene expression and protein function. In this light, the

predominant influence of agents such as HDACi as therapies may prove permissive for correction of pathologic alterations in physiologic gene expression and function rather than obligate and therefore less conducive to homeostasis.

Although we were able to demonstrate a beneficial effect of AR-42 treatment on neurogenesis at two different ages (1-2 months and 5-6 months), suggesting that this sub-phenotype of Kabuki syndrome may be treatable even in adulthood, it is well established that neurogenesis potential is age-restricted (Martinez-Canabal et al., 2013). It will be essential to further refine the window of opportunity to influence neurogenesis in the granule cell layer in both mouse models and patients. While our data suggest that neurogenesis and hippocampal memory can be recovered after 2 weeks of treatment with AR-42, it is unclear if this response can be sustained even in the presence of chronic treatment. It is also possible, but as yet unproven, that brief treatment in early postnatal stages will result in the expansion of a stable population of cells within the granule cell layer (despite an ongoing relative deficiency of methyltransferase function) and hence achieve long-term recovery of neurologic function. Finally, our ChIP-seq experiments suggest that AR-42 at a dose of 10mg/kg/day led to the most improvement in functional studies (Fig. 4D), but over-correction of genome-wide H3K4me3 (Fig. 4E). Given the favorable tolerance profile of high-dose HDACi when used for cancer treatment, this may not be a limiting factor. However, new challenges may arise when HDACi are used chronically for Kabuki syndrome or other neurodevelopmental disorders. The combination of *in vivo* ChIP-seq analyses and *in vitro* reporter allele performance with regard to H3K4me3 status may ultimately allow optimization in the selection of agent and dose for therapeutic purposes.

Potential limitations of this study include the use of a single heterozygous *Kmtd2* targeted allele that introduces a βGeo expression cassette into the open reading frame. While this strategy should recapitulate haploinsufficiency for KMT2D, as seen in Kabuki syndrome patients heterozygous for nonsense alleles, a gain-of-function contribution of the fusion protein cannot be formally excluded. There are also inherent limitations in the use of mouse models in the study of human neurocognitive disorders. Finally, lineage specific cell targeting will be required to mechanistically validate the correlative link between performance deficits and defects in adult neurogenesis in the dentate gyrus.

In conclusion, our work suggests that a postnatally ongoing and reversible deficiency of granule cell layer H3K4me3, in association with alterations in adult neurogenesis, underlies intellectual disability in a mouse model of KS. This work adds to the emerging view that multiple genetic etiologies of intellectual disability may be amenable to postnatal therapies (Guy et al., 2007; Das et al., 2013; Henderson et al., 2012).

Materials and Methods

Study design

The purpose of this study was to explore the pathophysiological sequence in Kabuki syndrome, a Mendelian disorder of the epigenetic machinery, and to seek robust disease associated phenotypes, which could be used to monitor therapeutic response. We hypothesized that since both causes of Kabuki syndrome involve the transition from

closed to open chromatin, this disorder might be caused by a general imbalance between open and closed chromatin states (favoring closed chromatin) and this ongoing deficiency might be ameliorated with agents that favor chromatin opening such as HDACi. At least 3-4 biological replicates were used for each biochemical analysis, while a sample size of at least 8-10 per group was used for behavioral testing. Data collection occurred for a pre-determined period of time, as dictated by literature-based or core facility-based standards and no exclusion criteria were applied. All analyses were performed by examiners blinded to genotype and/or treatment arm. For drug treatments, animals were randomly assigned to treatment arms with approximately equivalent numbers in each group. Box and whisker plots identify RStudio-defined outliers (shown as circles), but all data points were used in statistical analyses.

Retrospective analysis of neuropsychological testing on patients with Kabuki syndrome

A retrospective chart review was performed using data from patients that had clinically indicated neuropsychological testing at the Kennedy Krieger Institute in years 2004-2014. We analyzed test results from the three individuals with most extensive testing available and a known disease associated mutation in KMT2D. All patient data was collected after consenting patients and stored in secure electronic database at KKI. For this particular analysis per Kennedy Krieger and Johns Hopkins organizational policy, additional IRB reviews was not required (three or fewer patients). We divided the individual tasks into 16 categories, and used literature to identify tasks known to be

associated with dentate gyrus (Kesner et al., 2013; Morris et al., 2012; Epp et al., 2011) or hippocampus (non-dentate gyrus; Brickman et al., 2011).

Epigenetic reporter alleles

Epigenetic reporter alleles were synthesized (OriGene, Rockville, MD) using published sequences for component elements (Baird et al., 1999; Souslova et al., 2007). Single nucleotide mutations were created using the QuickChange Lightening kit (Agilent Technologies Inc, Santa Clara, CA). For H4ac indicator we introduced K5R, K8R, K12R, K16R and K20R (MUT indicator). For H3K4me3 indicator we introduced K4Q and D890A/W891A and M882A (three separate constructs). For transient transfections mouse embryonic fibroblasts (see below) were transfected with Fugene HD (Promega, Madison, WI), 48 hours prior to FACS. Transfection efficiency of reporter alleles was comparable in transiently-transfected murine embryonic fibroblasts (MEFs) derived from mice of both genotypes (*Kmt2d*$^{+/\beta Geo}$ and *Kmt2d*$^{+/+}$), as measured by real-time PCR of genomic DNA. For drug stimulation, drug was added to the media 24 hours prior to FACS. For stable transfections in T293 (American Type Culture Collection) cells, 10 μg/ml of Blastocidin (Life Technologies, Carlsbad, CA) was added to the media for several weeks. For stable transfection in MEFs, the reporter was transferred to a ViraPower Lentiviral Expression System (Life Technologies, Carlsbad, CA). After selection with Blastocidin, the drug of interest was added 24 hours prior to FACS. SAHA, AR-42 and MS275 were purchased from Selleck (Selleck Chemicals, Houston, TX). FACS was performed using either a FACSCalibur (BD Biosciences, San Jose, CA) or FACSverse (BD Biosciences, San Jose, CA) system with comparable results. FACS data were analyzed using FlowJo

(Tree Star Inc, Ashland, OR). A plasmid expressing HDAC3 was acquired from Addgene (Cambridge, MA, plasmid 13819) and transfected into a stable cell line carrying the H4 acetyl reporter allele.

Animals

Our mouse model, *Kmt2d*$^{+/\beta Geo}$, also named Mll2Gt $^{(RRt024)\ Byg}$, was acquired from Bay Genomics (University of California). All experimental mice were on a mixed C57BL/6J and 129/SvEv background. Expected Mendelian ratios were observed when heterozygous animals were bred to wild-type. In heterozygous crosses, however, there was uniform embryonic lethality of homozygotes by ED12, the earliest developmental stage assayed. For treatment with AR-42, mice were orally gavaged daily with drug (Selleck Chemicals, Houston, TX) solubilized in vehicle (0.5% methylcellulose, 0.1% Tween-80, water) or with vehicle alone. Drug delivery information was kindly provided by Drs. Chen and Kulp from Ohio State University (Huang et al., 2011). Drug was administered for 14 days and mice were sacrificed on day 15. Morris water maze testing was initiated at day 7 and a dose of 10 mg/kg/day was used for these studies. For quantification of DCX positive cells, doses of 0, 5, 10 and 25 mg/kg/day were used. Genotyping was performed using primers B-GeoF-(CAAATGGCGATTACCGTTGA) and B-GeoR-(TGCCCAGTCATAGCCGAATA) that are specific for the targeted allele and TcrdF-(CAAATGTTGCTTGTCTGGTG) and TcrdR-(GTCAGTCGAGTGCACAGTTT) that control for sufficient DNA concentration. Real-time PCR using the same primers allows discrimination between the heterozygous and homozygous state for the targeted allele.

Thymus was dissected from a wild-type neonatal mouse and flash frozen in OCT. Slides were fixed with 4% PFA for 30 minutes. All experiments were performed using mouse protocols approved by the Animal Care and Use Committee of Johns Hopkins University School of Medicine. The mouse protocols used for this study are in accordance with the guidelines used by the NIH for mouse care and handling.

Morris water maze testing

Mice were placed in a 1.1 meter diameter tank filled with room temperature water dyed with non-toxic white paint. For analysis purposes, the tank was divided into four quadrants, with one quadrant containing a small platform submerged 1.5 cm beneath the water. On each day of training mice were placed in the tank in a random quadrant facing away from the center and were allowed to swim until they found the platform and were left there for 30 seconds. If they did not reach the platform after 60 seconds they were placed on it for 30 seconds. Each mouse was given 4 trials per day (for 5 days) with no inter-trial interval and subsequently returned to its home cage. Latency to reach the platform was measured during each trial. The day after the final day of training, the platform was removed for a probe trial where mice were placed in the tank for 90 seconds. Average number of crossings of the platform's previous location was recorded. Visible/flagged platform training was also performed for 3 days either before the hidden platform or after the probe trial, where a visible flag was placed on the submerged platform, and the time for each mouse to reach the platform was measured for each 60 second trial, four of which were run in the same way as the hidden platform training. For

all training and probe testing, data was recorded both manually and electronically with ANY-maze software (San Diego Instruments, San Diego, CA) when applicable. Differences in the number of platform crossings during the probe trial were compared between groups with a Student's t-test with significance value set at $P < 0.05$.

Additional behavioral testing

For all behavioral testing, all data were collected and analyzed by an individual blinded to genotype and treatment group. Mice ranged from two to three months of age in all tests, and all experiments were performed in the late morning or early afternoon. Novel object recognition: On the first day of the novel object recognition test, mice were individually placed into a square plastic arena (25cmx25cmx25cm) that contained two identical plastic objects along the midline of the arena. Each mouse was allowed to explore the objects for 10 minutes and then placed back in its home cage. The following day, each mouse was placed in the same arena with the same two identical objects and the time interacting with each object was recorded over 10 minutes. On the third day, one object was removed and replaced by a novel object. Mice were placed in the arena for five minutes and timed for interaction with the familiar object compared to the novel object. Differences in interaction time between the novel object and the familiar object for $Kmt2d^{+/+}$ and $Kmt2d^{+/\beta Geo}$ mice were calculated by computing time spent with the novel object divided by the total time spent with both objects. These values were analyzed for significance with a Student's t-test with significance value set at $P < 0.05$. Fear conditioning testing: On day 1 both $Kmt2d^{+/\beta Geo}$ mice and $Kmt2d^{+/+}$ littermates were placed in chamber and allowed to explore the chamber freely. After 120 seconds (2

minutes), a 2000 Hz sound was played for 30 seconds. For the last 2 seconds of sound (seconds 148-150), the sound co-occurred with a 0.35 mAmp electrical shock (2 seconds) administered through the floor grid. Mice were observed for a total of 300 seconds. Freezing behavior was measured using the FreezeScan software (CleverSys Inc, Reston, VA). On days 2 and 14 (fig. S3) contextual freezing was assessed over 300 seconds (no cue). On days 3 and 15, cued freezing was assessed over 300 seconds. Open field testing: Mice were placed in the open field chamber and activity was monitored using the Photobeam activity system (San Diego Instruments, San Diego, CA). Activity levels (ten 180 second intervals) were pooled to yield a general activity level (Adamczyk, et al., 2012). Grip strength testing: Grip strength testing was performed as previously described (Adamczyk, et al., 2012). Three trials were performed and results were averaged for each mouse.

Perfusion and cryosectioning

Mice were sacrificed with a xylazine ketamine combination, transcardially flushed with PBS/Heparin and then perfused with 4% PFA/PBS. Brains were dissected and cryopreserved in 30% sucrose 0.1M phosphate solution overnight at 4°C. Brains were frozen and sectioned using a Microm HM 550 cryostat (Thermo Scientific, Waltham, MA). Sectioning was performed at 30 μm intervals and every section of the brain was collected and stored in glycerine ethylene glycol phosphate storage solution.

EdU administration and staining

For EdU experiments, mice were injected IP over ten days, with injections on the first three and last three days, with 50 mg/kg EdU (Life Technologies, Carlsbad, CA). Mice were sacrificed 30 days after the initial start of injection, and EdU staining was done with the Click-iT EdU Alexa Fluor 488 Imaging Kit (Life Technologies, Carlsbad, CA) as well as DAPI mounting with Vectamount (Vector Laboratories, Burlingame, CA). EdU quantification was performed by an individual blinded to genotype. Positive cells were counted in every sixth slice in the granule cell layer and the average number per slice was calculated for each brain.

Real time PCR

Real-time PCR was performed using Kmt2d-specific probes for exons 20 and 52 (Mm_02600438 and Mm_01717664, respectively) from TaqMan® Gene Expression Assays (Life Technologies, Carlsbad, CA). For a comparison of transfection efficiencies for indicator constructs in transient transfection studies, we performed real-time PCR using SYBR Green Real-Time PCR Master Mix (Life Technologies, Carlsbad, CA) and primers IND-F-(CTGCGCGCAAGTCAACGGGTG) and IND-R-(ATGCCGTTCTTCTGCTTGTCG) that are specific for the H3K4 methylation indicator. For expression analysis for KMT2D target gene KLF10 we performed real-time PCR using Klf10-specific expression assay (Mm00449812_m1) from TaqMan® Gene Expression Assays (Life Technologies, Carlsbad, CA).

Immunoblotting

Total protein lysates from *Kmt2d*$^{+/\beta Geo}$ and *Kmt2d*$^{+/+}$ littermates were isolated and immunoprecipitated with an antibody against the amino terminus of KMT2D (sc-292359, Santa Cruz Biotechnology, Dallas, TX). Isolated protein was applied to a membrane and immunoblotted with an antibody against beta-galactosidase (ab9361, Abcam, Cambridge, ENG) as previously described (Loeys et al., 2010).

Immunofluorescence

Every 6th brain section was selected and then blocked with 5% Bovine Serum Albumin (BSA) at room temperature followed by incubation with primary antibodies overnight at 4°C. Secondary antibodies were then applied for 1 hour at room temperature, after which sections were mounted onto microscope slides with Vectamount with DAPI (Vector Laboratories, Burlingame, CA). Primary antibodies included Doublecortin (DCX) (SC-8066, Santa Cruz Biotechnology, Dallas, TX, 1:200 goat), trimethylated H3K4 (9727L, Cell Signaling Technology, Beverly, MA, 1:500 rabbit), Kmt2d H-300 (SC-292359, Santa Cruz Biotechnology, Dallas, TX, 1:500 rabbit) and activated caspase 3 (AB3623, Millipore, Billerica, MA, 1:100, Rabbit). Non-specific binding was not observed when we sequentially exposed sections to serum (or IgG when appropriate) from the same species as the primary antibody for each experiment (i.e. rabbit for KMT2D and H3K4me3 and goat for doublecortin), followed by the secondary antibody used for KMT2D and H3K4me3 (anti-rabbit) or doublecortin (anti-goat).

Confocal microscopy

Z-stack images of slides were taken at either 10x using Zeiss Axiovert 200 with 510-Meta confocal module (Carl Zeiss, Jena, GER) or 25x using Zeiss AxioExaminer with 710NLO-Meta multiphoton (Carl Zeiss, Jena, GER). From 10x pictures, the granule cell layer was highlighted and fluorescent intensities for both DAPI and H3K4me3 were measured at the midpoint of the entire z-stack (Zen software, Carl Zeiss, Jena, GER) with the value for *Kmt2d*$^{+/+}$ animals set equal to one. A Students t-test with significance value set at $P < 0.05$ was used to compare H3K4 trimethylation intensity referenced to DAPI intensity.

Granule cell layer and doublecortin area

The area of both the granule cell layer and DCX+ cells was measured using the NS elements 2.0 software (Nikon, Tokyo, JPN). Normalized DCX area was calculated by measuring the DCX+ area of the granule cell layer and setting the baseline (*Kmt2d*$^{+/+}$) fraction to 1. A Student t-test with significance value set at $P < 0.05$ was used for comparison of DCX+ area referenced to granule cell layer area between genotypes and treatment arms.

Evaluation of maxillary protrusion

Maxillary protrusion was evaluated by ten investigators blinded to genotype and they were asked to rate maxillary protrusion on radiographs as either large (2) or small (1). When results were un-blinded and average scores for each animal determined, the *Kmt2d*$^{+/\beta Geo}$ animals had a significantly lower score than *Kmt2d*$^{+/+}$ littermates.

ChIP-seq

Spleens were dissected from eight mice, four from each *kmt2d* genotype (+/βGeo or +/+) where half of each genotype was treated with AR-42 and half with vehicle only. Spleens were minced and passed through a 40μm cell strainer to obtain single cell suspensions. 10 million cells were used for each ChIP-seq experiment following the native chromatin immunoprecipitation protocol, as previously described (Gilfillan et al., 2012), using a ChIP-grade antibody against H3K4me3 (9727, Cell Signaling Technology, Beverly, MA).

ChIP-seq data analysis

Sequencing was performed using a MiSeq system (Illumina, San Diego, CA). 4.8-9.6 million paired-end 26 bp reads were obtained per sample (Supplementary Table 1). Reads were aligned to the *M. musculus* genome, version mm10, using Bowtie 2 (Langmead et al., 2012). We examined each sample with regard to alignment rate as well as FRIP (fraction of reads in peaks), a measure of the ChIP efficiency (Supplementary Table 1). FRIP was computed based on peaks called only on specific samples using MACS version

1.4.2 (Zhang et al., 2008). For analysis, reads were merged into one meta-sample and peak calling was performed using MACS version 1.4.2 (Zhang et al., 2008). This allowed definition of a superset of 33,517 peaks in one or more samples. The number of reads overlapping a peak was computed using bedtools version 2.17.0 (Quinlan et al., 2010) in the following way: each paired-end read was converted to a single interval containing both mate coordinates (effectively filling in the insert) and these intervals were examined for overlaps with the superset of peaks. This created a peak by sample matrix of read counts. Differential binding was assessed using the GLM functionality (McCarthy et al., 2012) in edgeR version 3.5.27 (Robinson et al., 2010). A single model was fit, using all 8 samples, with Tagwise variance estimation. Different contrasts were examined corresponding to the different hypotheses considered in the main text, and peaks were considered differentially bound if they had a Benjamini-Horchberg corrected P-values less than 5%. Fold change and overall abundance was calculated as per edgeR.

Evaluation of directional balance in ChIP-seq dataset

For figures 2.1D and 2.4E and supplementary fig. 2.17 each point corresponds to a genomic location with an H3K4me3 peak in at least one of the samples. A positive value indicates that the peak is higher in the *Kmt2d*$^{+/\beta Geo}$ compared to the *Kmt2d*$^{+/+}$. Peaks which are significantly differentially bound are shown in red, and other peaks are shown in gray. In supplementary fig. 2.17, the expected medium is demonstrated with a broken line, but unbroken line shows the median in our observed comparison. Supplementary fig. 2.18 illustrates whether the balance is shifting up (blue) or down in a particular

comparison. To examine whether there was a directional balance between differentially bound genes we developed the following test. For *Kmt2d*$^{+/+}$(vehicle) compared to *Kmt2d*$^{+/\beta Geo}$(vehicle), we observed 454 peaks to be stronger bound in the mutant, 1,499 to be stronger bound in the wild-type and 27,052 peaks to not be differentially bound. Our model assumes that these three numbers follow a multinomial distribution with a probability vector (p1, p2, p3). To test for directional balance, we constructed a standard likelihood-ratio test for the hypothesis p1 = p2. Per standard results, two times the negative log-likelihood ratio test statistic was asymptotically chi-square distributed with 1 degree of freedom.

Statistics and plots

For all box plots generated through RStudio (RStudio Inc, Boston, MA), the margins of the box show the upper and lower quartiles, the central line the median, and the whiskers the range. Circles denote outliers as defined by the RStudio algorithm. For all column, line, and scatter-plot graphs (generated through Microsoft Excel), the error bars represent standard error of the mean, with the data point representing the mean of each applicable group. Unless otherwise stated, significance between two groups was calculated with a Student's t-test with a significance value of $P < 0.05$. Two-way repeated measures ANOVAs were calculated with SPSS (IBM, Armonk, NY). For every calculated P value the stated N represents the number of animals for each group contributing to that comparison. For *P* value nomenclature, * = $P < 0.05$, ** = $P < 0.01$, † = $P < 0.005$, †† = $P < 0.001$.

Figure 2.1: *Kmt2d*$^{+/\beta Geo}$ mouse model of Kabuki syndrome demonstrates hippocampal memory defects. (A) Domain organization of *KMT2D* in human and mouse, with the H3K4 methyltransferase SET domain indicated in red and other domains by additional colors, as well as The human and murine chromosomal assignment **(B)** The *Kmt2d*$^{\beta Geo}$ targeting event introduced a β-Geo cassette including a strong splice acceptor (SA) sequence and a 3' cleavage and polyadenylation signal (pA) into intron 50 of *Kmt2d* on mouse chromosome 15 (Sup. Fig. 2.2A). **(C)** Real-time PCR using primers for exons 20 or 52 of *Kmt2d* (arrows) confirmed a 50% reduction in mRNA corresponding to sequences distal to the β-Geo insertion site when compared to proximal sequences in *Kmt2d*$^{+/\beta Geo}$ mice, in comparison to *Kmt2d*$^{+/+}$ littermates. Results reflected three technical replicates for each of 3 *Kmt2d*$^{+/+}$ and 2 *Kmt2d*$^{+/\beta Geo}$ mice. **(D)** ChIP-seq revealed a genome-wide deficiency of H3K4me3 in cells from *Kmt2d*$^{+/\beta Geo}$ mice, when compared to cells from *Kmt2d*$^{+/+}$ littermates. A positive value indicates a higher locus-specific peak in *Kmt2d*$^{+/\beta Geo}$ mice. Each point corresponds to a genomic location with a peak in at least one sample. Significantly differentially bound loci are red, while others are gray. **(E)** No difference was seen in positional preference between genotypes during the habituation phase [identical objects (L/R)] of the novel object recognition test. *Kmt2d*$^{+/\beta Geo}$ mice spent less time with a novel object (L) and more with a habituated object (R) compared to *Kmt2d*$^{+/+}$ littermates. *Kmt2d*$^{+/+}$ littermates also demonstrated significant improvement from habituation phase [Novel object (L)] while *Kmt2d*$^{+/\beta Geo}$ mice did not. N = 13 (+/+), N = 10 (+/βGeo). **(F)** *Kmt2d*$^{+/\beta Geo}$ mice showed a reduced frequency in platform zone crossings during the probe trial phase of Morris water maze testing, N = 48 (+/+), N = 32 (+/βGeo). *$P < 0.05$. $^{\dagger}P < 0.005$; $^{\dagger\dagger}P < 0.001$, t-test.

-

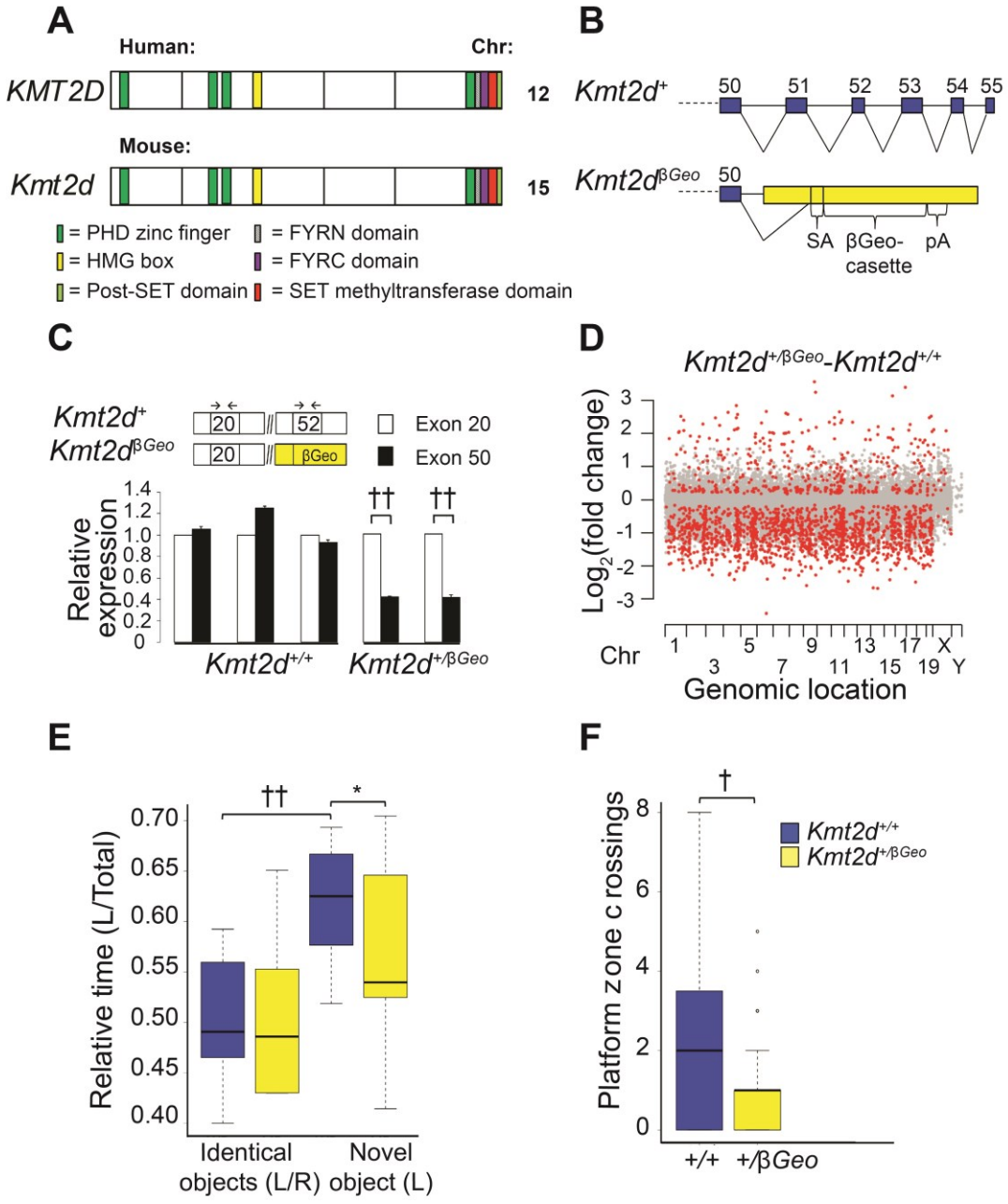
A
Human:
Chr:
KMT2D
12
Mouse:
Kmt2d
15
= PHD zinc finger
= FYRN domain
= HMG box
= FYRC domain
= Post-SET domain
= SET methyltransferase domain
B
Kmt2d+
50 51 52 53 54 55
Kmt2dβGeo
50
SA βGeo- pA
casette
C
Kmt2d+
Kmt2dβGeo
20
52
βGeo
Exon 20
Exon 50
Relative expression
Kmt2d+/+
Kmt2d+/βGeo
D
Kmt2d+/βGeo-Kmt2d+/+
Log2(fold change)
Chr
Genomic location
E
Relative time (L/Total)
Identical objects (L/R)
Novel object (L)
F
Platform zone c rossings
Kmt2d+/+
Kmt2d+/βGeo
+/+
+/βGeo

Figure 2.2: *Kmt2d*$^{+/\beta Geo}$ mice demonstrate a global deficiency of H3K4me3 in the dentate gyrus associated with reduced granule cell layer volume and neurogenesis. **(A)** Immunofluorescence revealed intense expression of KMT2D (red signal) in the dentate gyrus granule cell and pyramidal layers of *Kmt2d*$^{+/+}$ mice. **(B)** Immunofluorescence for H3K4me3 (red) and DAPI (blue) in the granule cell layer of *Kmt2d*$^{+/\beta Geo}$ mice and *Kmt2d*$^{+/+}$ littermates. **(C)** Quantification revealed a reduced H3K4me3/DAPI signal intensity ratio within the granule cell layer of *Kmt2d*$^{+/\beta Geo}$ mice compared to *Kmt2d*$^{+/+}$ littermates. N = 9 (+/+), N = 5 (+/βGeo). **(D)** Calculation of granule cell layer area (red outline) in every sixth brain slice allowed demonstration of reduced granule cell layer volume **(E)** in *Kmt2d*$^{+/\beta Geo}$ mice compared to *Kmt2d*$^{+/+}$ littermates. N = 4 (+/+), N = 5 (+/βGeo). **(F, G)** Immunofluorescence revealed reduced representation of cells positive for doublecortin (DCX), a marker for neurogenesis, in the granule cell layer of *Kmt2d*$^{+/\beta Geo}$ mice compared to *Kmt2d*$^{+/+}$ littermates. N = 4 (+/+), N = 4 (+/βGeo). *$P < 0.05$; $^{\dagger\dagger}P < 0.001$, t-test.

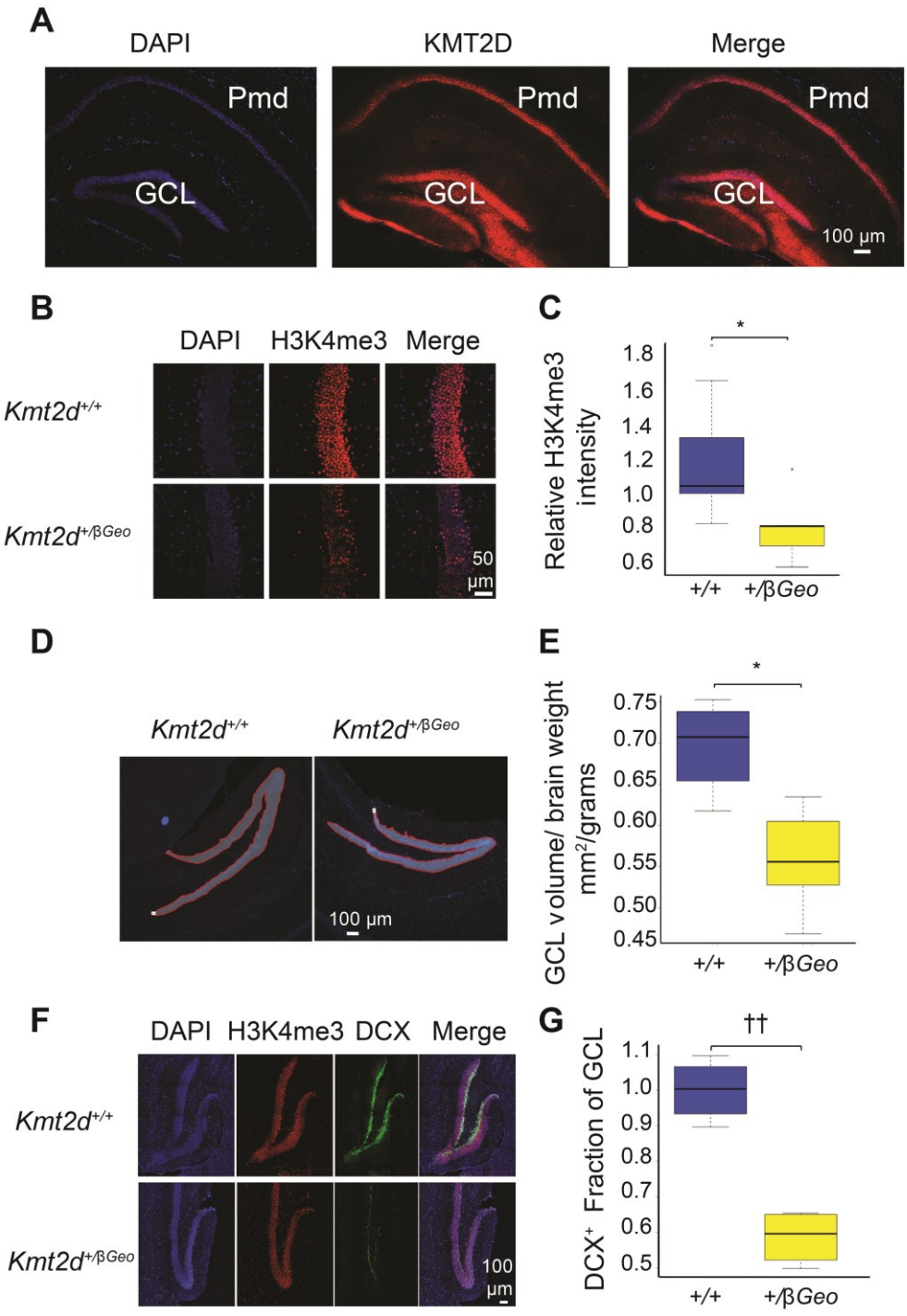
A
DAPI
KMT2D
Merge
Pmd
GCL
100 µm
B
DAPI
H3K4me3
Merge
Kmt2d+/+
Kmt2d+/βGeo
50 µm
C
Relative H3K4me3 intensity
1.8
1.6
1.4
1.2
1.0
0.8
0.6
*
+/+
+/βGeo
D
Kmt2d+/+
Kmt2d+/βGeo
100 µm
E
GCL volume/ brain weight mm2/grams
0.75
0.70
0.65
0.60
0.55
0.50
0.45
*
+/+
+/βGeo
F
DAPI
H3K4me3
DCX
Merge
Kmt2d+/+
Kmt2d+/βGeo
100 µm
G
DCX+ Fraction of GCL
1.1
1.0
0.9
0.8
0.7
0.6
0.5
††
+/+
+/βGeo

Figure 2.3: H3K4me3 epigenetic reporter allele demonstrates decreased activity in *Kmt2d*$^{+/\beta Geo}$ cells. **(A)** Domain organization encoded by the H4ac and H3K4me3 reporter alleles. The H4ac indicator includes H4 (lysine positions indicated), the C- and N-terminal halves of E-GFP separated by a short linker (L), the TAFII binding domain (BD) and a repetitive nuclear localization signal (NLS). The H3K4me3 indicator includes the H3 and the TAF3-PHD. **(B)** Recognition of the histone tail mark by the relevant histone reader leads to reconstitution of GFP structure and function (fluorescence). **(C, D)** The acetylation indicator demonstrated increasing fluorescence with increasing amounts of the histone deacetylase inhibitor SAHA. **(E)** Activity of the H4ac indicator was lost upon mutagenesis of all potential acetylation sites from lysine to arginine. **(F)** The H3K4me3 indicator demonstrated a dose dependent response to the histone deacetylase inhibitor AR-42 with decreased cell numbers at higher doses (red line). **(G)** Activity was greatly reduced upon mutagenesis of K4 in the H3 tail and D890A/W891A and M882A in the reader pocket. **(H)** The H3K4me3 indicator showed reduced activity in murine embryonic fibroblasts (MEFs) derived from *Kmt2d*$^{+/\beta Geo}$ mice compared to *Kmt2d*$^{+/+}$ littermates. Both genotypes showed a dose-dependent response to AR-42, with *Kmt2d*$^{+/\beta Geo}$ MEFs achieving untreated wild-type levels of activity at a dose of 5 μM. N = 3 (+/+), N = 3 (+/βGeo), biological replicates for each dose. $^{**}P < 0.01$, $^{\dagger\dagger}P < 0.001$, t-test.

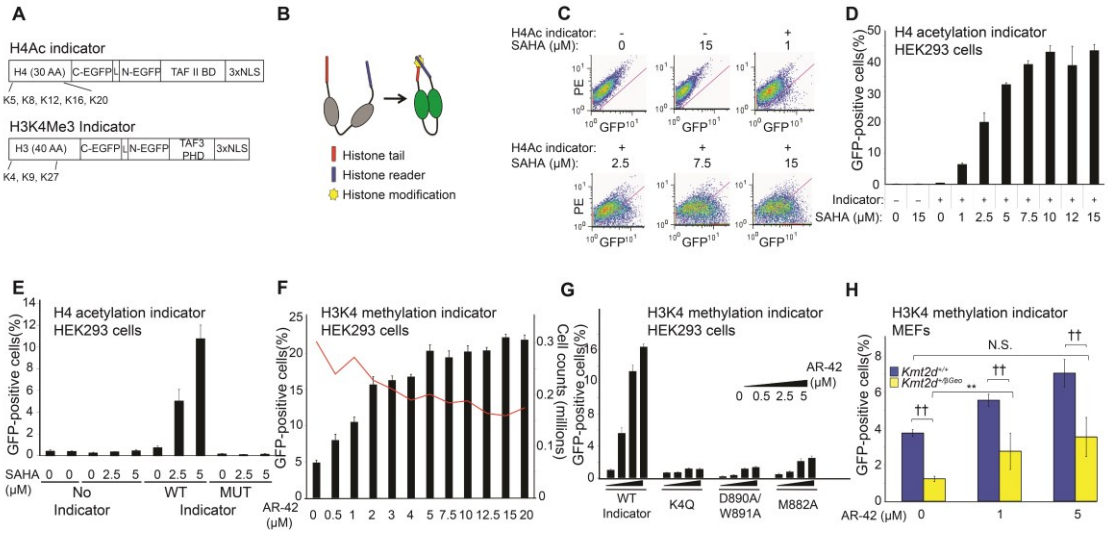
A
H4Ac indicator
H4 (30 AA)
C-EGFP
L
N-EGFP
TAF II BD
3xNLS
K5, K8, K12, K16, K20
H3K4Me3 Indicator
H3 (40 AA)
C-EGFP
L
N-EGFP
TAF3 PHD
3xNLS
K4, K9, K27
B
Histone tail
Histone reader
Histone modification
C
H4Ac indicator:
SAHA (μM):
PE
GFP
D
H4 acetylation indicator
HEK293 cells
GFP-positive cells(%)
Indicator:
SAHA (μM):
E
H4 acetylation indicator
HEK293 cells
GFP-positive cells(%)
SAHA (μM)
No Indicator
WT Indicator
MUT Indicator
F
H3K4 methylation indicator
HEK293 cells
GFP-positive cells(%)
Cell counts (millions)
AR-42 (μM)
G
H3K4 methylation indicator
HEK293 cells
GFP-positive cells(%)
AR-42 (μM)
WT Indicator
K4Q
D890A/ W891A
M882A
H
H3K4 methylation indicator
MEFs
GFP-positive cells(%)
N.S.
Kmt2d+/+
Kmt2d−/−Geo
AR-42 (μM)

Figure 2.4: *In vivo* effects of AR-42. 1-2 month old mice of both genotypes showed an increase in H3K4me3 (**A, B**) [N = 5-6 per group] associated with a dose-dependent increase in neurogenesis in *Kmt2d*$^{+/\beta Geo}$ mice **(C, D)** (monitored by normalized DCX expression) [N = 4-6 per group] upon treatment with the HDACi AR-42. There was no difference of either H3K4me3 or neurogenesis between *Kmt2d*$^{+/\beta Geo}$ and *Kmt2d*$^{+/+}$ animals at a dose of 10mg/kg/day. **(E)** The genome-wide deficiency of H3K4me3 seen in *Kmt2d*$^{+/\beta Geo}$ mice was improved upon treatment with 10 mg/kg/day AR-42. **(F)** The reduced frequency of platform crossing seen during Morris water maze testing of *Kmt2d*$^{+/\beta Geo}$ mice was normalized upon treatment with 10 mg/kg/day of AR-42. [N = 48 (+/+, no treatment), N = 32 (+/βGeo, no treatment), N = 14 (+/+, 10 mg/kg/day AR-42), N = 9 (+/βGeo, 10 mg/kg/day AR-42)]. *P < 0.05; **P < 0.01; †P < 0.005; ††P < 0.001, t-test.

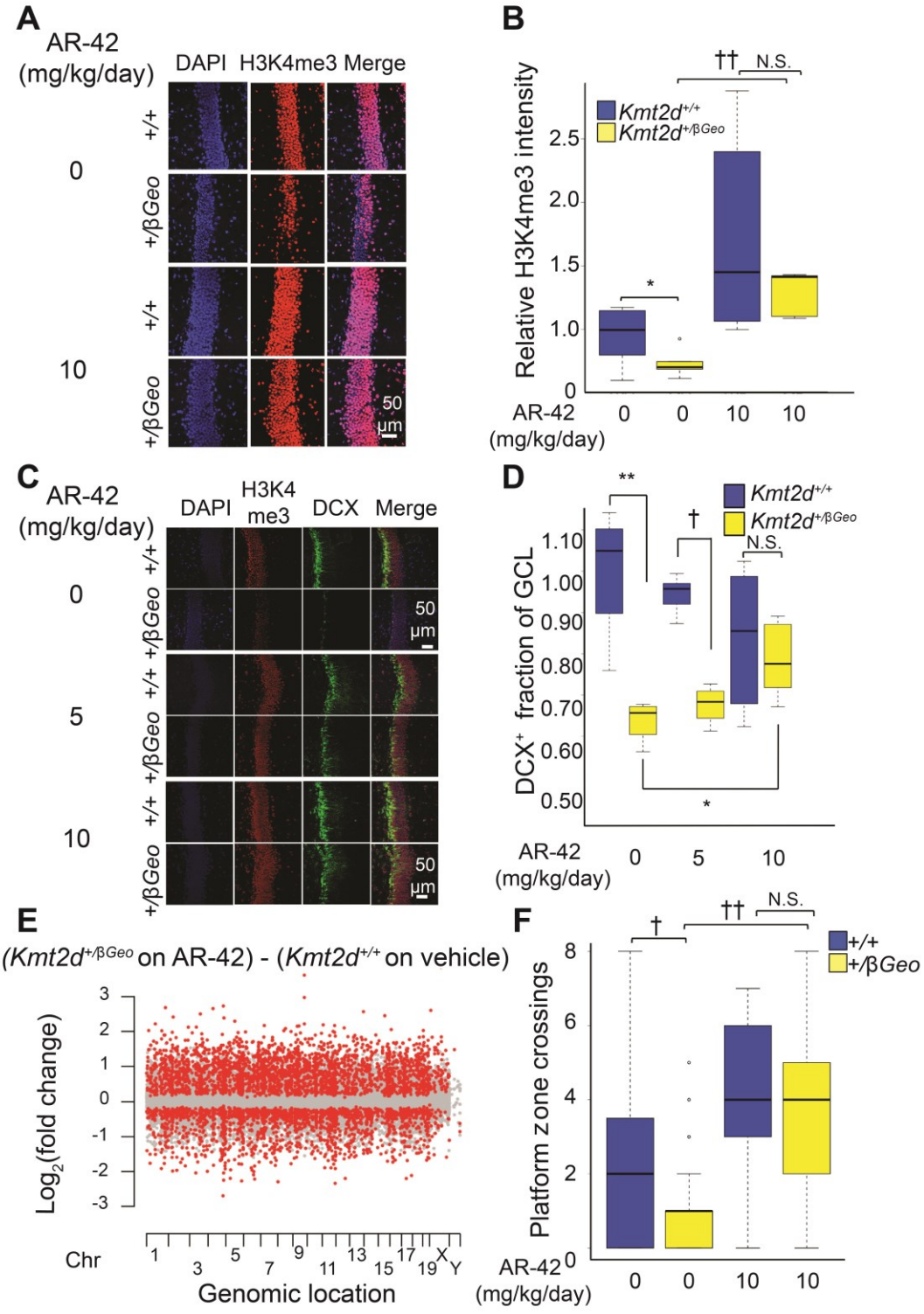
A
AR-42 (mg/kg/day)
DAPI H3K4me3 Merge
+/+
+/βGeo
0
10
50 μm
B
Relative H3K4me3 intensity
Kmt2d+/+
Kmt2d+/βGeo
††
N.S.
*
AR-42 (mg/kg/day)
C
AR-42 (mg/kg/day)
DAPI H3K4 me3 DCX Merge
0
5
10
50 μm
D
DCX+ fraction of GCL
**
†
N.S.
*
AR-42 (mg/kg/day)
E
(Kmt2d+/βGeo on AR-42) - (Kmt2d+/+ on vehicle)
Log2(fold change)
Chr
Genomic location
F
Platform zone crossings
†
††
N.S.
+/+
+/βGeo
AR-42 (mg/kg/day)

Table 2.1: Neuropsychological findings in patients with Kabuki syndrome. A retrospective analysis of neuropsychological testing on three patients with mutations in KMT2D reveals consistent abnormalities of functions that have been associated with the dentate gyrus. N/A, not adequately tested with testing regiment. ↓, deficient area (defined as >1 SD below the mean and lower than full-scale IQ or, if unavailable, highest individual test score); metrics linked to the dentate gyrus are in bold font (Kesner et al., 2013; Morris et al., 2012; Epp et al., 2011); metrics more broadly linked to the hippocampus are indicted with an asterisk (Brickman et al., 2011).

Neuropsychologic process/function	**Patient 1 28 years Female**	**Patient 2 15 years Female**	**Patient 3 14 years Male**
Affected gene	*KMT2D*	*KMT2D*	*KMT2D*
Full-scale IQ	87	84	66
Perceptual or nonverbal reasoning*	↓	↓	↓
Verbal reasoning/comprehension	Normal	Normal	↓
Verbal fluency*	↓	Normal	N/A
Naming*	Normal	Normal	Normal
Vocabulary/reading	Normal	Normal	N/A
Processing speed	↓	↓	↓
Basic math calculation	Normal	↓	N/A
Visual selective attention*	↓	↓	N/A
Visual working memory*	↓	↓	↓
Verbal working memory*	Normal	Normal	↓
Visual delayed memory*	↓	↓	↓
Verbal delayed memory*	↓	↓	Normal
Switching/inhibition	↓	↓	N/A
Verbal organization	Normal	Normal	N/A
Visual organization*	↓	↓	↓
Fine motor	↓	↓	↓

Supplementary Material

Supplementary figure 2.1: Integration site of gene trap in the *Kmt2d*$^{\beta Geo}$ allele. **(A)** DNA sequence of the targeted allele showing sequence for *Kmt2d* exon 50 (red) and intron 50 (blue) and the gene trap encoding the β-Geo cassette (purple). **(B)** Immunoprecipitated protein using an antibody directed against KMT2D showed immunoreactivity for β-galactosidase in cellular lysates from *Kmt2d*$^{+/\beta Geo}$ mice but not *Kmt2d*$^{+/+}$ littermates. The presence of this hybrid protein suggested that mRNA from the *Kmt2d*$^{\beta Geo}$ allele is both transcribed and translated.

A

Exact integration site:

CTGTGTGGAACCGCATCATTGAGCCTGTGGCTGCCATGAGAAAAGAAGCC
GACATGCTGAGACTCTTCCCCGAGTACCTGAAAGGCGAAGAACTCTTTGG
GCTGACAGTGCATGCAGTGCTTCGCATAGCTGAATCGGTAAGCAAGCGGC
AAGGAGCTGGGGCCAAGGTGGGAATACTTACTGTATGGCGTGCGGGTGT
GTGTGACCGTGGGTACACTTAAAACACCGGGTTTTGGATCTGCACTGTCCC
GGATGTCCTCTGGTGCTCAAAGACCCTTTTGGGTTTGCCCTTTGGTAAGA
GCGCCGGGATCTACTTGTCTGGAGGCCAGGGAGTCCTCAGCCGAGGCTT
GCCGCCCCTGACTGCACTGCACTGAGTAGT

B

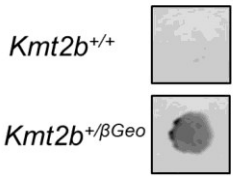

Supplementary figure 2.2: *Kmt2d*$^{+/\beta Geo}$ mice show overlapping phenotypic features with patients with Kabuki syndrome. Decreased protrusion of the maxilla over the mandible could be seen when skin was removed (A) and on radiographs (B) in *Kmt2d*$^{+/\beta Geo}$ mice, when compared to *Kmt2d*$^{+/+}$ littermates (N ≥ 5 for both groups). This was verified by a group of investigators blinded to genotype which gave *Kmt2d*$^{+/+}$ mice a significantly higher maxillary protrusion score than *Kmt2d*$^{+/\beta Geo}$ littermates (C). $^{\dagger}P < 0.005$.

A **B** **C**

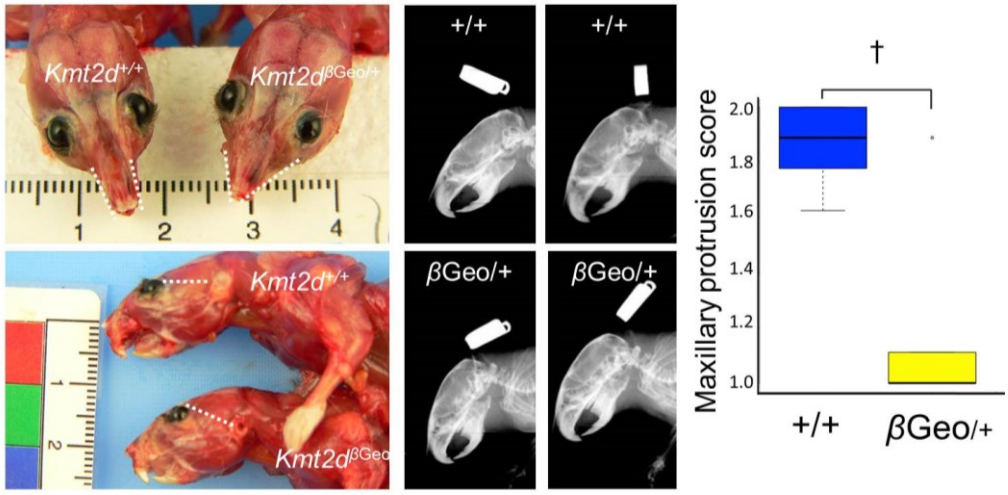

Supplementary figure 2.3: *Kmt2d*$^{+/\beta Geo}$ mice have context related memory defects. *Kmt2d*$^{+/\beta Geo}$ showed impaired performance in a fear-conditioning assay, when compared to *Kmt2d*$^{+/+}$ littermates. N = 20 (+/+), 8 (+/βGeo). $P < 0.05$ (repeated measures ANOVA comparing two genotypes in all time points).

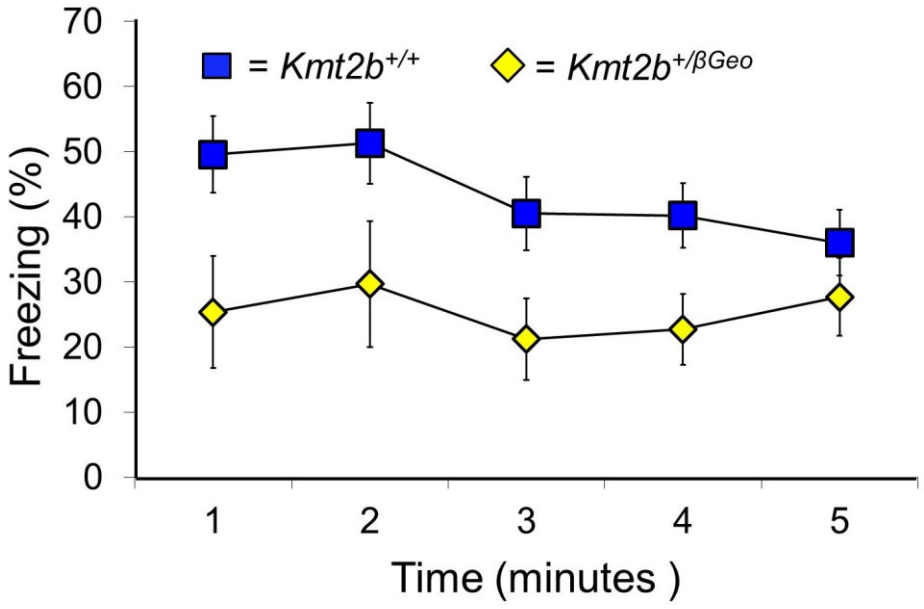

Supplementary figure 2.4: *Kmt2d*$^{+/\beta Geo}$ mice show no deficit in flag trial. *Kmt2d*$^{+/\beta Geo}$ mice and *Kmt2d*$^{+/+}$ littermates showed similar performance during flag trials prior to Morris water maze testing (as reflected by no significant difference in a repeated measures ANOVA), suggesting no inherent impairment to task completion such as visual impairment, in subsequent memory-based testing. N.S., N = 15 (+/+), 9 (+/βGeo).

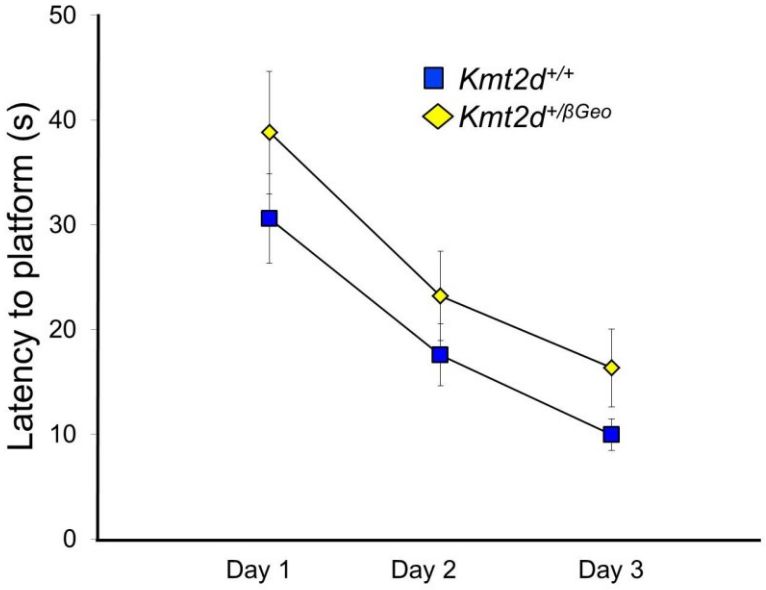

Supplementary figure 2.5: Assessment of motor function in *Kmt2d*$^{+/\beta Geo}$ and *Kmt2d*$^{+/+}$ mice. *Kmt2d*$^{+/\beta Geo}$ mice did not show any deficit in general activity level (as monitored by beam breaks in open field testing) **(A)** or grip strength **(B)**, when compared to *Kmt2d*$^{+/+}$ littermates and had comparable swimming speed in the probe trial of the Morris Water Maze (**C**). Open field testing: N.S., N = 11 (+/+), 11 (+/βGeo); grip strength: N.S., N= 18 (+/+), 8 (+/βGeo). MWM probe trial: N.S., N = 29 (+/+), 23 (+/βGeo).

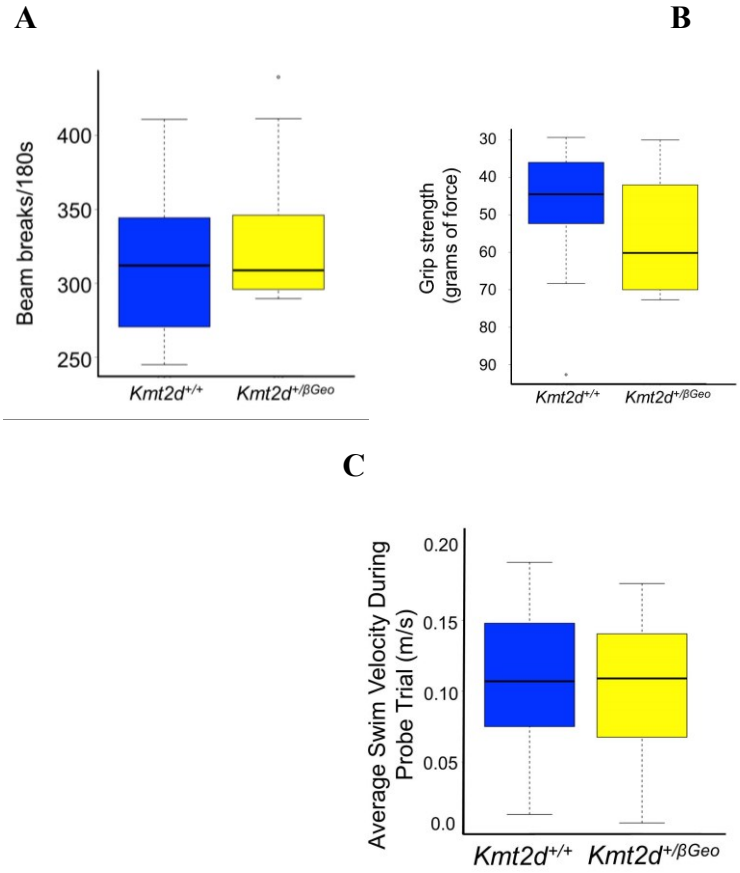

Supplementary figure 2.6: Escape latencies during Morris water maze training. (**A**) Average latency to platform zone for *Kmt2d*$^{+/\beta Geo}$ (yellow) and *Kmt2d*$^{+/+}$ animals (blue). Repeated measures ANOVA showed no significant difference between groups across all time points. (**B**) *Kmt2d*$^{+/\beta Geo}$ mice on 10 mg/kg/day of AR-42 (yellow triangle) and *Kmt2d*$^{+/+}$ animals on 10 mg/kg/day of AR-42 (blue circle). No significant difference was observed. (**C**) *Kmt2d*$^{+/+}$ animals with (blue circle) and without (blue square) 10 mg/kg/day of AR-42. A significant difference was observed with P <0.01. (**D**) *Kmt2d*$^{+/\beta Geo}$ animals with (yellow rhombus) and without (yellow triangle) 10 mg/kg/day of AR-42. No significant difference was observed. N = 32 (+/βGeo, vehicle), 44 (+/+, vehicle), 9 (+/βGeo, AR-42), 14 (+/+, AR-42).

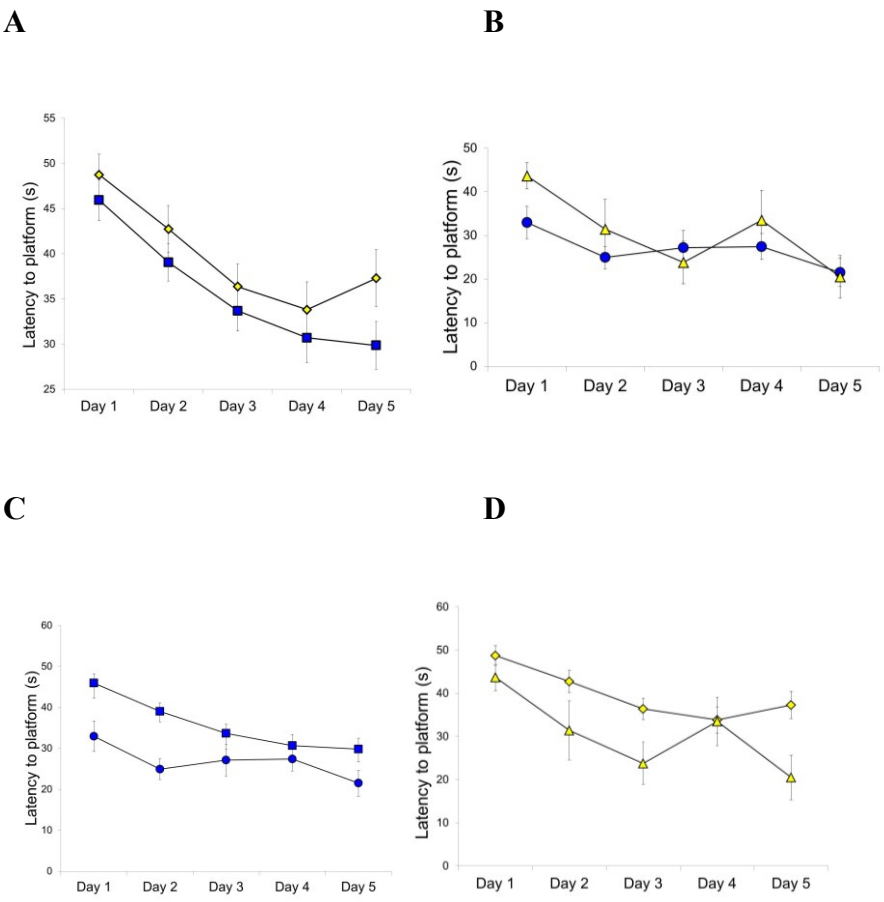

Supplementary figure 2.7: H3K4me3 is decreased in the pyramidal layer in *Kmt2d*$^{+/\beta Geo}$ mice compared to *Kmt2d*$^{+/+}$ littermates. H3K4me3 was also significantly reduced in the pyramidal layer of the hippocampus, another cell layer with strong expression of the KMT2D protein. N = 5 (+/+), 5 (+/βGeo). **P < 0.01.

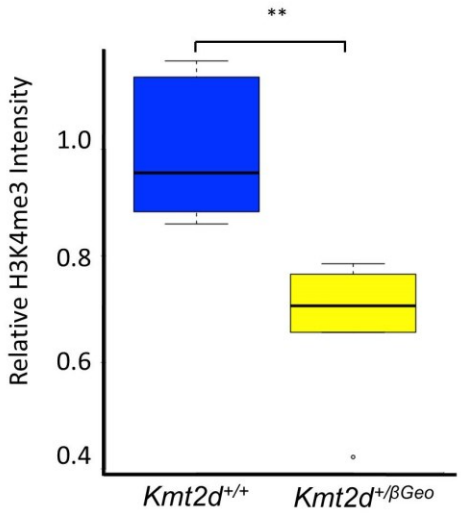

Supplementary figure 2.8: Body and brain size in *Kmt2d*$^{+/\beta Geo}$ mice. While *Kmt2d*$^{+/\beta Geo}$ animals showed a significant reduction in body weight, at 5 months of age when compared to *Kmt2d*$^{+/+}$ littermates **(A)** there was no significant difference in brain weight **(B)**. Body, N = 10 (+/+), 5 (+/βGeo). Brain, N.S., N = 14 (+/+), 12(+/βGeo), *P < 0.05.

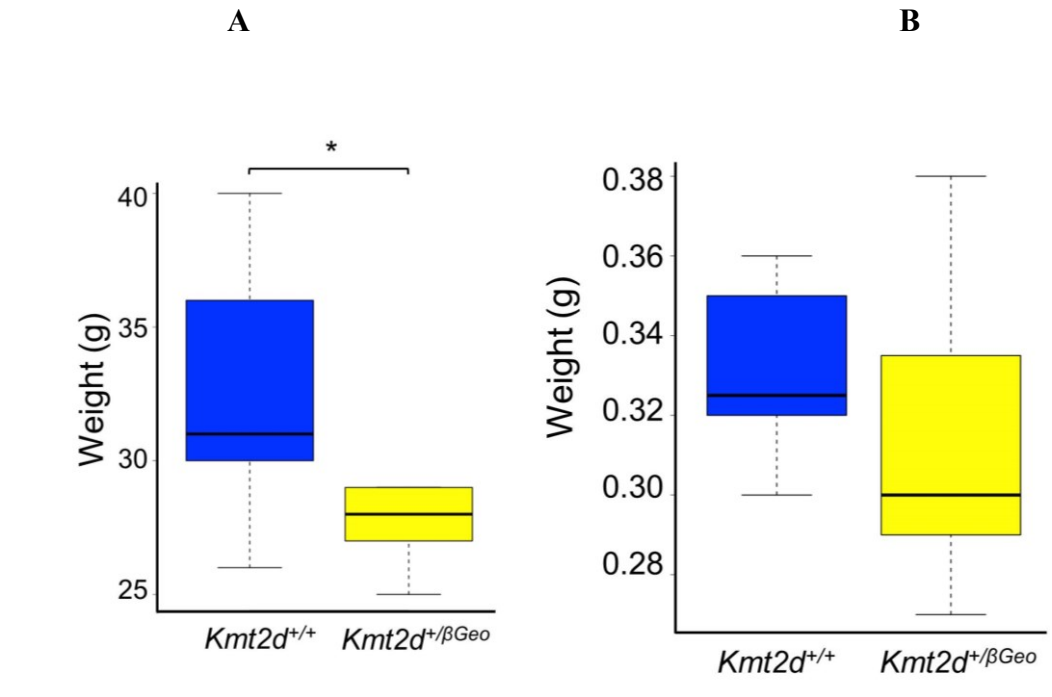

Supplementary figure 2.9: EdU incorporation. *Kmt2d*$^{+/\beta Geo}$ mice showed reduced incorporation of EdU in the granule cell layer 30 days after the onset of injection, suggesting reduced neurogenesis and long-term neuronal survival, when compared to *Kmt2d*$^{+/+}$ littermates, as assessed by observers blinded to genotype. Eleven animals were analyzed, each brain was fully sectioned and every 6th slice was stained for each animal (N= 7 (+/+), 4 (+/βGeo)) **P < 0.01.

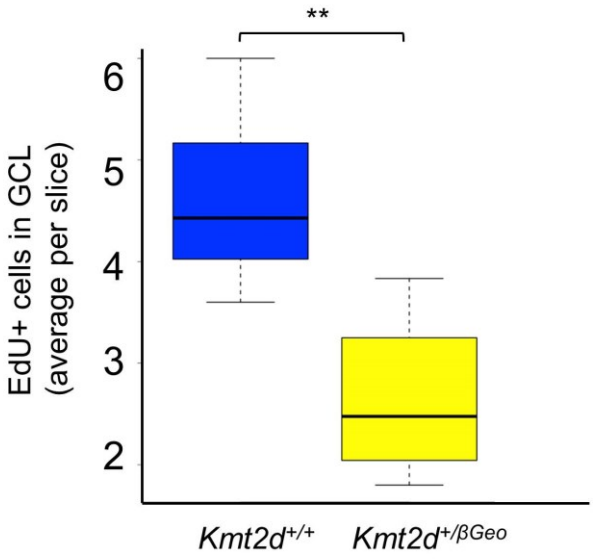

Supplementary figure 2.10: Decreased dendrites in DCX+ cells in the granule cell layer of *Kmt2d*$^{+/\beta Geo}$ mice. Immunofluorescence showed that *Kmt2d*$^{+/\beta Geo}$ animals demonstrate an apparent decrease in dendritic arborization of cells that are DCX+, when compared to *Kmt2d*$^{+/+}$ littermates.

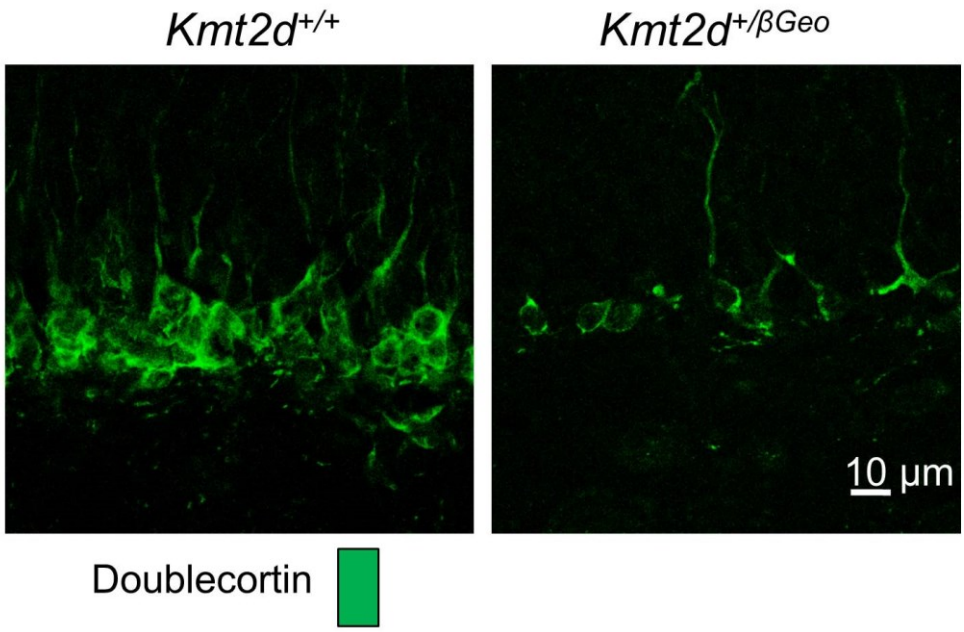

Supplementary figure 2.11: Staining for activated caspase 3 does not reveal increased apoptosis in the granule cell layer of *Kmt2d*$^{+/\beta Geo}$ mice compared to *Kmt2d*$^{+/+}$ littermates. Immunofluorescence staining using an antibody against activated caspase 3 (red) with a DAPI counter-stain (blue) did not reveal an increased number of positive cells (indicating apoptosis) in *Kmt2d*$^{+/\beta Geo}$ animals compared to *Kmt2d*$^{+/+}$ littermates, nor did animals treated with 1 mg/kg/day of AR-42 have increased apoptosis. We also performed immunofluorescence with the same antibody using newborn thymus as a positive control.

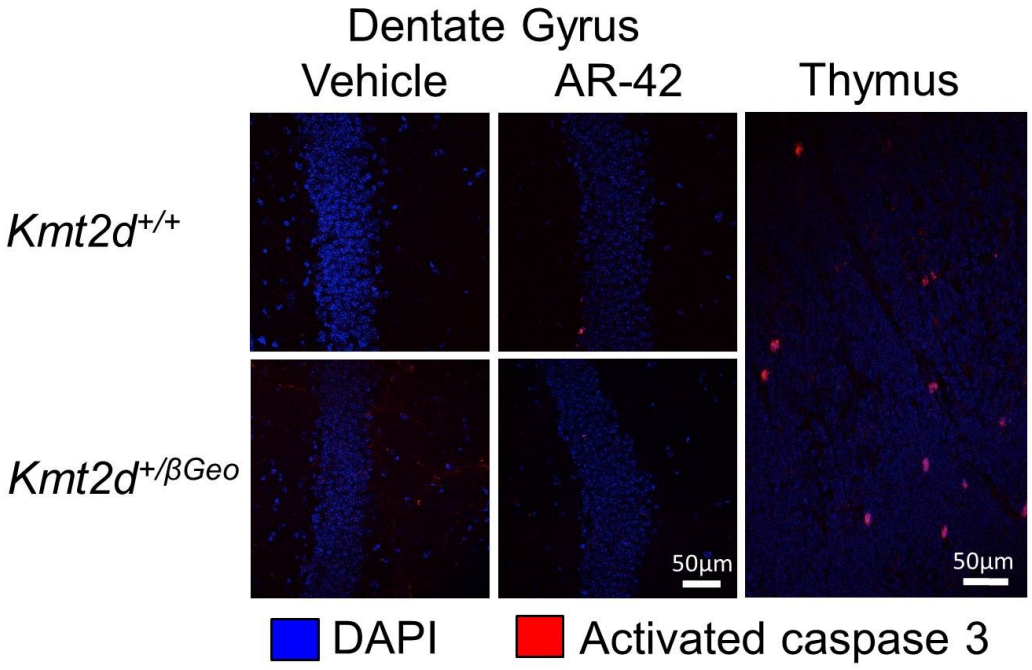

Supplementary figure 2.12: HDAC3 attenuates signal of the H4ac indicator. HEK293 cells stably expressing the H4ac indicator showed increased signal upon stimulation with the histone deacetylase SAHA that was attenuated by recombinant expression of HDAC3. N = 3 biologic replicates for each state, stable transfection. **P < 0.01.

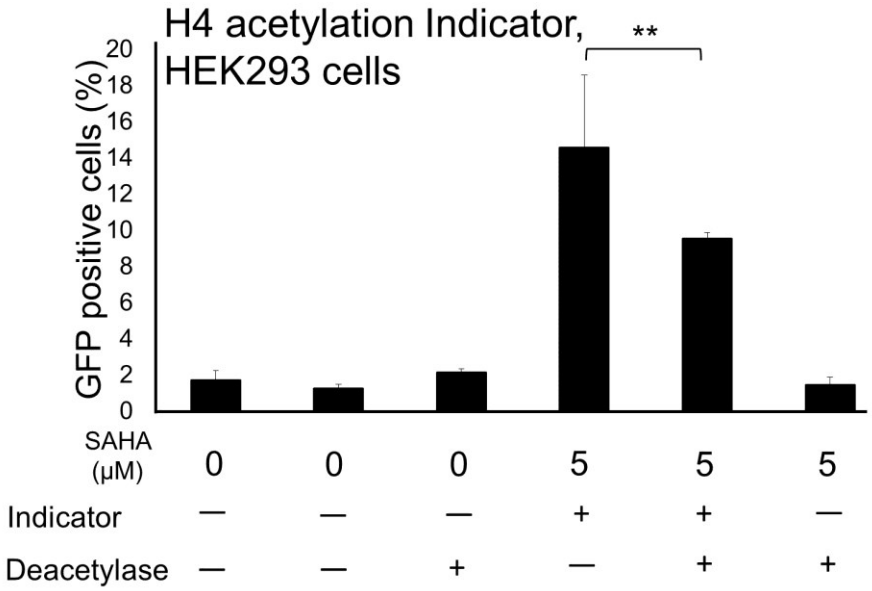

Supplementary figure 2.13: Both indicators demonstrate a deficiency in *Kmt2d*$^{+/\beta Geo}$ mice. Stable expression of the specified indicator into mouse embryonic fibroblasts (MEFs) demonstrated significant deficiencies in both histone H4 acetylation and H3K4 trimethylation activity in *Kmt2d*$^{+/\beta Geo}$ MEFs compared to *Kmt2d*$^{+/+}$ cells, as assessed by the percentage of GFP positive cells. N = 4 (+/+), 3 (+/βGeo). *P < 0.05.

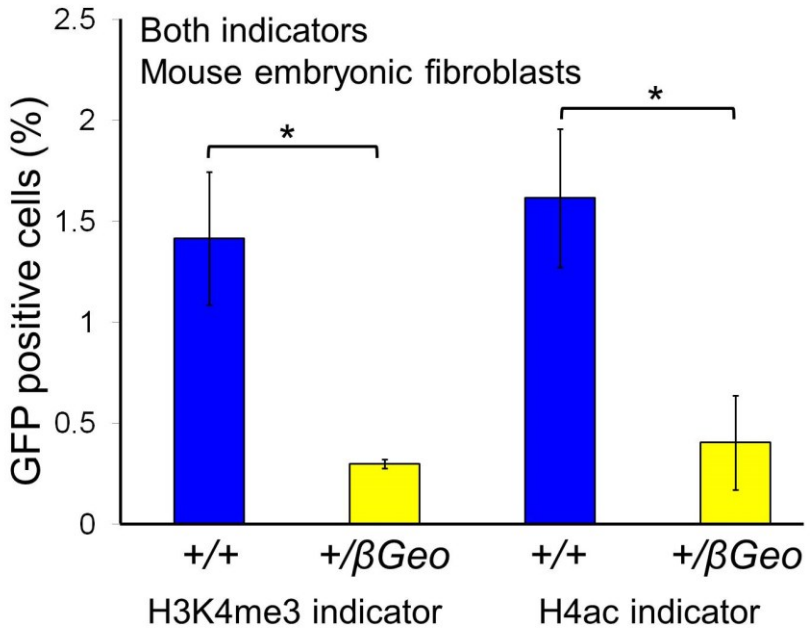

Supplementary figure 2.14: Improved H3K4 trimethylation activity in *Kmt2d*$^{+/\beta Geo}$ cells transiently transfected with H3K4 trimethylation indicator and treated with MS275. *Kmt2d*$^{+/\beta Geo}$ MEFs showed reduced H3K4 trimethylation activity, when compared to *Kmt2d*$^{+/+}$ cells, that was improved upon treatment with the histone deacetylase MS275 (**A**). Transiently transfected cells of both genotypes demonstrated comparable transfection efficiency as estimated by real time PCR when compared to a genomic control (**B**). N = 6 (+/+), 6 (+/βGeo), biological replicates for each concentration, transient transfection. *P < 0.05; **P < 0.01; ††P < 0.001.

A **B**

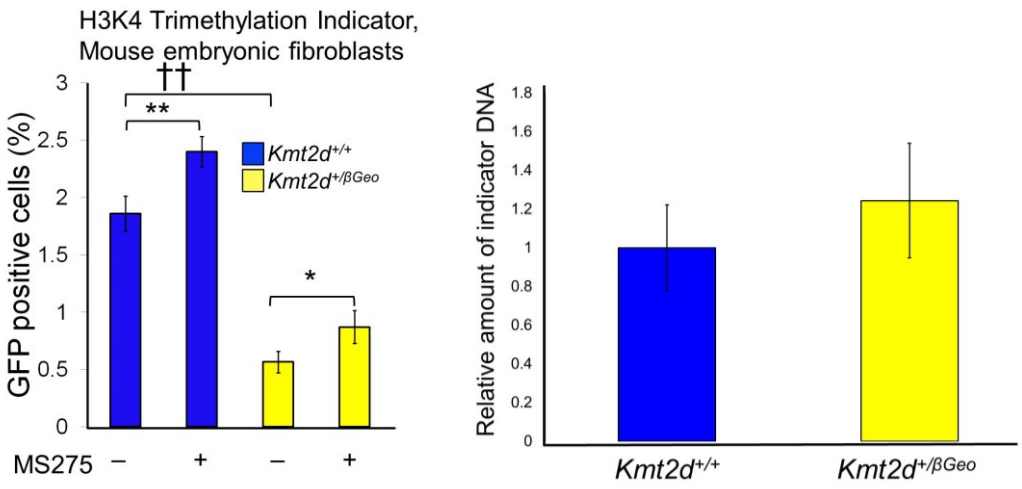

Supplementary figure 2.15: *In vivo* responses to AR-42. (A-B) Immunofluorescence revealed increased H3K4me3 in the granule cell layer of *Kmt2d*$^{+/+}$ and *Kmt2d*$^{+/\beta Geo}$ mice upon treatment with 25 mg/kg/day of AR-42, with no difference between genotypes in the treated groups, N = 4-5 per group. **(C)** 25mg/kg/day of AR-42 did not improve DCX expression in *Kmt2d*$^{+/\beta Geo}$ mice and reduced DCX expression in *Kmt2d*$^{+/+}$ animals, N = 4-6 per group, **(D)** DCX expression was improved in older mice (5-6 months) upon treatment of *Kmt2d*$^{+/\beta Geo}$ mice with 10mg/kg/day of AR-42. N = 3-4 per group. *P < 0.05; **P < 0.01; ††P < 0.001.

A

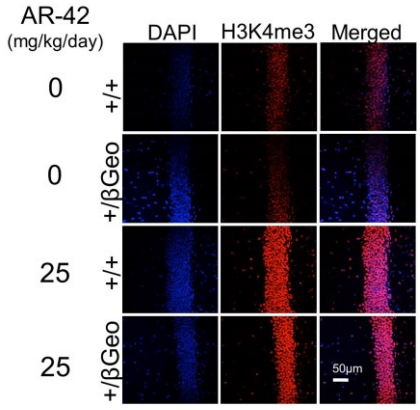

B

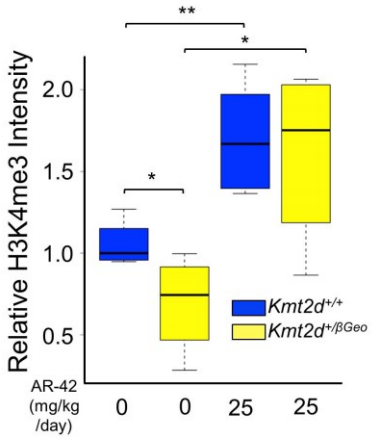

C

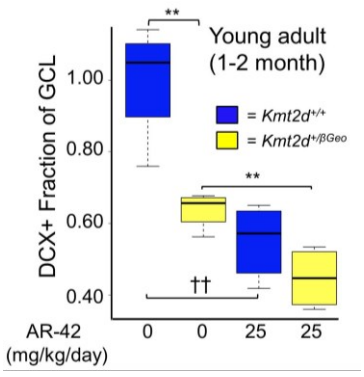

D

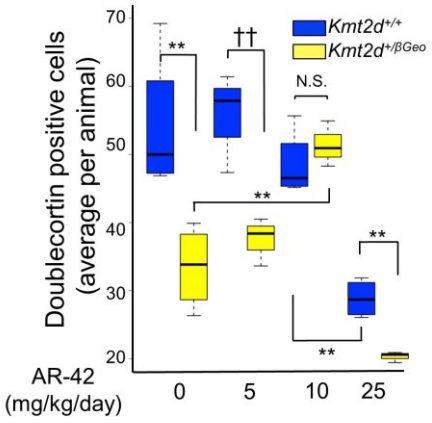

Supplementary figure 2.16: AR-42-induced expression of a known Kmt2d target gene. Klf10, a known target gene of Kmt2d (Guo et al., 2012), demonstrated reduced expression in spleen cells of *Kmt2d*$^{+/\beta Geo}$ mice that was normalized upon treatment with AR-42 N = 4 per group. *P < 0.05, †P < 0.005.

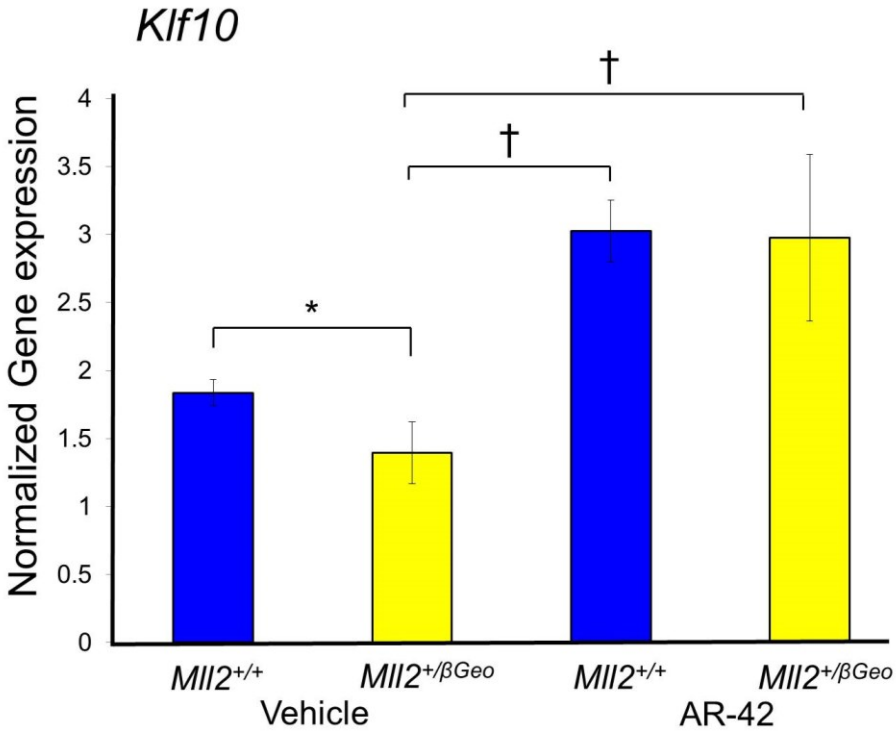

Supplementary figure 2.17: MA plots indicate a shift in the balance of H3K4me3 upon treatment with AR-42. Significant differences in the locus-specific intensity of H3K4me3 are indicated in red, with the directionality and magnitude of each peak height reflecting the difference between the indicated states (genotype and AR-42 treatment status). *Kmt2d*$^{+/\beta Geo}$ animals demonstrated a downward shift compared to *Kmt2d*$^{+/+}$ littermates (**A**), which was recovered with AR-42 (**B**). These data indicate there may be some overcorrection, which could be improved in future studies by using ChIP-seq as a biomarker. The difference between AR-42 treated and vehicle treated *Kmt2d*$^{+/+}$ animals was less notable (**C**), but obvious when comparing *Kmt2d*$^{+/\beta Geo}$ on AR-42 compared to *Kmt2d*$^{+/\beta Geo}$ littermates on vehicle (**D**) or both genotypes on AR-42 (**E**). CPM: counts per million, FC: fold change. N= 2 (+/βGeo, vehicle), 2 (+/+, vehicle), 2 (+/βGeo, AR-42), 2 (+/+, AR-42).

A **B**

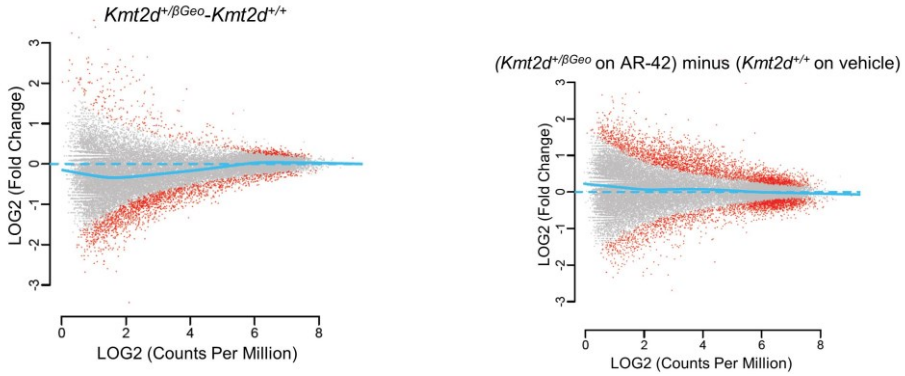

C

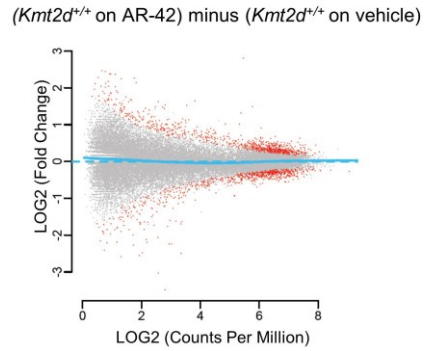
(Kmt2d+/+ on AR-42) minus (Kmt2d+/+ on vehicle)
LOG2 (Fold Change)
LOG2 (Counts Per Million)

D

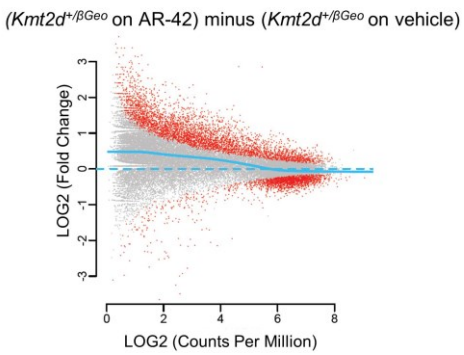
(Kmt2d+/βGeo on AR-42) minus (Kmt2d+/βGeo on vehicle)
LOG2 (Fold Change)
LOG2 (Counts Per Million)

E

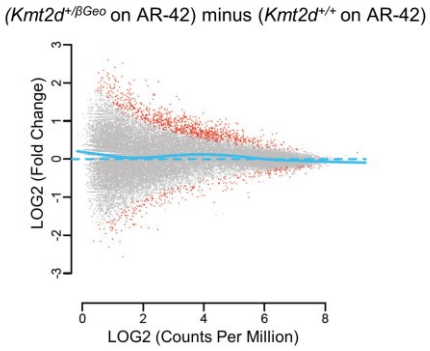
(Kmt2d+/βGeo on AR-42) minus (Kmt2d+/+ on AR-42)
LOG2 (Fold Change)
LOG2 (Counts Per Million)

Supplementary figure 2.18: A visualization of shifts in balance between states (genotype or AR-42) as a function of intensity demonstrates an abnormality in *Kmt2d*$^{+/\beta Geo}$ that is responsive to AR-42. *Kmt2d*$^{+/\beta Geo}$ animals demonstrated a downward shift compared to *Kmt2d*$^{+/+}$ littermates (**A**; -2logQ: 589.5, P < 2.2e-16), which was normalized (but somewhat over corrected) with AR-42 (**B**; -2logQ: 146.0, P < 2.2e-16). The difference between AR-42-treated *Kmt2d*$^{+/+}$ mice and vehicle treated *Kmt2d*$^{+/+}$ littermates was less notable (**C**), but more evident when comparing *Kmt2d*$^{+/\beta Geo}$ on AR-42 to *Kmt2d*$^{+/\beta Geo}$ littermates on vehicle (**D**) or on both genotypes on AR-42 (**E**, -2logQ: 359.9, P < 2.2e-16). N = 2 (+/βGeo, vehicle), 2 (+/+, vehicle), 2 (+/βGeo, AR-42), 2 (+/+, AR-42).

A

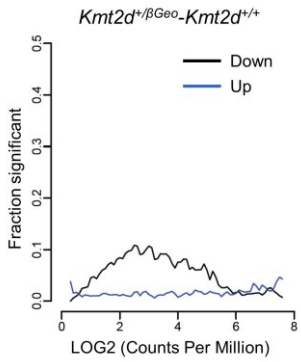
Kmt2d+/βGeo-Kmt2d+/+
Down
Up
Fraction significant
LOG2 (Counts Per Million)

B

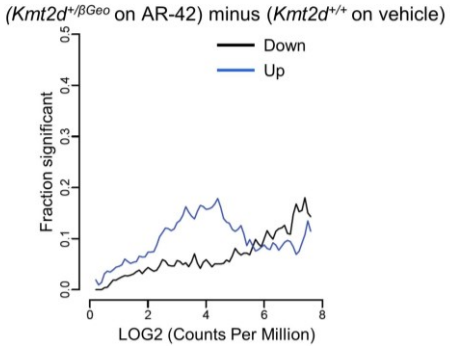
(Kmt2d+/βGeo on AR-42) minus (Kmt2d+/+ on vehicle)
Down
Up
Fraction significant
LOG2 (Counts Per Million)

C

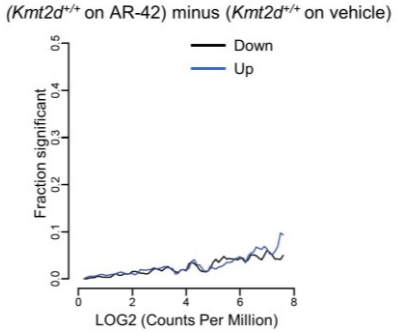
(Kmt2d+/+ on AR-42) minus (Kmt2d+/+ on vehicle)
Down
Up
Fraction significant
LOG2 (Counts Per Million)

D

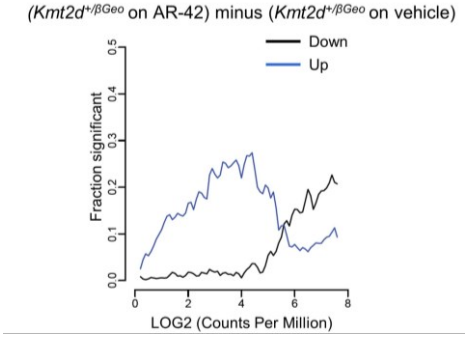
(Kmt2d+/βGeo on AR-42) minus (Kmt2d+/βGeo on vehicle)
Down
Up
Fraction significant
LOG2 (Counts Per Million)

E

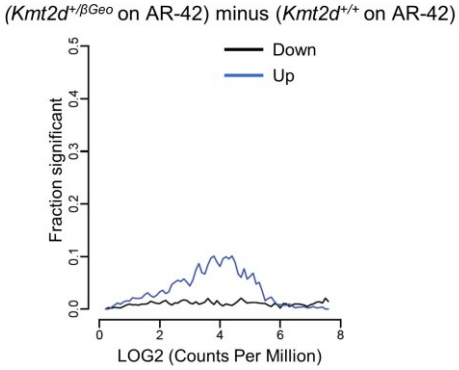
(Kmt2d+/βGeo on AR-42) minus (Kmt2d+/+ on AR-42)
Down
Up
Fraction significant
LOG2 (Counts Per Million)

Supplementary figure 2.19: Serum control experiments for antibodies used for immunofluorescence. Non-specific binding was not observed when we sequentially exposed sections to serum from the same species matching the primary antibody for each experiment (i.e. rabbit for KMT2D and H3K4me3 and goat for doublecortin), followed by the secondary antibody used for KMT2D and H3K4me3 (anti-rabbit) or doublecortin (anti-goat).

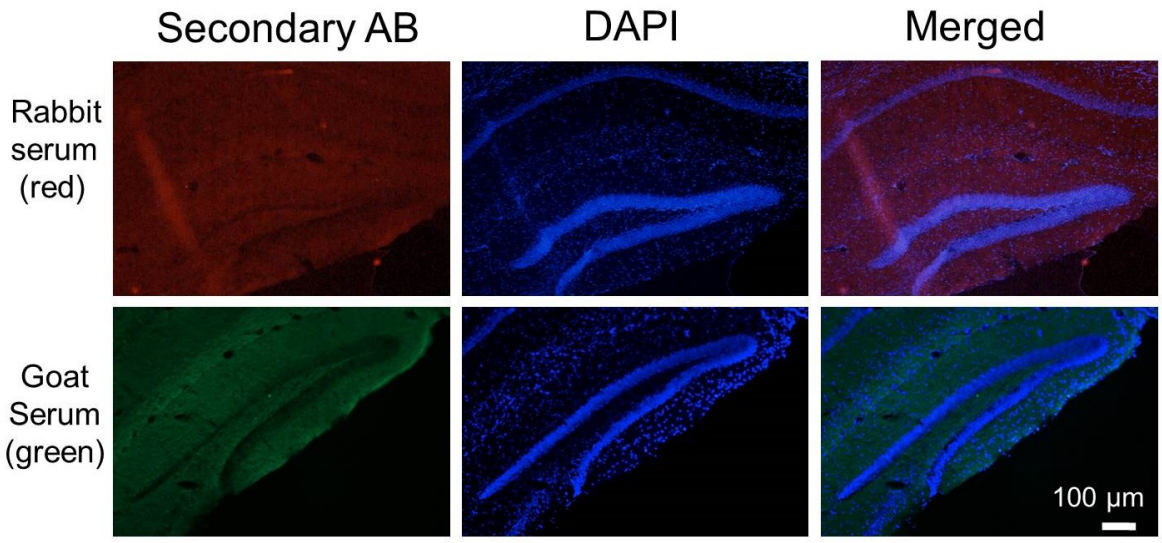

Supplementary table 2.1: A summary of genotypes, drugs and quality measures of ChIP-seq experiments. N Reads = number of reads, alignRate = fraction aligned to genome; FRIP = fraction of reads in peaks.

Genotype	Drug	Run	nReads	alignRate	FRIP
Kmt2d$^{+/\beta Geo}$	AR-42	run4	5690117	0.92	0.508
Kmt2d$^{+/\beta Geo}$	Vehicle	run4	7520215	0.93	0.556
Kmt2d$^{+/+}$	AR-42	run4	9614420	0.92	0.48
Kmt2d$^{+/+}$	Vehicle	run4	6828962	0.92	0.571
Kmt2d$^{+/\beta Geo}$	AR-42	run5	7604137	0.93	0.53
Kmt2d$^{+/\beta Geo}$	Vehicle	run5	6016687	0.92	0.55
Kmt2d$^{+/+}$	AR-42	run5	4846490	0.93	0.545
Kmt2d$^{+/+}$	Vehicle	run5	8682723	0.93	0.573

Chapter 3: Dietary treatment of *Kmt2d*$^{+/\beta Geo}$

Introduction

Kabuki syndrome (KS) is a rare genetic disease with cardinal manifestations including intellectual disability, postnatal growth retardation, immunological dysfunction, and characteristic facial features. Mutations in either *KMT2D* or *KDM6A* are known to lead to KS (Ng et al., 2010; Lederer et al., 2012; Miyake et al., 2013). Interestingly, each of these genes plays an independent role in the process of chromatin opening as KMT2D adds an open chromatin mark (histone 3, lysine 4 trimethylation; H3K4me3) and KDM6A removes a closed chromatin mark (histone 3, lysine 27 trimethylation; H3K27me3). If a deficiency of chromatin opening plays a role in KS pathogenesis, agents that promote open chromatin states, such as histone deacetylase inhibitors (HDACi), could ameliorate ongoing disease processes (Fahrner and Bjornsson, 2014).

Previously, we observed a deficiency of adult neurogenesis, a dynamic process in adult life (Ming et al., 2011), in a mouse model of KS ($Kmt2d^{+/\beta Geo}$), seen in association with hippocampal memory deficits. These deficits normalized following a two-week course with the HDACi AR-42 (Bjornsson et al., 2014), an antineoplastic agent. Recently, beta-hydroxybutyrate (BHB), one of the ketone bodies has been shown to have endogenous HDACi activity (Shimazu et al., 2013). Since BHB is actively transported into the central nervous system during ketosis (Hasselbalch et al., 1995), it could theoretically modulate histone modifications in relevant cells (neurons), and thereby ameliorate the neurological dysfunction previously observed in $Kmt2d^{+/\beta Geo}$ mice.

Here we demonstrate normalization of histone 3 acetylation (H3Ac), H3K4 trimethylation (H3K4me3) and the deficiency of neurogenesis seen in the granule cell layer (GCL) of the dentate gyrus (DG) in association with rescue of the hippocampal

memory defects in *Kmt2d*$^{+/\beta Geo}$ mice after administration of a ketogenic diet (KD) for two weeks. Furthermore, administration of exogenous BHB also rescued the neurogenesis defect in *Kmt2d*$^{+/\beta Geo}$ mice, suggesting that the increase in BHB plays a major role in the observed therapeutic effect of the KD. Our data show that the effects of a debilitating mutation can be offset by modifying the epigenome, thereby serving as proof-of-principle that dietary manipulation may be a viable strategy for selected causes of intellectual disability.

Results

Our previously characterized (Bjornsson et al., 2014) mouse model of Kabuki syndrome (*Kmt2d*$^{+/\beta Geo}$), demonstrates several cardinal features which include hippocampal memory defects (Fig. 3.1A, Sup. Fig. 3.1), a deficiency of adult neurogenesis (Fig. 3.1B, Sup. Fig. 3.1) and growth retardation (Sup. Fig. 3.2), on both mixed and genetically homogenized C57BL/6J backgrounds (>10 generations; Sup. Fig. 3.3).

Given the global deficiency of H3K4me3 seen in the GCL of *Kmt2d*$^{+/\beta Geo}$ mice (Bjornsson et al., 2014), we have hypothesized that the pathogenesis of KS relates to an inability to open chromatin and consequently express critical disease-relevant target genes (Fahrner and Bjornsson, 2014). In support of this hypothesis, we now describe that 17 genes show significantly (>1 $\log_2$ fold change; <0.05 adjusted p-value) decreased expression in *Kmt2d*$^{+/\beta Geo}$ mice compared to *Kmt2d*$^{+/+}$ littermates, as measured by gene expression microarray (Fig. 3.1C, Sup. Tab. 3.1). In contrast, no genes showed significantly increased expression in *Kmt2d*$^{+/\beta Geo}$ mice compared to *Kmt2d*$^{+/+}$ littermates (Fig. 3.1C). Additionally, pathway analysis of the entire filtered dataset showed

downregulation of several pathways relevant to the phenotype observed in *Kmt2d*$^{+/\beta Geo}$ mice (Sup. Tab. 3.2).

Based on the reported histone deacetylase inhibitory activity of BHB (Shimazu et al., 2013), we hypothesized that BHB could be used for therapeutic purposes. To independently confirm the HDACi activity of BHB (Shimazu et al., 2013), we used a previously described (Bjornsson et al., 2014) *in vitro* epigenetic reporter allele assay to quantify the enzymatic activity of the H3K4me3 and H4Ac machinery, and observed a dose-dependent increase of both reporter with increasing amounts of BHB (Fig. 3.1D). In an effort to increase BHB levels *in vivo,* we placed *Kmt2d*$^{+/\beta Geo}$ and *Kmt2d*$^{+/+}$ mice on a KD using a regimen frequently used in humans (4:1 fat to protein; Freeman et al., 1998). We observed a significant increase of urine BHB from KD-treated mice compared to regular diet-treated counterparts (Fig. 3.1E). KD-treated *Kmt2d*$^{+/\beta Geo}$ mice also showed an increased BHB/AcAc ratio, indicating a disproportionally increased BHB (Sup. Fig. 3.4) when compared to *Kmt2d*$^{+/+}$ littermates. Further studies indicated that this metabolic defect is likely based on an altered NADH/NAD^{+} ratio in the *Kmt2d*$^{+/\beta Geo}$ mice (Sup. Fig. 3.5). Interestingly, these effects are not observed in a mouse model of Rubinstein-Taybi syndrome (*Crebbp*$^{+/-}$; Kung et al., 2000; Sup. Fig. 3.6), another genetically imposed deficiency of open chromatin marks (Alarcon et al., 2004), suggesting that this finding is not secondary to the global loss of open chromatin modifications (Kurdistani et al., 2014, Castonguay et al., 2014).

After administration of a KD to *Kmt2d*$^{+/\beta Geo}$ and *Kmt2d*$^{+/+}$ mice for two weeks, we saw an increase in levels of H3K4me3 and H3Ac in the GCL of the DG in *Kmt2d*$^{+/\beta Geo}$ mice (Fig. 3.2A-B). Overall, the KD did not lead to global gene expression changes in

Kmt2d$^{+/\beta Geo}$ mice, and none of the 17 previously defined candidates (Fig. 3.1C*;* Sup. Tab. 3.1) showed significant normalization (Sup. Fig. 3.7A, orange dots). However, we suspected that critical target genes could have been missed given the small sample size and stringent p-value based criteria. As a complementary approach, we ranked genes from the microarray based on fold change differences between *Kmt2d*$^{+/\beta Geo}$ mice on the KD compared to a standard diet (Sup. Fig. 3.7B, right edge of line). Among the top 50 genes, we picked the five genes (10%) that showed the most dramatic rescue on the KD. Three of these genes demonstrated significantly less expression (RT-qPCR) in the hippocampus of *Kmt2d*$^{+/\beta Geo}$ compared to *Kmt2d*$^{+/+}$ mice on a standard diet which significantly normalized in the *Kmt2d*$^{+/\beta Geo}$ mice on a KD (Sup. Fig. 3.7C-D).

The impact of the KD on neurogenesis was assessed by two independent markers; quantification of either EdU^{+} or doublecortin-positive (DCX^{+}) cells in the GCL of the DG. We first counted the number of EdU^{+} cell in the GCL both immediately after a course of EdU injections (proliferation) or 30 days later (survival); both measures showed significant increase in numbers in *Kmt2d*$^{+/\beta Geo}$ mice on a KD compared to *Kmt2d*$^{+/\beta Geo}$ mice on a regular diet (Fig. 3.2C). We next quantified the DCX^{+} fraction of the GCL and found a significant increase in *Kmt2d*$^{+/\beta Geo}$ mice on a KD compared to mice on a standard diet, with no significant difference when compared to KD-treated *Kmt2d*$^{+/+}$ littermates (Fig. 3.2D).

Following a two-week treatment with the KD, *Kmt2d*$^{+/\beta Geo}$ mice showed a significant increase in the number of platform zone crossings (Fig. 3.2E) during the probe trial of a Morris water maze (MWM), a measure previously shown to be particularly sensitive for detecting a disruption of adult neurogenesis (Garthe et al., 2013).

Kmt2d$^{+/\beta Geo}$ mice also showed decreased escape latency during the hidden platform testing, with no significant differences when compared to KD-treated *Kmt2d*$^{+/+}$ controls, along with no significant differences during the visible flag testing (Sup. Fig. 3.8). Additional control tests for strength, activity and anxiety-like behaviors (grip strength and open field testing) were unaffected by genotype (Sup. Fig. 3.9).

Finally, we asked whether exogenous administration of BHB was sufficient to rescue the neurogenesis defect in *Kmt2d*$^{+/\beta Geo}$ mice. Once daily intraperitoneal (IP) injection of 10 mM/kg/day of BHB led to peak urine levels of BHB comparable to levels seen in animals on the KD (Sup. Fig. 3.10), and led to a significant increase in EdU^{+} cells in the GCL of the DG (Fig. 3.3A) although not to the same extent as the KD (Fig. 3.2C). Given the short half-life of BHB (1-2 hours; Clarke et al., 2012), the overall daily exposure to BHB after a single injection was much less than with the KD (Fig. 3.3B). Consequently, we employed a combination strategy of a mini osmotic pump (Sup. Fig. 3.11) and three daily IP injections (10 mM/kg BHB) that was able to achieve BHB levels comparable to the KD (Fig. 3.3C). This combination strategy led to a significant increase in neurogenesis, as measured by the number of EdU^{+} cells in the GCL of the DG, in *Kmt2d*$^{+/\beta Geo}$ compared to vehicle-treated *Kmt2d*$^{+/\beta Geo}$ mice (Fig. 3.3D), that closely mirrored the neurogenesis rescue seen after treatment with a KD (Fig. 3.2C).

Discussion

Although BHB has previously been shown to demonstrate HDACi activity (Shimazu et al., 2013; Lim et al., 2011), any clinical relevance remained speculative. Here, we show that therapeutically relevant levels of BHB are achieved with a KD

modeled upon protocols that are used and sustainable in humans (Wheless, 2008; Gasior et al., 2006). Furthermore, we demonstrate for the first time a therapeutic rescue of a genetic disorder by taking advantage of the HDACi activity of BHB. This work serves as a proof-of-principle that dietary manipulation may be a viable strategy for Kabuki syndrome, and suggests that BHB may underlie the mechanism of action of the previously observed therapeutic benefits of the KD.

While we cannot exclude a contribution from other biochemical actions of BHB such as direct butyrylation of the histone tail (Chen et al., 2007), our data provide strong, albeit correlative, evidence that the therapeutic effect of the KD relates to BHB-mediated modulation of epigenetic marks. The global epigenetic abnormalities seen in *Kmt2d*$^{+/\beta Geo}$ mice occur in association with altered expression of genes important to neuronal function including genes that participate in CREB signaling in neurons, synaptic long-term potentiation, and glutamate signaling. Furthermore, some genes show rescue with the KD, making BHB-induced normalization of gene expression a plausible mechanism for the observed therapeutic effect even though the specific disease relevant disease genes are unknown at this time.

Our findings that exogenous BHB treatment lead to similar effects on neurogenesis as the KD support the hypothesis that it is the BHB that mediates the therapeutic effect. In our previous study, AR-42 led to improved performance in the probe trial of the Morris water maze for both *Kmt2d*$^{+/\beta Geo}$ and *Kmt2d*$^{+/+}$ mice (Bjornsson et al., 2014***;*** genotype independent improvement), however here we report that KD administration only led to improvement for *Kmt2d*$^{+/\beta Geo}$ mice (genotype dependent improvement). This discrepancy may relate to the fact that AR-42 acts as an HDACi but

also affects expression levels of histone demethylases (Huang et al., 2011), resulting in increased potency but less specificity. Alternatively, the physiological levels of BHB might be unable to reach levels that would lead to such genotype independent effects.

Our work also uncovered a metabolic phenotype in *Kmt2d*$^{+/\beta Geo}$ mice which lead to increased BHB/acetoacetate and lactate/pyruvate ratios during ketosis; an increased NADH/NAD$^+$ ratio could explain both observations. This increased NADH/NAD$^+$ ratio may relate to a previously described propensity of *Kmt2d*$^{+/\beta Geo}$ mice towards biochemical processes predicted to produce more NADH, including glycolysis, and a resistance to high fat diet induced obesity (Kim et al., 2015). If this exaggerated BHB elevation holds true in patients with KS, this may make the KD a particularly effective treatment strategy for this patient population. Alterations of the NADH/NAD$^+$ ratio could also impact chromatin structure through action of the sirtuins, a class of histone deacetylases (HDACs) that are known to be NAD$^+$ dependent (Cohen et al., 2004).

In summary, our work suggests that a particular dietary regimen (in this case a KD) may be useful for a particular genotype (haploinsufficiency of *KMT2D*). Advocates of personalized medicine have predicted such targeted dietary interventions, although currently there are few robust examples (Elliot et al., 2002; Ordovas et al., 2004; García-Canas et al., 2010). Our data suggest that the ketogenic diet may prove to be an effective therapeutic approach for Kabuki syndrome.

Materials and methods

Animals and treatment

Our mouse model, *Kmt2d*$^{+/\beta Geo}$, also known as (*Mll2Gt*$^{(RRt024)Byg}$) was generated by BayGenomics (San Francisco, CA, USA) through the insertion of a gene trap vector. The KD (4:1 ratio, F6689 Rodent Diet, Ketogenic, Fat: Paste) was acquired from Bio-Serv (Flemington, NJ, USA). Mice were given 2 weeks *ad libitum* access to KD paste, with the paste replaced several times per week. During MWM testing, given the length of testing (more than a week), we treated for three weeks. *Crebbp*$^{+/-}$, also known as *Crebbp*^{tm1Dli} (Kung et al., 2000), were acquired from the Jackson laboratories (Bar Harbor, ME, USA). All mice used in these studies were between 1-2 months of age unless otherwise noted. All experiments were performed on mice fully backcrossed to C57BL/6J background unless otherwise noted.

BHB injection and assay

Either 10mM/kg of (R)-(-)-3-Hydroxybutyric acid sodium salt (Santa Cruz Biotechnology, Dallas, TX, USA) or saline was injected (100µl) intraperitoneally once or three times a day. Urine BHB was quantified by the β-Hydroxybutyrate (Ketone Body) Colorimetric Assay Kit (Cayman Chemical Company, Ann Arbor, MI, USA). Urine from injected mice was collected approximately 1.5-2 hours after injection and urine from mice on a KD was taken in the early afternoon unless otherwise stated in the text.

Osmotic pumps

An Alzet (Durect co., Cupertino, CA, USA) micro-osmotic pump (model 1002) made to allow for 14 days of diffusion was filled (84 µl reservoir) with either 2.5mg/ml (R)-(-)-3-

Hydroxybutyric acid sodium salt (Santa Cruz Biotechnology) in saline vehicle or saline vehicle alone. Animals were anesthetized, after which a small incision was made on the skin of the lower back and pump was placed directly under the skin.

Reporter alleles

HEK 293 cells were transfected with lipofectamine LTX (Thermo Fisher, Waltham, MA, USA) with either our H3K4me3 or H4ac reporter alleles that have been previously described (Bjornsson et al., 2014). Stable transfections were induced and maintained with positive selection with blasticidin at a dose of 10mg/ml (Life Technologies, Life Technologies, Carlsbad, CA, USA). Blasticidin selection was stopped 24 hours prior to exposure to BHB. For BHB treatment, (R)-(-)-3-Hydroxybutyric acid sodium salt (Santa Cruz Biotechnology) was added to the medium 24 hours before FACSVerse flow sorting (BD Sciences, San Jose, CA, USA). Data were analyzed using FlowJo (Tree Star Inc., Ashland, OR, USA).

Serum lactate and pyruvate analysis

Serum was extracted from whole blood by centrifugation at 3500g for 10 minutes. Subsequently, the supernatant was removed and stored at -20 degrees C. Serum samples were then assayed for levels of lactate and pyruvate with the Lactate Assay Kit (Sigma Aldrich, Saint Louis, MO, USA) and Pyruvate Assay Kit (Sigma Aldrich).

Mass spectrometry for acetoacetate and beta-hydroxybutyrate

Acetoacetate and beta-hydroxybutyrate were prepared via acid extraction and BSTFA (N,O-bis(trimethylsilyl)trifluoroacetamide) derivatization, and detected via gas chromatography-mass spectrometry. The mass spectrometer was set in SCAN mode to detect all mass fragments in a range of m/z 50-600. Compounds were identified based on their characteristic retention time and ion peaks. Results were reported as a ratio of acetoacetate to beta-hydroxybutyrate.

Microarray experiment

Hippocampi were dissected from three wild type and three *Kmt2d*$^{+/\beta Geo}$ mice on a standard diet, as well as four *Kmt2d*$^{+/\beta Geo}$ mice on the KD. RNA was extracted from whole hippocampi using the Qiagen RNeasy kit or TRIzol reagents (Ambion Life Technologies, Carlsbad, CA) followed with DNase I treatment (Qiagen, Valencia, CA, USA). For microarray cDNA was synthesized by the JHMI High Throughput Biology Center and hybridized to Affymetrix (Santa Clara, CA, USA) Mouse Gene 1.0 microarrays.

RT-qPCR validation

For RT-qPCR validation cDNA was synthesized using the Applied Biosciences High Capacity cDNA Reverse Transcription Kit (Applied Biosciences, Foster City, CA).

RT-qPCR was done on RNA from the same mice used for microarray but also an additional second cohort treated in an identical fashion with the KD (N=5-7). The Taqman (Life Technologies) probes used were (*Pld5*, Mm00620912_m1, Fam, S; *Atp2b4* Mm01285597_m1, Fam, S; *Glp1r*, Mm00445292_m1, Fam, S; *Tmsf14*,

Mm00447009_m1, Fam, S; *Nts* Mm00481140_m1 Fam, S), with control probes (*Pgk1,* Mm00435617_m1, Vic, S and *Gapdh*, Mm00445292_m1 Vic, S). All assays were multiplexed except *Nts*, as multiplexing was unsuccessful for this assay. The two experimental groups were run and normalized to untreated wildtype and then combined for analysis.

Analysis of microarray data

The data were normalized using the gene expression barcode method (Zilliox et al., 2007; McCall et al., 2011; McCall et al., 2014) as implemented in the fRMA package (McCall et al., 2012). The array was normalized using frozen RMA and probe sets, which were declared present in more than two arrays, were kept leaving 5,614 probe sets. Additional data handling was performed using the oligo package (Carvalho et al., 2010) from Bioconductor (Gentleman et al., 2004; Huber et al., 2015). Normalized data was analyzed using the empirical Bayes methods (Smyth, 2004) implemented in the limma package (Richie et al., 2015). P-values were adjusted for multiple testing and genes were declared significantly differentially expressed if they had an adjust p-value less than 5% and an absolute $\log_2$(fold change) greater than 1. The 5,641 probe sets were uploaded to QIAGEN's Ingenuity Pathway Analysis (IPA, QIAGEN Redwood City, CA USA) for further pathway and functional analysis. Of these, 4,559 probe sets were recognized in the IPA software knowledgebase and four IPA analyses were performed: Canonical Pathways, Upstream Analysis, Disease & Function, and Networks. These analyses were completed for the comparison of $Kmt2d^{+/\beta Geo}$ and $Kmt2d^{+/+}$ mice on a standard diet.

Perfusion, sectioning and staining

Perfusion, cryosectioning and immunofluorescence staining were performed as previously described (Bjornsson et al., 2014). EdU (Life Technologies) in PBS/6%DMSO (10mg/ml) injections (50μg/g/day), was delivered either for seven consecutive days followed by immediate perfusion (proliferation) or seven consecutive days of injection and then perfusion on the 30th day after the first injection (survival). For staining, every sixth brain section was used, and blocking was done with 5% BSA. EdU was labeled with Click-iT EdU Alexa Fluor 488 Imaging Kit (Thermo Fisher) as well as DAPI mounting with Vectamount (Vector Laboratories, Burlingame, CA, USA). EdU quantification was done blinded to genotype and treatment. Labeled cells were counted in every sixth slice in the GCL of the DG and average number per slice was calculated for each brain. Immunofluorescence was performed with the following primary antibodies: Doublecortin (Santa Cruz Biotechnology, 1:200 goat), trimethylated H3K4 (Cell Signaling, 1:500 rabbit), acetylated H3K9 and H3K14 (1:5000) (Cell Signaling, Danvers, MA, USA). Incubations were done overnight at 4 degrees C in blocking buffer. Previous experiments done on normal serum from which the antibodies were derived showed no non-specific immuno-reactivity (Bjornsson et al., 2014*)*.

Confocal microscopy

Z-stack images were taken at either 10x using Zeiss Axiovert 200 (Carl Zeiss) or 25x using Zeiss AxioExaminer multiphoton (Carl Zeiss) with genotypes and treatment blinded to the researcher. Fluorescence intensity of the highlighted GCL layer at the midpoint of the z-stack was measured at 10x magnification using the Zen software (Carl

Zeiss, Jena, Germany). Fluorescence intensity of either the H3K4me3 or H3Ac antibody was divided by the DAPI fluorescence intensity to normalize for cell numbers. For ease of interpretation, values were normalized to *Kmt2d*$^{+/+}$ levels. Group comparisons were done using a Student's t-test, with significance set at $p<0.05$.

Doublecortin area measurement

The doublecortin (DCX) positive fraction of the GCL was measured by taking 4x pictures and using the Bezier tool on NS elements 2.0 software (Nikon, Melville, NY, USA) to measure the area of DCX^{+} cells that expressed DCX as well as the entire granule cell layer with researcher blinded to mouse genotype and treatment. The fraction of the GCL that showed DCX^{+} cells was then calculated, and group differences were analyzed using a Student's t-test with significance value set at $p<0.05$.

Behavior testing

Behavioral testing was conducted on mice between 1-2 months of age, and performed and analyzed blinded to genotype and treatment, with all experiments performed in the late morning or early afternoon. Each particular behavioral test was performed at a consistent time of day. For open field testing, *Kmt2d*$^{+/+}$ and *Kmt2d*$^{+/\beta Geo}$ mice were placed individually in an open field chamber (San Diego Instruments, San Diego, CA, USA) for ten 180 second intervals. These intervals were combined to give an average activity level, and treatment and genotype groups were compared using a Student's t-test with significance value set at $p<0.05$. For grip strength, mice were allowed to grab onto the grip strength meter (Columbus Instruments, Columbus, OH, USA), and were lightly

pulled by the tail with increasing force until they released their grip. This was repeated 5 times for each mouse with the highest and lowest value being discarded. Remaining three values were then averaged. Average grip strength for treatment and genotype groups were compared with a Student's t-test with significance value set at $p<0.05$. For the Morris water maze, all testing was performed in a standard 1.1 meter diameter tank filled with room temperature water stained with white tempera paint (Crayola, Forks Township, PA, USA). The tank had a small platform submerged 2 cm below the water level in the middle of one of the four tank quadrants. For the first three days the platform had a visible flag on top (Flag training), and each mouse was placed in the tank for four consecutive 60s trials in which they were trained to reach the visible platform. During each trial the platform was moved to a different quadrant, but the mouse was always entered into the tank in the same location. Latency for each trial for each mouse was recorded, and if the mouse could not reach the platform in 60s they were placed there. Following flag training, the visible flag was removed and for five days mice were trained to reach the now hidden platform (Hidden platform training), with four consecutive trials per mouse per day, with a maximum allotment of 60s per trial. The platform was never moved, but each trial the mouse was entered into a different quadrant, with the order of these quadrants randomized for each day. On the final day (Probe trial) the platform was removed and mice were allowed to swim for 90s and the number of crossings over the previous location of the platform was measured. For training and probe tests, data were recorded both manually and electronically, with ANY-maze software (San Diego Instruments). The four genotype and treatment groups were analyzed for differences

using a Student's t-test during the probe trial and with repeated measures ANOVA within subjects test for the latencies.

Figure 3.1: The potential use of the KD to treat markers of disease in a mouse model of Kabuki syndrome (*Kmt2d*$^{+/\beta Geo}$ mice). (**A**) Fully backcrossed (C57BL/6J) *Kmt2d*$^{+/\beta Geo}$ mice demonstrate a significant decrease ($p<0.005$) in platform zone crosses during MWM probe trial compared to *Kmt2d*$^{+/+}$ littermates (N=23-27 per group) similar to what was previously seen on a mixed background. (**B**) Fully backcrossed (C57BL/6J) *Kmt2d*$^{+/\beta Geo}$ mice demonstrate significantly fewer ($p<0.005$) EdU^{+} cells in the GCL of the DG compared to *Kmt2d*$^{+/+}$ littermates (N=4-7 per group) similar to what was previously observed a mixed background. (**C**) Gene expression microarray from the hippocampus reveals 17 genes that show significantly (>1 $\log_2$ fold change; >0.05 adjusted p value) decreased expression in *Kmt2d*$^{+/\beta Geo}$ mice compared to *Kmt2d*$^{+/+}$ littermates (N=3-4 per group). (**D**) Stably transfected HEK293T cells with either an H4Ac or an H3K4me3 reporter allele both show a dose dependent increase in fluorescence with increasing amounts of BHB in culture media (N=5-7 replicates per condition). (**E**) Mice treated with a KD for two weeks show a significant ($p<0.001$) increase of urine BHB compared to standard diet treated controls (N=12-17 per group). *P <0.05; **P <0.0.01; †P <0.005; ††P <0.001.

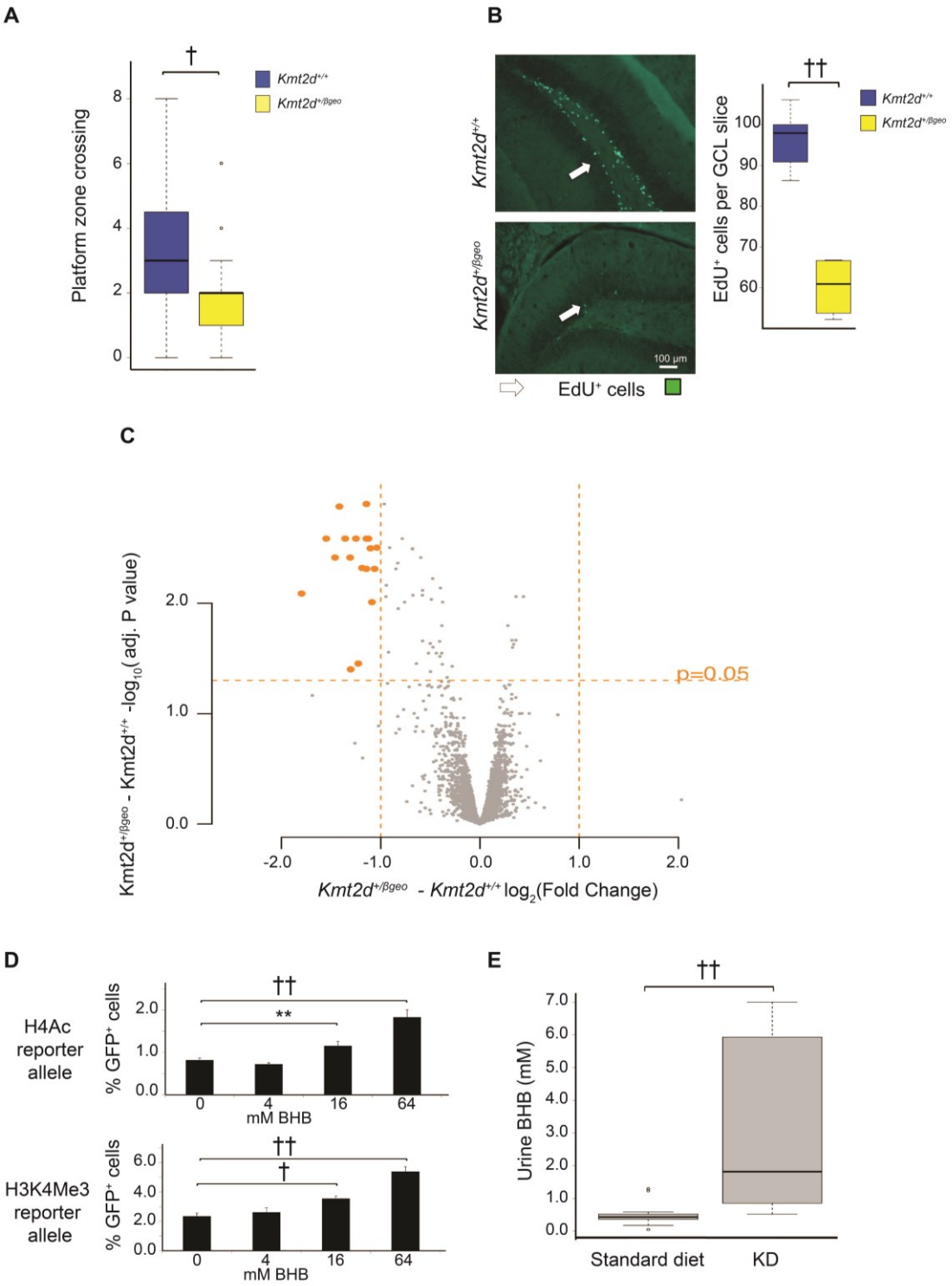
A
†
Kmt2d+/+
Kmt2d+/βgeo
Platform zone crossing
0
2
4
6
8
B
Kmt2d+/+
Kmt2d+/βgeo
100 μm
EdU+ cells
††
EdU+ cells per GCL slice
60
70
80
90
100
C
p=0.05
Kmt2d+/βgeo - Kmt2d+/+ -log10(adj. P value)
0.0
1.0
2.0
-2.0
-1.0
0.0
1.0
2.0
Kmt2d+/βgeo - Kmt2d+/+ log2(Fold Change)
D
H4Ac reporter allele
% GFP+ cells
††
**
0.0
1.0
2.0
0
4
16
64
mM BHB
H3K4Me3 reporter allele
% GFP+ cells
††
†
0.0
2.0
4.0
6.0
0
4
16
64
mM BHB
E
††
Urine BHB (mM)
0.0
1.0
2.0
3.0
4.0
5.0
6.0
7.0
Standard diet
KD

Figure 3.2: *In vivo* responses of either genotype to the KD. (**A**) *Kmt2d*$^{+/\beta Geo}$ mice demonstrate a significantly ($p<0.005$) decreased H3K4me3/DAPI fluorescence ratio in the GCL of the DG compared to *Kmt2d*$^{+/+}$ littermates on a standard diet. Upon two weeks of a KD, there is a significant ($P <0.05$) increase in the H3K4me3/DAPI fluorescence in *Kmt2d*$^{+/\beta Geo}$ mice and no significant difference ($P =0.09$) between the two genotypes (N=10-12 per group). (**B**) *Kmt2d*$^{+/\beta Geo}$ mice show a significant decrease ($P <0.005$) in the H3Ac/DAPI fluorescence ratio compared to *Kmt2d*$^{+/+}$ littermates, this ratio significantly increased ($P <0.05$) in *Kmt2d*$^{+/\beta Geo}$ mice after two weeks of a KD (N=11-14 per group). (**C**) *Kmt2d*$^{+/\beta Geo}$ mice demonstrate significantly fewer EdU^{+} cells in the GCL of the DG both immediately after 7 days of EdU injection (proliferation, $P <0.001$) or 30 days after start of EdU injection (survival, $P <0.001$). Both measures increase significantly ($P <0.001$; $P <0.05$) in *Kmt2d*$^{+/\beta Geo}$ mice on a KD for two weeks (N=5-9, proliferation; N=8-15, survival). (**D**) *Kmt2d*$^{+/\beta Geo}$ mice on a standard diet demonstrate a significantly smaller DCX^{+} cell population in the GCL of the DG ($P <0.001$), compared to *Kmt2d*$^{+/+}$ littermates. This ratio significantly increases ($P <0.01$) in *Kmt2d*$^{+/\beta Geo}$ mice following two weeks of a KD (N=7-12 per group). (**E**) The number of platform crossings during the probe trial portion of the MWM increased significantly ($p<0.05$) in *Kmt2d*$^{+/\beta Geo}$ mice on KD compared to a standard diet. When compared to KD-treated *Kmt2d*$^{+/+}$ mice, KD-treated *Kmt2d*$^{+/\beta Geo}$ mice showed no significant difference in platform crossings ($P =0.239$; N=19-32 per group). *$P <0.05$; **$P <0.0.01$; †$P <0.005$; ††$P <0.001$.

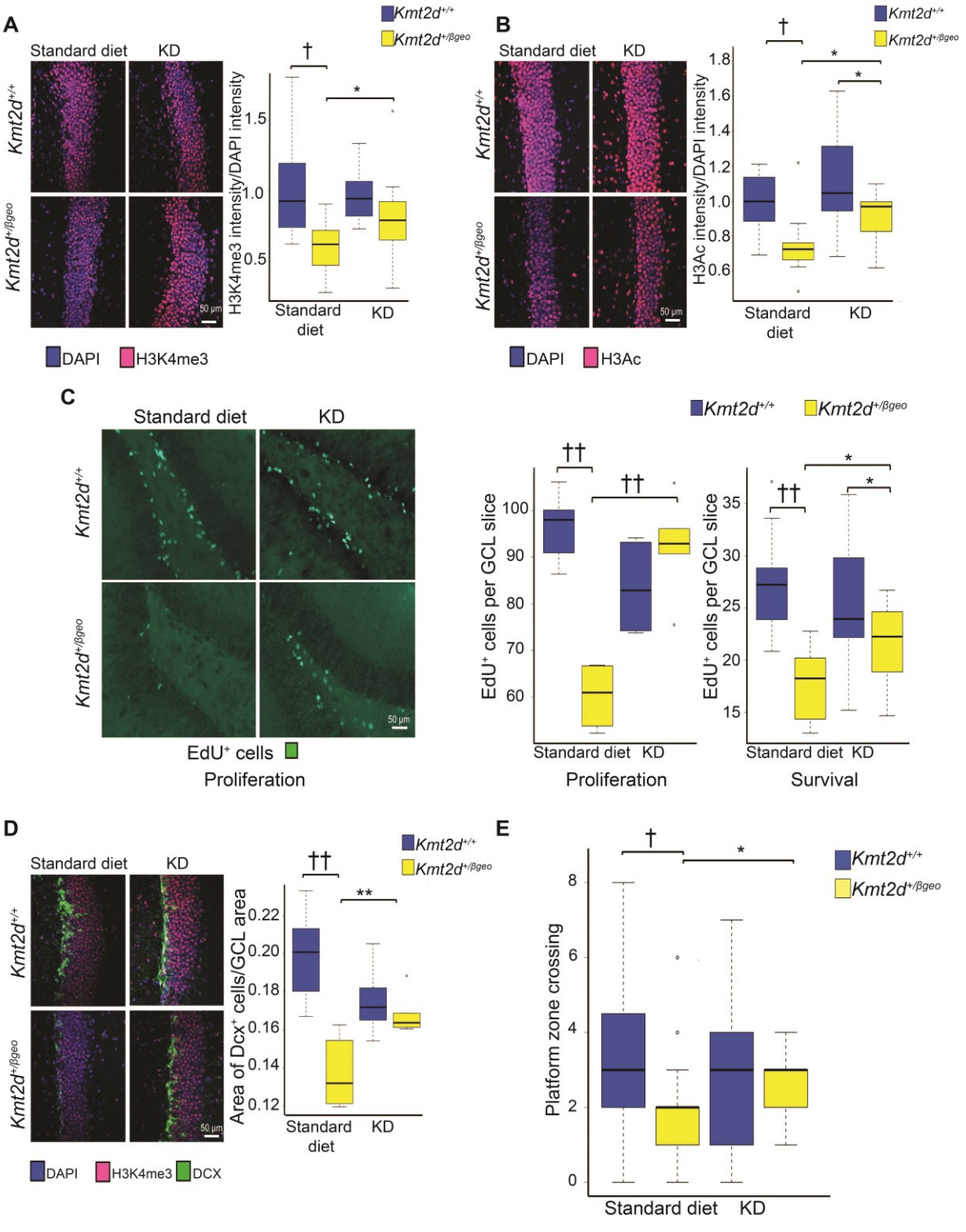
A
Standard diet
KD
Kmt2d+/+
Kmt2d+/βgeo
50 μm
H3K4me3 intensity/DAPI intensity
Standard diet
KD
DAPI
H3K4me3
B
H3Ac intensity/DAPI intensity
DAPI
H3Ac
C
EdU+ cells
Proliferation
EdU+ cells per GCL slice
Survival
D
Area of Dcx+ cells/GCL area
DAPI
H3K4me3
DCX
E
Platform zone crossing

Figure 3.3: Effects of exogenous BHB administration on either genotype. (**A**) *Kmt2d*$^{+/\beta Geo}$ mice injected with BHB showed a significant ($p<0.05$) increase in EdU^{+} cell numbers in the GCL of the DG of the mice compared to *Kmt2d*$^{+/\beta Geo}$ mice injected with saline vehicle. This was not a comparable rescue to what was seen with a KD since *Kmt2d*$^{+/\beta Geo}$ mice injected with BHB had significantly less ($p<0.05$) GCL EdU^{+} cells compared to BHB injected *Kmt2d*$^{+/+}$ (N=5-9 per group). (**B**) Urine time course (12 hours) from mice on a KD, mice treated with a single 10mM/kg BHB injection (9AM) or saline vehicle reveals notably less daily BHB exposure from a single injection than what was seen from a KD treatment (N=4-5 per group). (**C**) The combination of osmotic pumps to provide a constant level of BHB and three injections of 10mM/kg BHB at 9AM, 2PM, and 7PM showed a more similar BHB profile to KD-treated mice. (**D**) Following a two-week treatment with this combined BHB implementation scheme, we observed a significant ($P <0.001$) increase in EdU^{+} cells in the GCL of *Kmt2d*$^{+/\beta Geo}$ mice injected with BHB compared to *Kmt2d*$^{+/\beta Geo}$ mice injected with saline control and no significant difference between *Kmt2d*$^{+/\beta Geo}$ mice on treatment compared to *Kmt2d*$^{+/+}$ mice on and off treatment ($P =0.34$, $P =0.30$). *$P <0.05$; ††$P <0.001$.

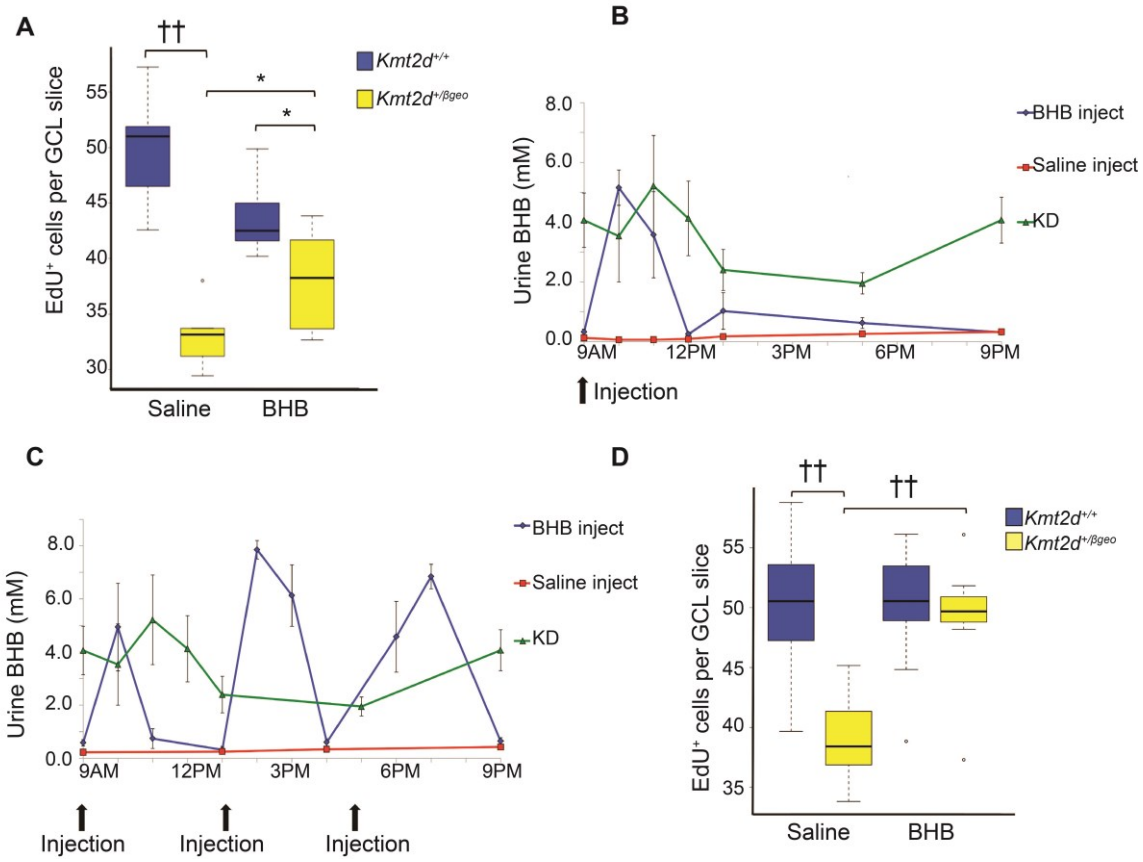
A
††
*
*
Kmt2d+/+
Kmt2d+/βgeo
EdU+ cells per GCL slice
55
50
45
40
35
30
Saline
BHB
B
8.0
6.0
4.0
2.0
0.0
Urine BHB (mM)
BHB inject
Saline inject
KD
9AM
12PM
3PM
6PM
9PM
Injection
C
8.0
6.0
4.0
2.0
0.0
Urine BHB (mM)
BHB inject
Saline inject
KD
9AM
12PM
3PM
6PM
9PM
Injection
Injection
Injection
D
††
††
Kmt2d+/+
Kmt2d+/βgeo
EdU+ cells per GCL slice
55
50
45
40
35
Saline
BHB

Supplementary figures

Supplementary figure 3.1: Previous findings of *Kmt2d*$^{+/\beta Geo}$ mice on a mixed background. *Kmt2d*$^{+/\beta Geo}$ mice on a mixed C57BL/6J and 129SvEv background demonstrated a global deficiency of the open chromatin mark H3K4me3 in association with decreased neurogenesis in the GCL of the DG and decreased platform crossing performance in a Morris water maze when compared to littermate *Kmt2d*$^{+/+}$ mice (First two columns). These defects were rescued with AR-42, an HDACi (third column, Bjornsson et al., 2014***).*** These findings therefore raise the possibility that BHB (an endogenous HDACi) may be able to provide similar therapeutic benefits to *Kmt2d*$^{+/\beta Geo}$ mice (bottom).

Pharmacological rescue

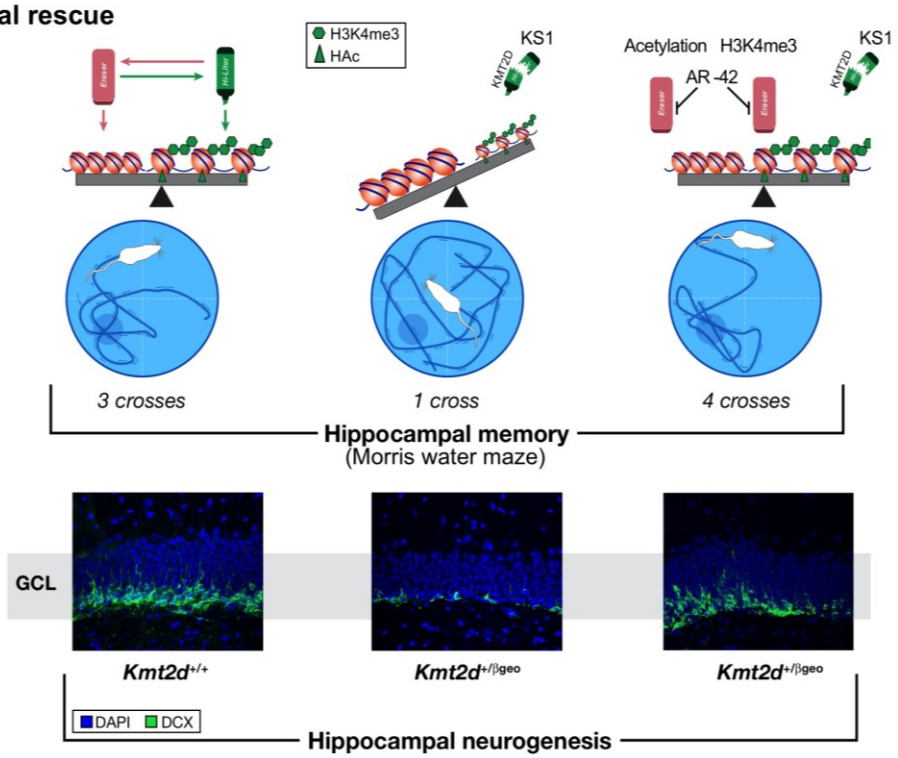

Dietary rescue

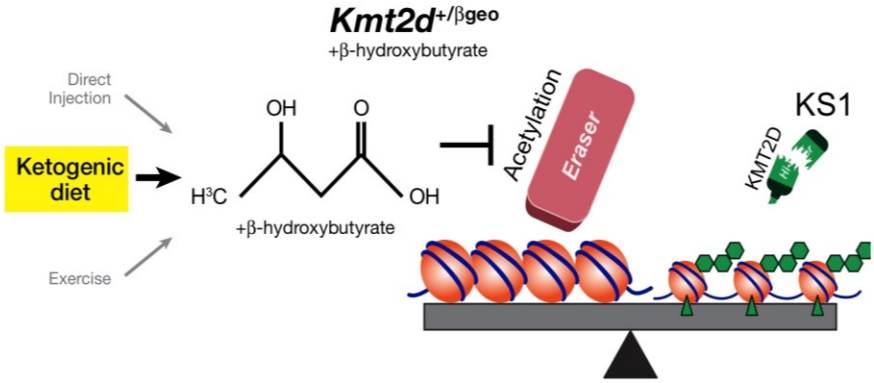

Supplementary figure 3.2: *Kmt2d*$^{+/\beta Geo}$ mice show growth retardation compared to *Kmt2d*$^{+/+}$ mice, which becomes more pronounced in old age. (**A**) Fully C57BL/6J backcrossed *Kmt2d*$^{+/\beta Geo}$ mice are significantly lighter than age matched *Kmt2d*$^{+/+}$ at 3 months, and this weight difference becomes larger at 12 months (N=4-10 per group). (**B**) *Kmt2d*$^{+/\beta Geo}$ mice on a mixed C57BL/6J and 129SvEv background show decreased weight when compared to *Kmt2d*$^{+/+}$ littermates, and the difference increases with advanced age (N=5-15 per group). The increased weight differences of the two genotypes with age suggest that *Kmt2d*$^{+/\beta Geo}$ mice may be resistant to the age related obesity seen in most mice (Bachmanov et al., 2001). Interestingly, another *Kmt2d*$^{+/\beta Geo}$ mouse model was recently described to be resistant to high fat diet induced obesity due to an intrinsic metabolic defect (Kim et al., 2015). *P <0.05; **P <0.01. ††P <0.001.

A

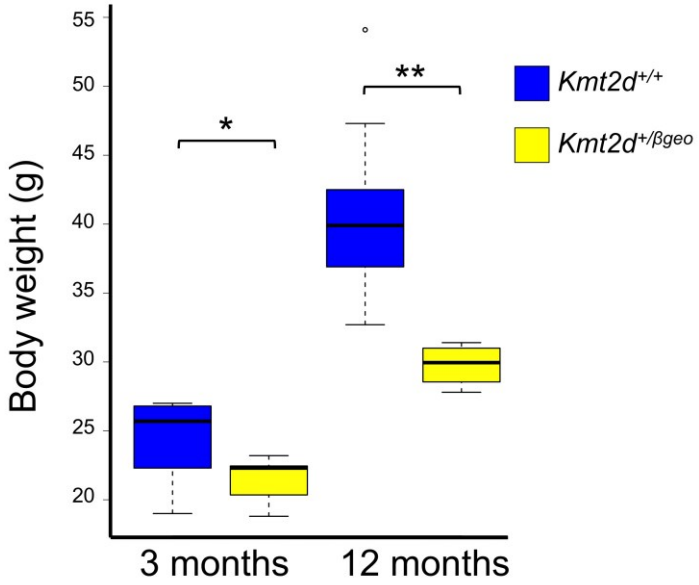
Body weight (g)
55
50
45
40
35
30
25
20
*
**
3 months
12 months
Kmt2d+/+
Kmt2d+/βgeo

B

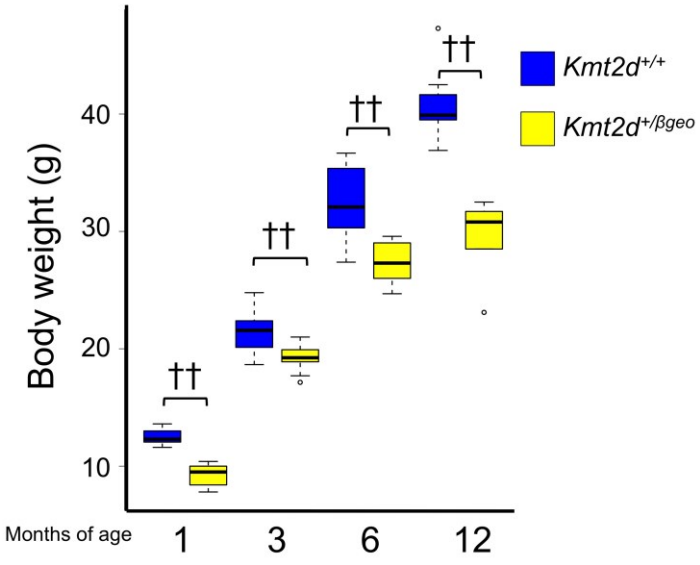
Body weight (g)
40
30
20
10
††
††
††
††
Months of age
1
3
6
12
Kmt2d+/+
Kmt2d+/βgeo

Supplementary figure 3.3: The *Kmt2d*$^{+/\beta Geo}$ mouse model has been fully backcrossed. Schematic diagram showing the backcrossing of *Kmt2d*$^{+/\beta Geo}$ mice onto a homogenized (10 generations) C57BL/6J genetic background.

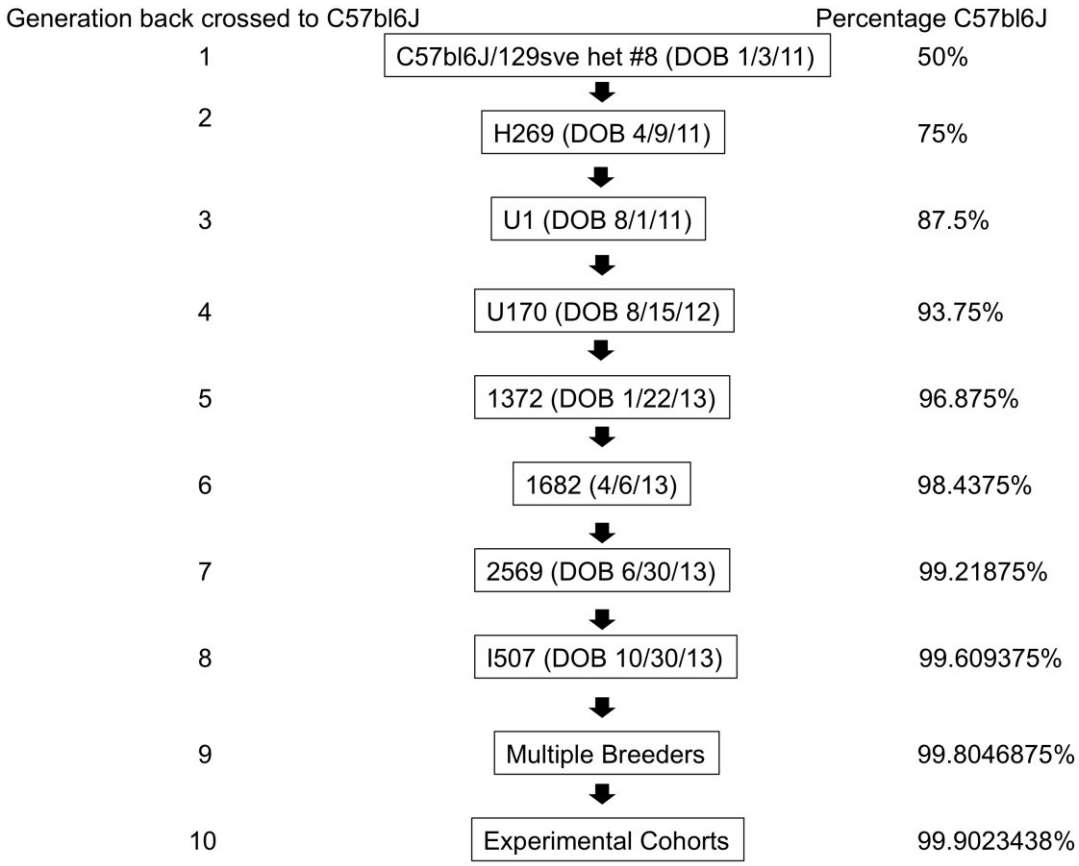

Supplementary figure 3.4: *Kmt2d*$^{+/\beta Geo}$ mice show a predisposition to disproportionately elevate BHB when on a KD. (**A**) When separated by genotype, urine from KD-treated mice revealed significantly increase urine BHB levels ($P < 0.05$) in *Kmt2d*$^{+/\beta Geo}$ mice compared to *Kmt2d*$^{+/+}$ controls suggesting that *Kmt2d*$^{+/\beta Geo}$ mice are predisposed to preferentially increase BHB levels during ketosis (N=4-12 per group). (**B**) GC-MS analysis confirmed this observation and revealed that this increase in BHB is in fact due to an altered beta-hydroxybutyrate to acetoacetate (BHB/AcAc) ratio, which is significantly elevated in KD-treated *Kmt2d*$^{+/\beta Geo}$ mice compared to controls (N=3 per group; *$P < 0.05$).

A

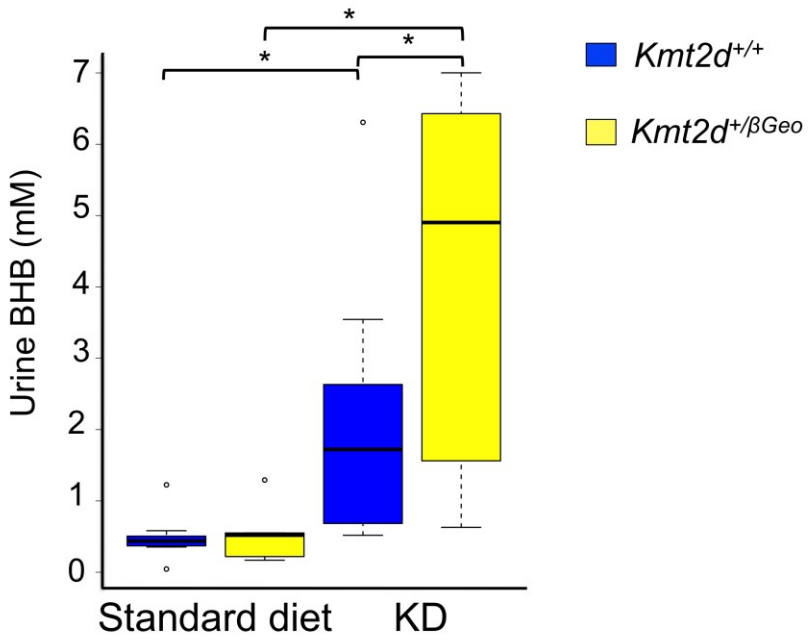

B

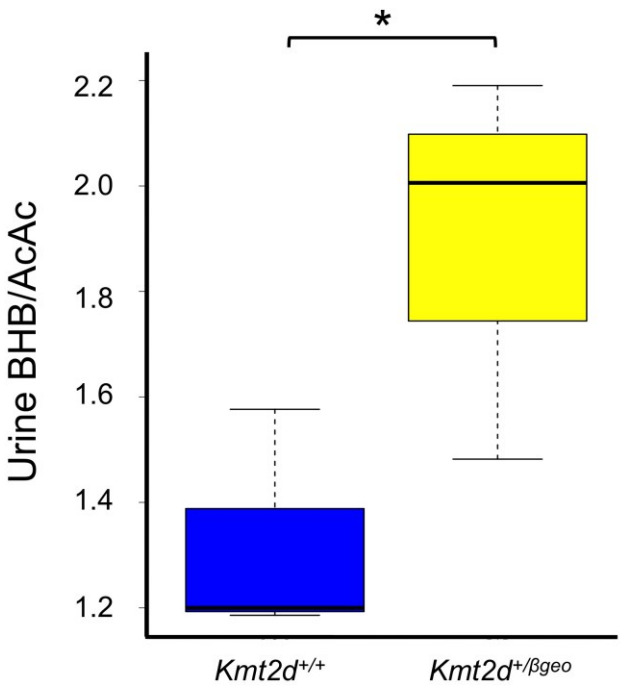

Supplementary figure 3.5: An increase in both BHB/AcAc and Lac/Pyr ratios in KD-treated *Kmt2d*$^{+/\beta Geo}$ mice suggest a potential NADH/NAD$^+$ imbalance. In addition to the increased BHB/AcAc ratio seen in Sup. Fig. 3.4, serum analysis from KD-treated animals shows *Kmt2d*$^{+/\beta Geo}$ mice had a significant increase ($P < 0.05$) in the lactate to pyruvate (Lac/Pyr) ratio compared to KD-treated *Kmt2d*$^{+/+}$ littermates (N=12-15 per group). This schematic demonstrates how both of these processes are controlled by the cellular NADH/NAD$^+$ ratio (Feron et al., 2009; White and Venkatesh, 2011), suggesting that *Kmt2d*$^{+/\beta Geo}$ mice maintain relatively higher NADH levels during ketosis. *$P < 0.05$.

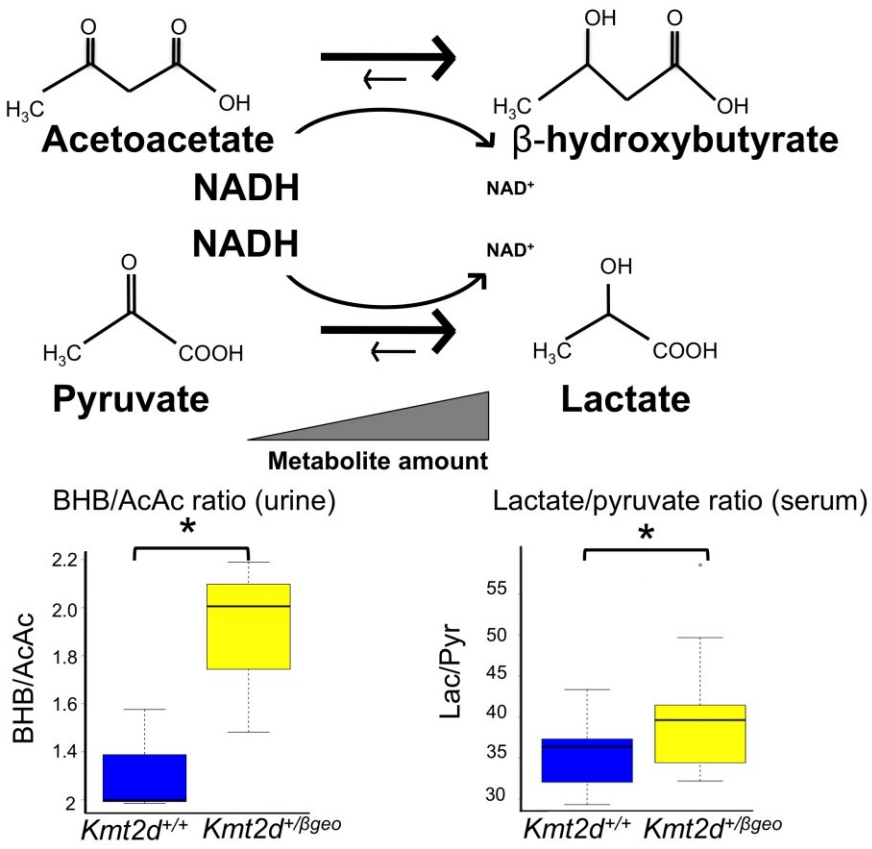

Supplementary figure 3.6: A mouse model of Rubinstein-Taybi syndrome does not demonstrate an elevation of urine BHB compared to wildtype littermates on a KD. Rubinstein-Taybi syndrome (RTS) is another Mendelian disorder of the epigenetic machinery, caused by deficiency of an histone acetyltransferase (CREBBP), which secondarily leads to a global deficiency of histone acetylation (Alarcon et al., 2004). The histone tails have previously been considered to be a potential acetyl-CoA sink (Kurdistani et al., 2014) and previously a link between NAD^+ and histone acetylation has been documented (Castonguay et al., 2014). A global deficiency of histone acetylation could therefore potentially lead to chronic acetyl-CoA elevation, thereby driving beta-oxidation and secondarily increasing NADH/NAD^+ ratio in both KS and RTS. (**A**) BHB levels from urine show a significant ($P < 0.05$) elevation in *Kmt2d*$^{+/\beta Geo}$ mice compared to *Kmt2d*$^{+/+}$ and *Crebbp*$^{+/-}$ mice (Kung et al., 2000; N=6-8 per group). However, no significant differences were seen between *Kmt2d*$^{+/+}$ and *Crebbp*$^{+/-}$ ($P = 0.36$). (**B**) GC-MS analysis further revealed no significant increase in the BHB/AcAc ratio of KD-treated *Crebbp*$^{+/-}$ mice compared to wildtype KD-treated controls ($P = 0.38$), while KD-treated *Crebbp*$^{+/-}$ mice showed a significant ($P < 0.05$) decrease compared to *Kmt2d*$^{+/\beta Geo}$ mice. These data suggest that the NADH/NAD^+ imbalance seen in *Kmt2d*$^{+/\beta Geo}$ mice, is unique to this condition and likely caused by specific target genes of Kmt2d, rather than a global abnormality. *$P < 0.05$.

A

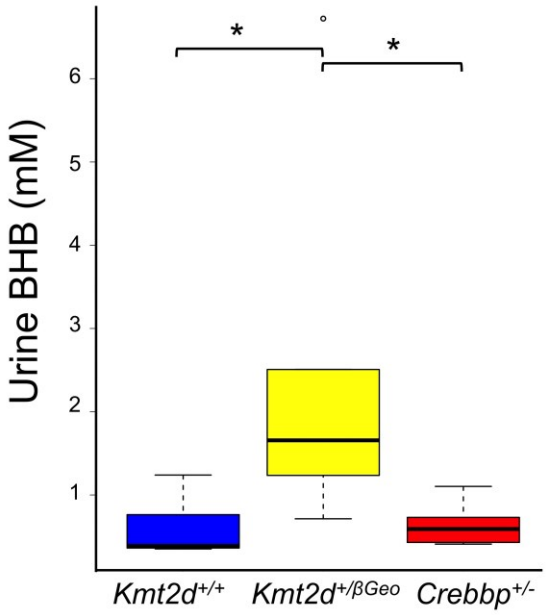
Urine BHB (mM)
1
2
3
4
5
6
*
°
*
Kmt2d+/+
Kmt2d+/βGeo
Crebbp+/-

B

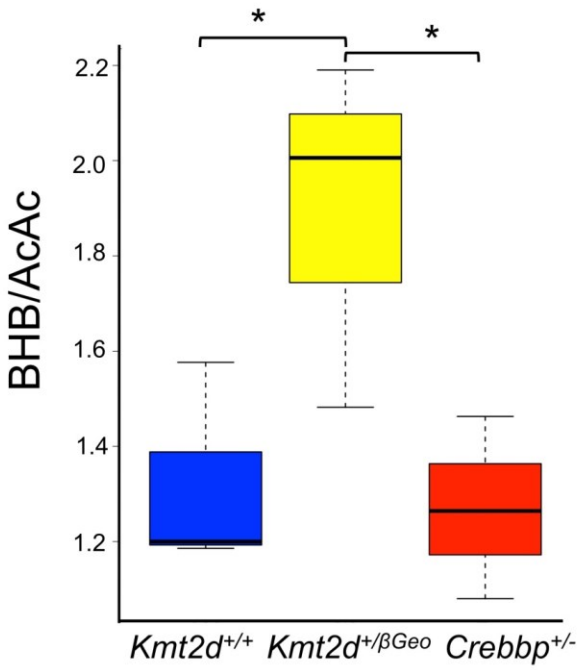
BHB/AcAc
1.2
1.4
1.6
1.8
2.0
2.2
*
*
Kmt2d+/+
Kmt2d+/βGeo
Crebbp+/-

Supplementary figure 3.7: Gene expression changes on the KD. (**A**) Overall, we did not observe a global change of gene expression in *Kmt2d*$^{+/\beta Geo}$ mice on a KD compared to mice on a standard diet. For instance, none of the 17 significantly down-regulated genes between *Kmt2d*$^{+/\beta Geo}$ and *Kmt2d*$^{+/+}$ mice (orange) showed significant change on the KD. (**B**) Ranked genes based on fold change difference in *Kmt2d*$^{+/\beta Geo}$ mice on and off the KD (right edge of line). From this list, we chose the highest five genes (10%) for RT-qPCR validation (red). Also displayed is the fold change difference between *Kmt2d*$^{+/\beta Geo}$ and *Kmt2d*$^{+/+}$ mice (left edge of line). (**C**) Validation of these five genes by RT-qPCR confirms that three of these genes (*Atp2b4*, *Pld5*, *Glp1r*) show a significantly decreased expression in *Kmt2d*$^{+/\beta Geo}$ mice compared to *Kmt2d*$^{+/+}$ littermates on a standard diet, with a significant increase in gene expression in the *Kmt2d*$^{+/\beta Geo}$ mice on a KD compared to *Kmt2d*$^{+/\beta Geo}$ mice on a standard diet (N=9-11 per group). (**D**) Additionally, the other two genes (*Tm4sf1, Nts*) showed a similar but non-significant trend. *P <0.05; **P <0.01. ††P <0.001.

A

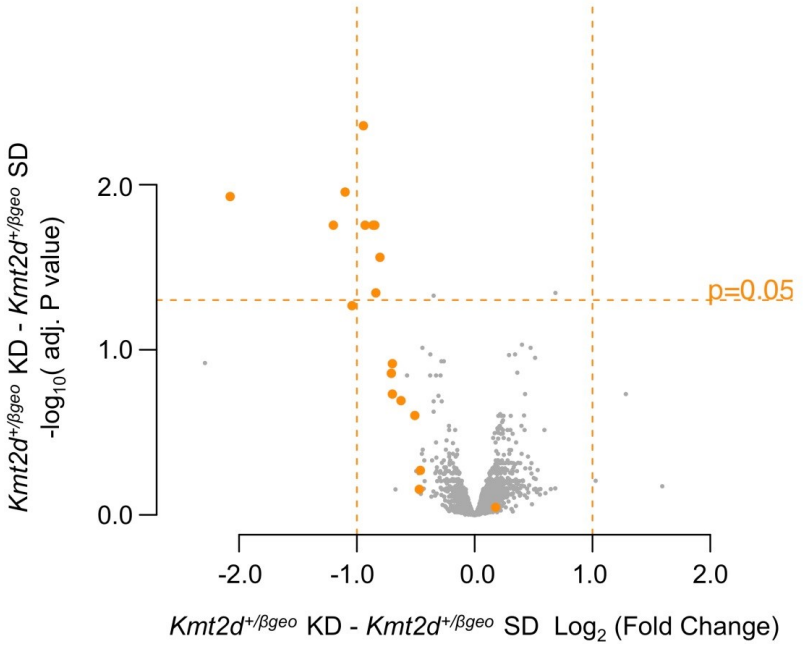
Kmt2d+/βgeo KD - Kmt2d+/βgeo SD
-log10(adj. P value)
2.0
1.0
0.0
p=0.05
-2.0
-1.0
0.0
1.0
2.0
Kmt2d+/βgeo KD - Kmt2d+/βgeo SD Log2 (Fold Change)

B

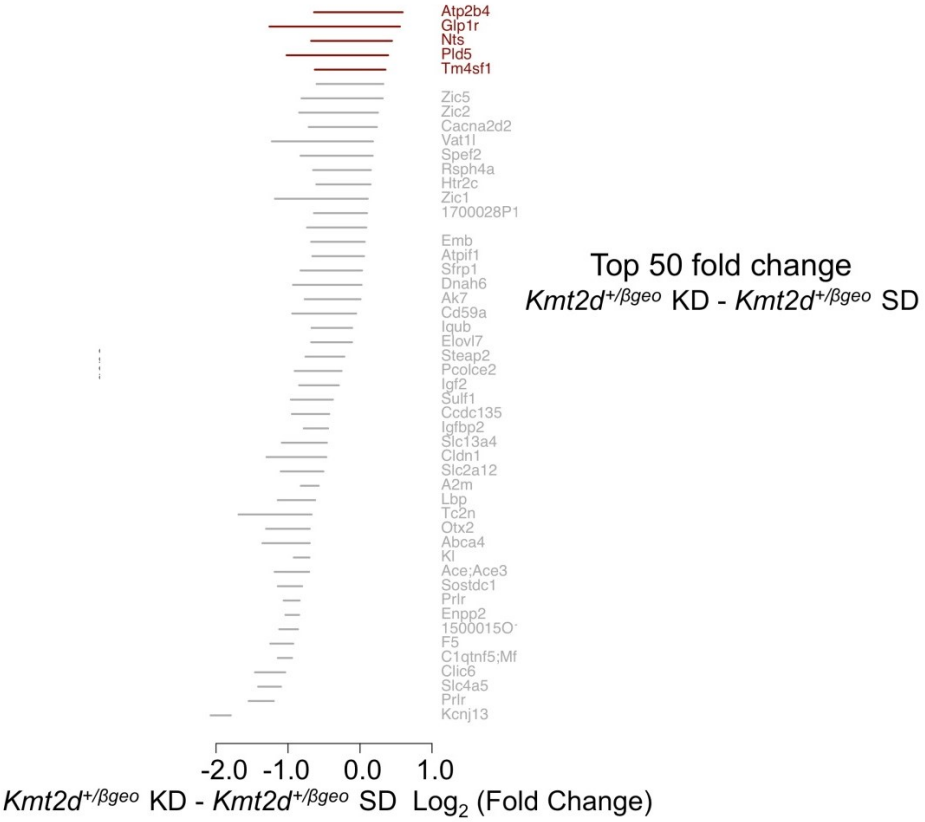
Atp2b4
Glp1r
Nts
Pld5
Tm4sf1
Zic5
Zic2
Cacna2d2
Vat1l
Spef2
Rsph4a
Htr2c
Zic1
1700028P1
Emb
Atpif1
Sfrp1
Dnah6
Ak7
Cd59a
Iqub
Elovl7
Steap2
Pcolce2
Igf2
Sulf1
Ccdc135
Igfbp2
Slc13a4
Cldn1
Slc2a12
A2m
Lbp
Tc2n
Otx2
Abca4
Kl
Ace;Ace3
Sostdc1
Prlr
Enpp2
1500015O
F5
C1qtnf5;Mf
Clic6
Slc4a5
Prlr
Kcnj13
Top 50 fold change
Kmt2d+/βgeo KD - Kmt2d+/βgeo SD
-2.0
-1.0
0.0
1.0
Kmt2d+/βgeo KD - Kmt2d+/βgeo SD Log2 (Fold Change)

C

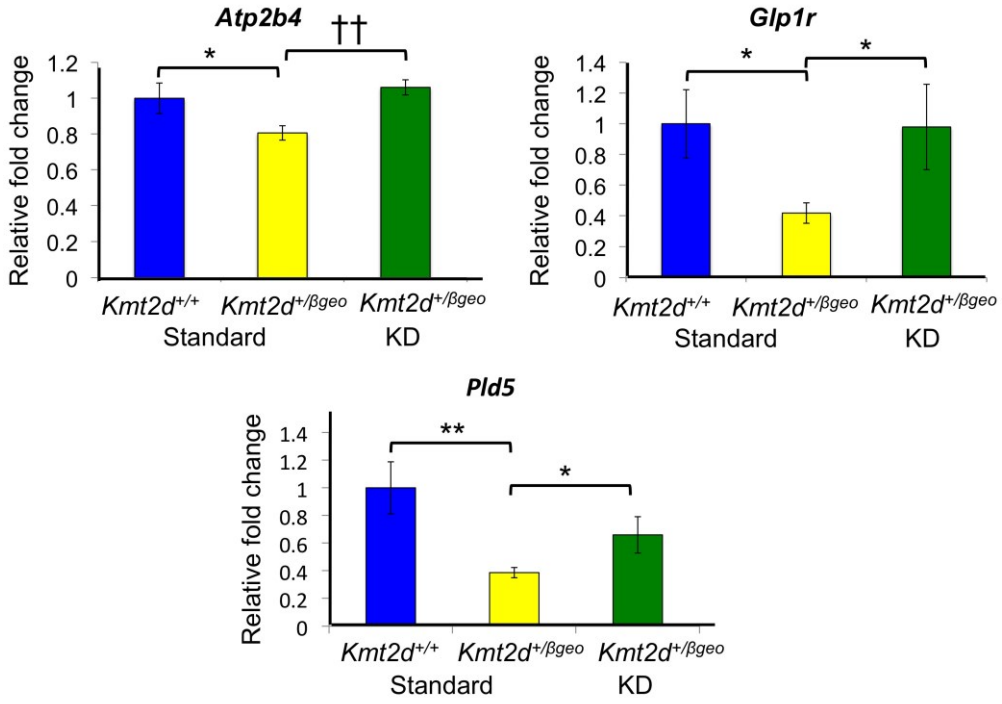
Atp2b4
Relative fold change
1.2
1
0.8
0.6
0.4
0.2
0
*
††
Kmt2d+/+
Kmt2d+/βgeo
Kmt2d+/βgeo
Standard
KD
Glp1r
Relative fold change
1.4
1.2
1
0.8
0.6
0.4
0.2
0
*
*
Kmt2d+/+
Kmt2d+/βgeo
Kmt2d+/βgeo
Standard
KD
Pld5
Relative fold change
1.4
1.2
1
0.8
0.6
0.4
0.2
0
**
*
Kmt2d+/+
Kmt2d+/βgeo
Kmt2d+/βgeo
Standard
KD

D

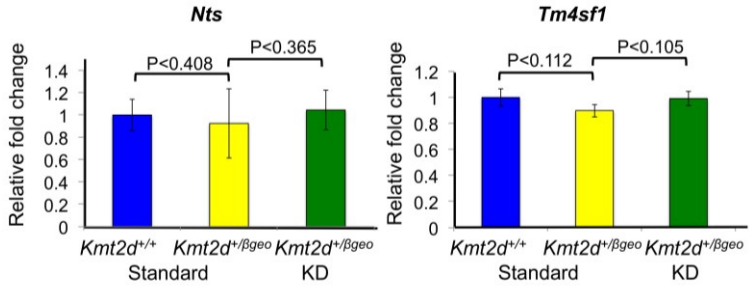
Nts
Relative fold change
1.4
1.2
1
0.8
0.6
0.4
0.2
0
P<0.408
P<0.365
Kmt2d+/+
Kmt2d+/βgeo
Kmt2d+/βgeo
Standard
KD
Tm4sf1
Relative fold change
1.2
1
0.8
0.6
0.4
0.2
0
P<0.112
P<0.105
Kmt2d+/+
Kmt2d+/βgeo
Kmt2d+/βgeo
Standard
KD

Supplementary figure 3.8: Hidden platform and flag latencies. (**A**) The latencies to find the hidden platform during the 5 days of training showed a significant interaction ($P < 0.05$) between genotype and treatment for *Kmt2d*$^{+/\beta Geo}$ compared to *Kmt2d*$^{+/+}$ mice as well as standard and a KD treatment as examined by a repeated measures ANOVA. (**B**) The latencies to find the platform during the flag training did not show a significant interaction for either genotype or treatment ($P = 0.142$), as examined by a repeated measures ANOVA (N=19-32 per group).

A

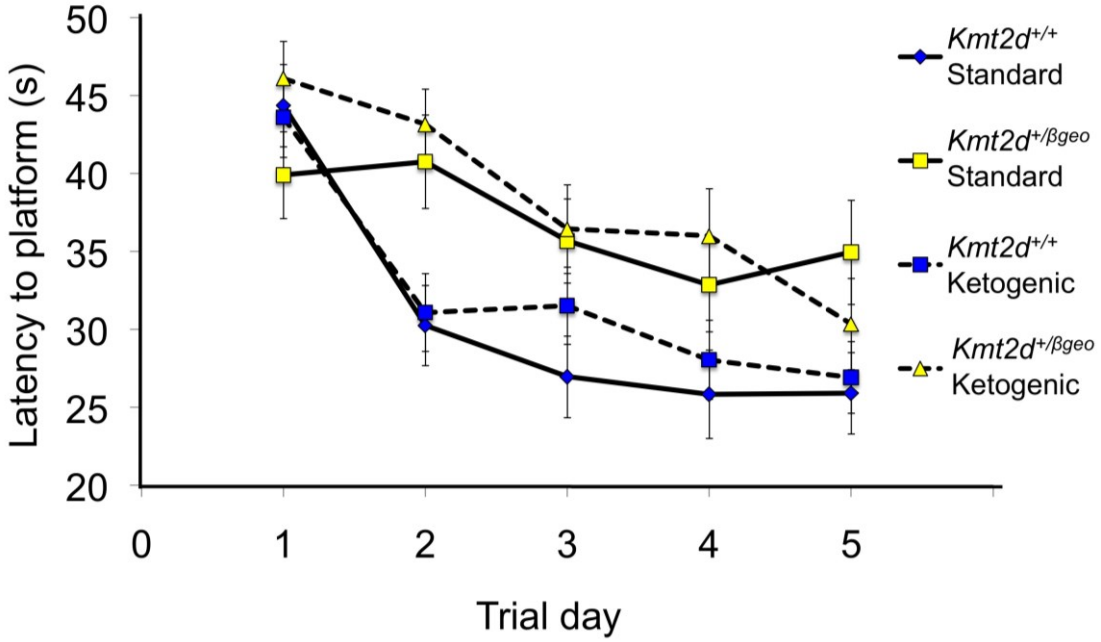
Latency to platform (s)
50
45
40
35
30
25
20
0
1
2
3
4
5
Trial day
Kmt2d+/+ Standard
Kmt2d+/βgeo Standard
Kmt2d+/+ Ketogenic
Kmt2d+/βgeo Ketogenic

B

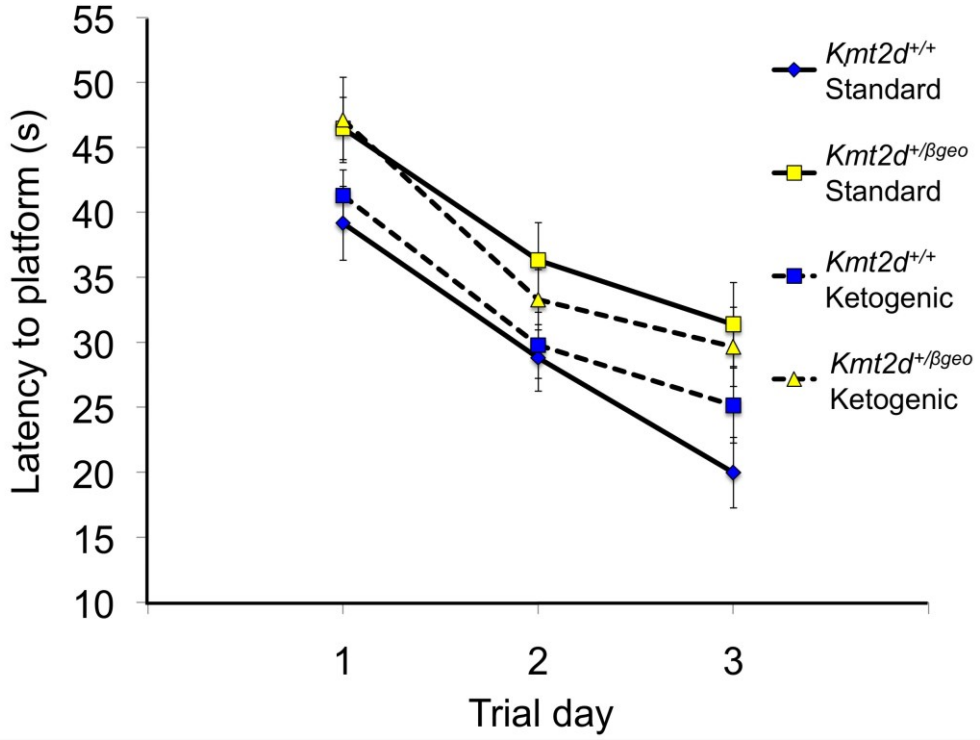
Latency to platform (s)
55
50
45
40
35
30
25
20
15
10
1
2
3
Trial day
Kmt2d+/+ Standard
Kmt2d+/βgeo Standard
Kmt2d+/+ Ketogenic
Kmt2d+/βgeo Ketogenic

Supplementary figure 3.9: There are no significant effect of diet or genotype on tests exploring strength or activity levels. (**A**) *Kmt2d*$^{+/\beta Geo}$ mice did not show a significant difference from *Kmt2d*$^{+/+}$ mice on the regular diet, and did not demonstrate decreased activity on the KD in an open field test, while *Kmt2d*$^{+/+}$ mice did show an increase ($P < 0.05$) in activity compared to *Kmt2d*$^{+/\beta Geo}$ mice only when both were treated with the KD. There were no differences for grip strength for either genotype or treatment (N=5-15 per group). (**B**) *Kmt2d*$^{+/\beta Geo}$ mice did not show a significant difference from *Kmt2d*$^{+/+}$ mice on the regular diet, and did not have decreased activity on a KD as measured by an open field test, while *Kmt2d*$^{+/+}$ mice did show an increase ($P < 0.001$) in activity compared to *Kmt2d*$^{+/\beta Geo}$ mice only when both were treated with the KD (N=13-26 per group). The increased activity seen in wild type animals on KD has been previously described *(*Zhao et al., 2004). *P <0.05; ††P <0.001.

A

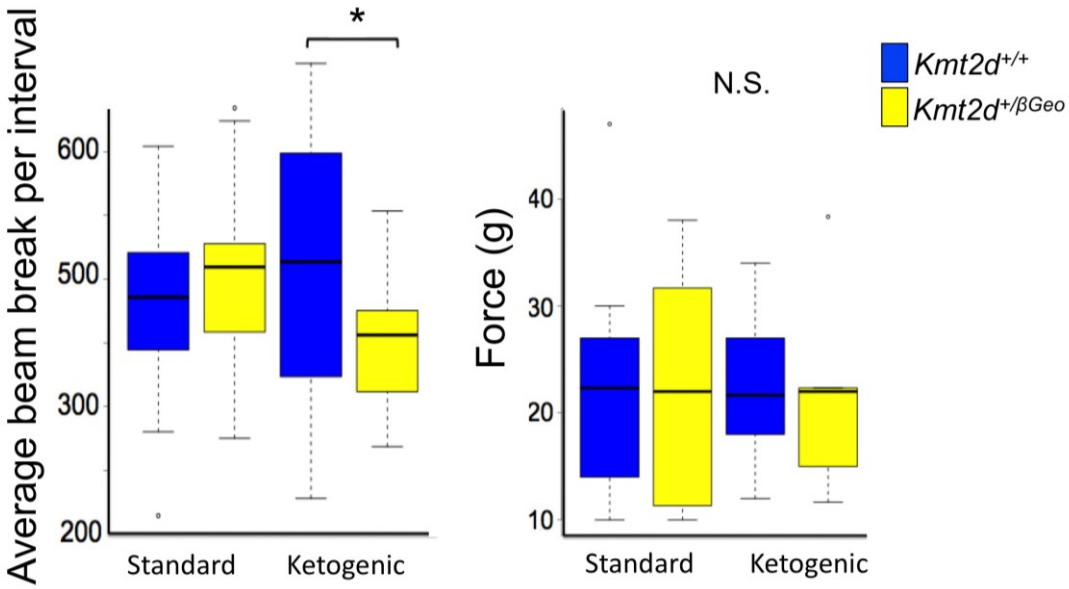
Average beam break per interval
600
500
300
200
*
Standard
Ketogenic
N.S.
Force (g)
40
30
20
10
Standard
Ketogenic
Kmt2d+/+
Kmt2d+/βGeo

B

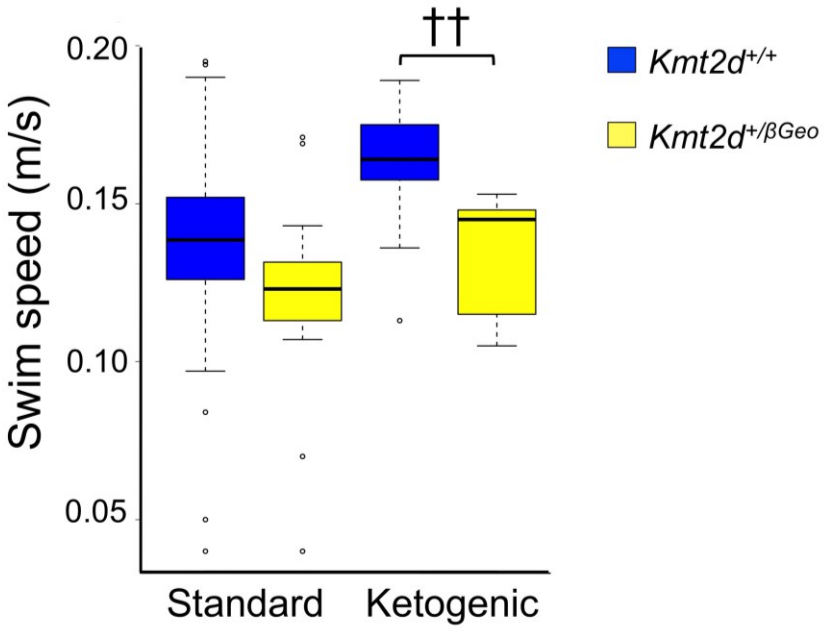
Swim speed (m/s)
0.20
0.15
0.10
0.05
††
Standard
Ketogenic
Kmt2d+/+
Kmt2d+/βGeo

Supplementary figure 3.10: Basis for the dose selection (10mM/kg) of exogenously administered BHB. Several different doses (0,5,10,20 mM/kg) of BHB were IP injected followed by urine collection 1.5 hours later (approximate time of BHB peak levels; Clarke et al., 2012). The 10mM/kg dose shows a BHB level that resembles the urine BHB profile (approximated in this figure with dashed lines) from KD-treated mice (N=22 total). *P <0.05; †P <0.005.

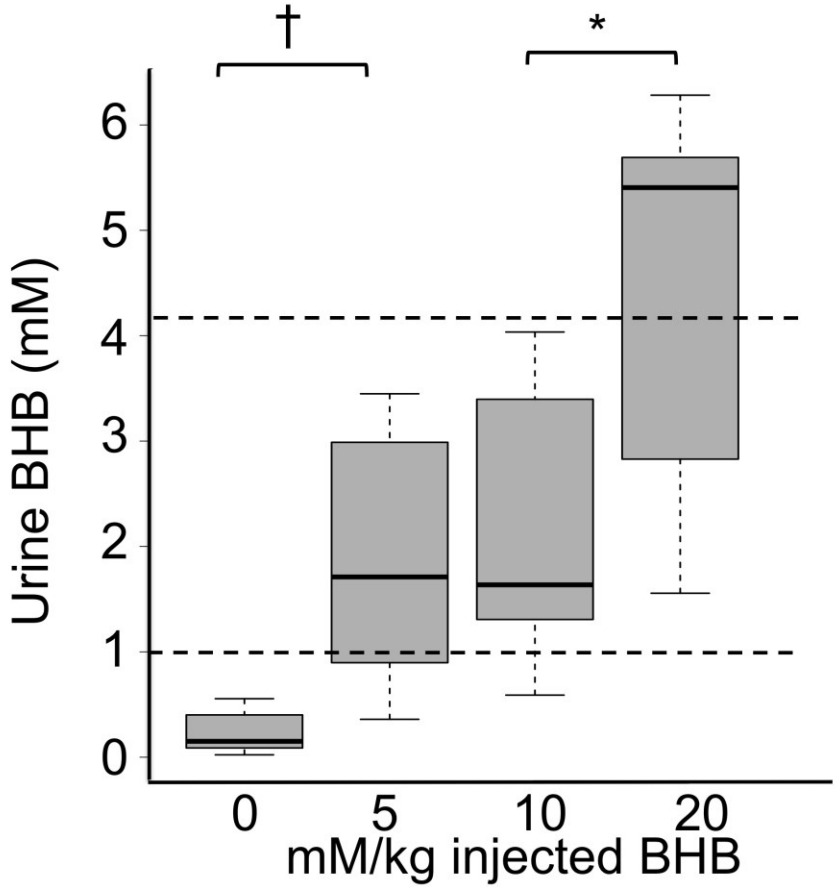

Supplementary figure 3.11: BHB administered by osmotic pump did not reach levels of BHB comparable to levels seen in mice on a KD. Mice implanted with a two-week BHB pump that provided 3mg/ml BHB at a rate of 0.25µl/hour showed a significant (P <0.05) increase in BHB measured from urine (N=10-12 per group). However, while the pump provided a constant stream of BHB, the urine BHB did not reach comparable levels to what was seen in mice on a KD (approximately 1-2 mM BHB). *P <0.05;

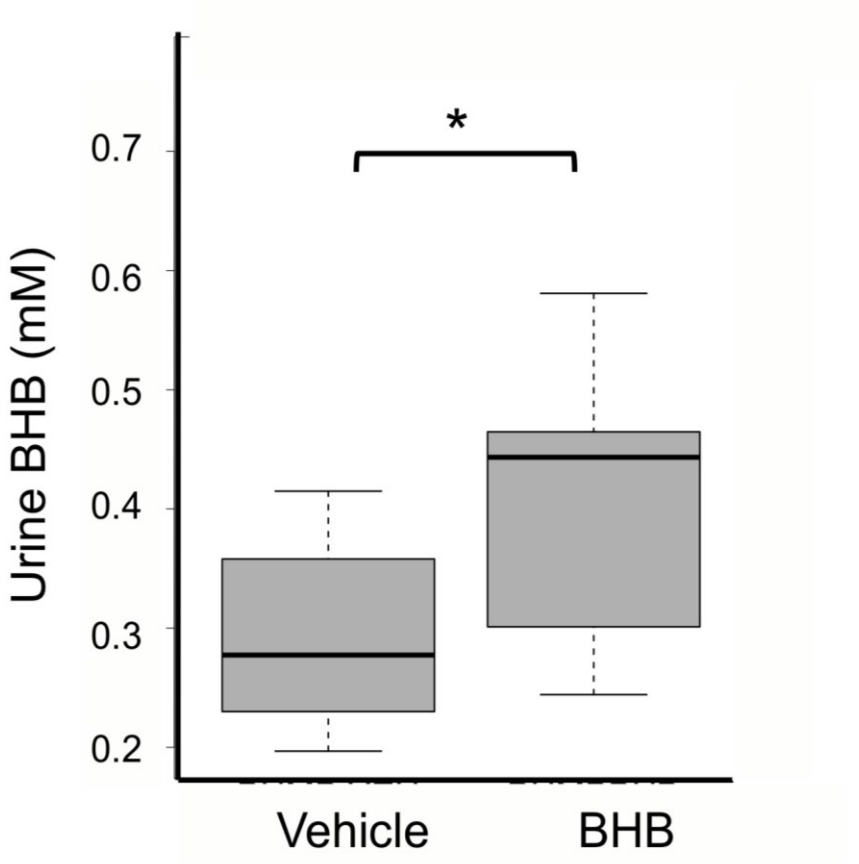

Supplementary Table 3.1: Genes downregulated in the hippocampus of *Kmt2d*$^{+/\beta Geo}$ compared to *Kmt2d*$^{+/+}$ mice. 18 probes demonstrated in (Fig. 3.1C; orange) represent 17 unique genes. Here we summarize gene symbol, gene function, examples of OMIM disease associated with each gene and information regarding fold change and p-values of each probe.

Probe ID	Gene symbol	Gene function	OMIM disease linked to this gene	Fold change (Log)	P value	Adjusted P value
10584653	*C1qtnf5;Mfrp*	Component of basement membrane	Late onset AD retinal degeneration (605670)	-1.14	2.44E-07	0.0013
10539393	*Slc4a5*	Sodium Bicarbonate Cotransporter	No known human disease	-1.42	7.07E-07	0.0013
10351224	*F5*	Clotting factor	Factor V deficiency (227400)	-1.25	2.29E-06	0.0026
10345921	*1500015O10Rik*	Unknown function	No known human disease	-1.12	3.22E-06	0.0026
10395389	*Sostdc1*	Bone morphogenetic protein antogonist	No known human disease	-1.14	3.24E-06	0.0026
10495712	*Abca4*	ABC transporter	Stargardt disease 1 (248200)	-1.36	3.45E-06	0.0026
10423049	*Prlr*	Prolactin receptor	Hyperprolactinemia (615555)	-1.55	4.14E-06	0.0026
10428619	*Enpp2*	Phosphodiesterase and phospholipase	No known human disease	-1.04	6.10E-06	0.0031
10362104	*Slc2a12*	Glucose transporter	No known human disease	-1.10	6.75E-06	0.0032
10436958	*Clic6*	Intracellular chloride channel	No known human disease	-1.46	1.14E-05	0.0038
10419356	*Otx2*	Transcription factor	Pituitary hormone deficiency (613986)	-1.31	1.16E-05	0.0038
10381962	*Ace;Ace3*	Angiotensin converting enzyme	Renal tubular dysgenesis (267430)	-1.19	1.61E-05	0.0048
10478048	*Lbp*	Lipopolysaccharide binding protein	No known human disease	-1.14	1.81E-05	0.0049
10423030	*Prlr*	Prolactin receptor	Hyperprolactinemia (615555)	-1.06	1.82E-05	0.0049
10356403	*Kcnj13*	Potassium channel	Leber congenital amaurosis 16 (614186)	-1.80	3.91E-05	0.0082
10543921	*Slc13a4*	Sodium/Sulfate symporter	No known human disease	-1.09	6.04E-05	0.0098
10575693	*Vat1l*	Unknown function	No known human disease	-1.22	0.000332649	0.0351
10438769	*Cldn1*	Component of tight junctions	NISCH syndrome (607626)	-1.30	0.000400921	0.0397

Supplementary table 3.2: Genetic pathways disrupted in the hippocampus of *Kmt2d*$^{+/\beta Geo}$ mice. We performed gene ontology and pathway analysis (IPA) on microarray data from the hippocampus of *Kmt2d*$^{+/\beta Geo}$ and *Kmt2d*$^{+/+}$ mice. Pathways, disease processes, and cellular functions that show biggest difference between the two genotypes are listed. The disruption of the CREB signaling pathway is of particular interest, as this pathway is disrupted in Rubinstein-Taybi syndrome, another disorder involving the global loss of an open chromatin modification (Alarcon et al., 2004, Kung et al., 2000).

Top Canonical Pathways

Name	p-value	Ratio
EIF2 Signaling	1.29E-22	90/159 (0.566)
CREB Signaling in Neurons	4.04E-18	86/167 (0.515)
Axonal Guidance Signaling	7.51E-18	165/419 (0.394)
Synaptic Long Term Potentiation	2.23E-17	66/115 (0.574)
Glutamate Receptor Signaling	1E-16	41/56 (0.732)

Top Diseases and Bio Functions

Diseases and Disorders

Name	p-value	# Molecules
Neurological Disease	9.79E-87 - 7.47E-07	1328
Psychological Disorders	4.11E-71 - 7.47E-07	921
Skeletal and Muscular Disorders	4.16E-62 - 6.30E-07	571
Hereditary Disorder	1.16E-58 - 1.57E-07	389
Metabolic Disease	4.58E-34 - 2.07E-07	553

Molecular and Cellular Functions

Name	p-value	# Molecules
Cellular Development	1.04E-83 - 6.72E-07	1182
Cell Morphology	5.50E-77 - 6.72E-07	1077
Cellular Assembly and Organization	5.50E-77 - 6.72E-07	982
Cellular Function and Maintenance	5.50E-77 - 6.72E-07	1216
Cell-To-Cell Signaling and Interaction	8.84E-64 - 8.08E-07	650

Bibliography

1) Alarcon JM, Malleret G, Touzani K, Vronskaya S, Ishii S, Kandel ER, Barco A.. Chromatin acetylation, memory, and LTP are impaired in CBP+/- mice: a model for the cognitive deficit in Rubinstein-Taybi syndrome and its amelioration. *Neuron.* **42**:947-59. (2004).

2) Altman J, Are new neurons formed in the brains of adult mammals? *Science*. **135**, 1127-8 (1962).

3) Ansorg A, Witte OW, Urbach A, Age-dependent kinetics of dentate gyrus neurogenesis in the absence of cyclin D2. *BMC Neurosci.* **13**, 46 (2012).

4) Azad N, Zahnow CA, Rudin CM, Baylin SB, The future of epigenetic therapy in solid tumors—lessons from the past. Nat Rev Clin Oncol. **10**(5):256-66 (2013).

5) Bachmanov AA, Reed DR, Tordoff MG, Price RA, Beauchamp GK. 2001. Nutrient preference and diet induced adiposity in C57BL/6ByJ and 129P3/J mice. *Physiology & Behavior.* **72**:603-613.

6) Baird GS, Zacharias DA, Tsien RY, Circular permutation and receptor insertion within green fluorescent proteins. *Proc Natl Acad Sci*. **96**, 11241-6 (1999).

7) Baranano KW, Hartman AL, The ketogenic diet: uses in epilepsy and other neurologic illnesses. *Curr Treat Options Neurol*. **10**(6):410-19 (2008).

8) Berdasco M, Esteller M, Genetic syndromes caused by mutations in epigenetic genes. *Hum Genet*. 132, 359-83 (2013).

9) Bhaumik S, Gangadharan S, Hiremath A, Russell PS, Psycological treatments in intellectual disability: the challenges of building a good evidence base. *Br J Psychiatry.* 198(6):428-30 (2011).

10) Bjornsson HT, Fallin MD, Feinberg AP, An integrated epigenetic and genetic approach to common human disease. *Trends Genet.* 20, 350-8 (2004).

11) Bjornsson HT, Benjamin JS, Zhang L, Weissman J, Gerber EE, Chen YC, Vaurio RG, Potter MC, Hansen KD, Dietz HC. Histone deacetylase inhibition rescues structural and functional brain deficits in a mouse model of Kabuki syndrome. *Science Translational Medicine*. **6**:256ra135. (2014).

12) Bjornsson HT, The Mendelian disorders of the epigenetic machinery. *Genome Res*. **25**: 1473-1481 (2015).

13) Bögershausen N, Bruford E, Wollnik B. Skirting the pitfalls: a clear-cut nomenclature for H3K4 methyltransferases. *Clin Genet*. 83, 212-4 (2013).

14) Bogershausen N, Wollnik B, Unmasking Kabuki syndrome. *Clin Genet.* **83**(3):201-11 (2013).

15) Bose P, Dai Y, Grant S, Histone deacetylase inhibitor (HDACI) mechanism of action: Emerging insights. *Pharm and Therap.* **143**(3):323-336 (2014).

16) Brickman AM, Stern Y, Small SA, Hippocampal subregions differentially associate with standardized memory tests. *Hippocampus*. 21, 923-8 (2011).

17) Brus M, Keller M, Lévy F, Temporal features of adult neurogenesis: differences and similarities across mammalian species. *Front Neurosci.* 7, 135 (2013).

18) Carvalho BS, Irizarry RA.. A framework for oligonucleotide microarray preprocessing. *Bioinformatics*. **26**:2363-7. (2010)

19) Castonguay Z, Auger C, Thomas SC, Chahma M, Appanna VD. Nuclear lactate dehydrogenase modulates histone modification in human hepatocytes. *Biochemical and Biophysical Research Communications*. **454**:172-7.

20) Chen Y, Sprung R, Tang Y, Ball H, Sangras B, Kim SC, Falck JR, Peng J, Gu W, Zhao Y. 2007. Lysine propionylation and butyrylation are novel post-translational modifications in histones. *Molecular & Cellular Proteomics*. **6**:812-19. (2014).

21) Choi SW, Friso S, Epigenetics: a new bridge between nutrition and health. *Adv Nutr.* **1**:8-16 (2010).

22) Clarke K, Tchabanenko K, Pawlosky R, Carter E, Todd King M, Musa-Veloso K, Ho M, Roberts A, Robertson J, Vanitallie TB, Veech RL. Kinetics, safety and tolerability of (R)-3-hydroxybutyl (R)-3-hydroybutyrate in healthy adult subjects. *Regulatory Toxicology and Pharmacology,* **63**:401-408. (2012).

23) Cohen HY, Miller C, Bitterman KJ, Wall NR, Hekking B, Kessler B, Howitz KT, Gorospe M, de Cabo R, Sinclair DA.. Calorie restriction promotes mammalian cell survival by inducing the Sirt1 deacetylase. *Science.* **305**:390-392. (2004).

24) Cohen-Armon M, Visochek L, Katzoff A, Levitan D , Susswein AJ, Klein R, Valbrun M, Schwartz JH, Long-term memory requires polyADP-ribosylation. *Science.* **304**, 1820-2 (2004).

25) Das I, Park JM, Shin JH, Jeon SK, Lorenzi H, Linden DJ, Worley PF, Reeves RH, Hedgehog agonist therapy corrects structural and cognitive deficits in a Down syndrome mouse model. *Sci Transl Med.* **5**, 201ra120 (2013).

26) Das I, Park JM, Shin JH, Jeon SK, Lorenzi H, Linden DJ, Worley PF, Reeves RH, Hedgehog agonist therapy corrects structural and cognitive deficits in a Down syndrome mouse model. *Sci Transl Med*. **5**(201):201ra120 (2013).

27) Dash PK, Orsi SA, Moore AN, Histone deacetylase inhibition combined with behavioral therapy enhances learning and memory following traumatic brain injury. *Neuroscience* **163**, 1-8 (2009).

28) Denis-Donini S, Dellarole A, Crociara P, Francese MT, Bortolotto V, Quadrato G, Canonico PL, Orsetti M, Ghi P, Memo M, Bonini SA, Ferrari-Toninelli G, Grilli M, Impaired adult neurogenesis associated with short-term memory defects in NF-kappaB p50-deficient mice. *J Neurosci.* **28**, 3911–3919 (2008).

29) Dokmanovic M, Clarke C, Marks PA, Histone deacetylase inhibitors: overview and perspectives. *Mol Cancer Res*. **5**(10):981-9 (2007).

30) Elliot R, Ong TJ. Nutritional genomics. *British Medical Journal*. **324**:1438-42. (2002).

31) ENCODE Project Consortium, Identification and analysis of functional elements in 1% of the human genome by the ENCODE pilot project. *Nature.* **447**: 799-816 (2007).

32) Epp JR, Haack AK, Galea LA, Activation and survival of immature neurons in the dentate gyrus with spatial memory is dependent on time of exposure to spatial learning and age of cells at examination. *Neurobiol Learn Mem*. **95**, 316-25 (2011).

33) Fahrner JA, Bjornsson HT. Mendelian disorders of the epigenetic machinery: tipping the balance of the chromatin states. *Annual Review of Genomics and Human Genetics*. **15**:269-93. (2014).

34) Feron O. Pyruvate into lactate and back: from the Warburg effect to symbiotic energy fuel exchange in cancer cells. *Radiotherapy and Oncology*. **92**:329-33. (2009).

35) Freeman JM, Vining EP, Pillas DJ, Pyzik PL, Casey JC, Kelly LM. The efficacy of the ketogenic diet-1998: a prospective evaluation of intervention in 150 children. *Pediatrics*. **102**:1358-63 (1998).

36) Fukako T, Mitchell G, Sasso JO, Hori T, Orii K, Ayoma Y, Ketone body metabolism and its defects. *J Inherit Metab Dis*. **37**(4):541-51 (2014).

37) García-Canas V, Simó C, León C, Cifuentes A. Advances in nutrigenomics research: novel and future analytical approaches to investigate the biological activity of natural compounds and food functions. *Journal of Pharmaceutical and Biomedical Analysis*. **51**:290–304 (2010).

38) Gasior M, Rogawski MA, Hartman AL. Neuroprotective and disease-modifying effects of the ketogenic diet. *Behavioral Pharmacology*. **17**:431-439. (2006).

39) Gentleman RC, Carey VJ, Bates DM, Bolstad B, Dettling M, Dudoit S, Ellis B, Gautier L, Ge Y, Gentry J, Hornik K, Hothorn T, Huber W, Iacus S, Irizarry R, Leisch F, Li C, Maechler M, Rossini AJ, Sawitzki G, Smith C, Smyth G, Tierney L, Yang JY, Zhang J. Bioconductor: open software development for computational biology and bioinformatics. *Genome Biology*. **5**:R80. (2004).

40) Gibbons RJ, Suthers GK, Wilkie AO, Buckle VJ, Higgs DR, X-linked alpha-thalaseemia/mental retardation (ATR-X) syndrome: localization to Xq12-q21.31. *Am J Hum Genet.* **51**(5):1136-49 (1992).

41) Gilfillan GD, Hughes T, Sheng Y, Hjorthaug HS, Straub T, Gervin K, Harris JR, Undlien DE, Lyle R, Limitations and possibilities of low cell number ChIP-seq. *BMC Genomics*. **13**, 645 (2012).

42) Goo YH, Sohn YC, Kim DH, Kim SW, Kang MJ, Jung DJ, Kwak E, Barlev NA, Berger SL, Chow VT, Roeder RG, Azorsa DO, Meltzer PS, Suh PG, Song EJ, Lee KJ, Lee YC, Lee JW, Activating signal cointegrator 2 belongs to a novel steady-state complex that contains a subset of trithorax group proteins. *Mol Cell Biol.* **23**(1):140-9 (2003).

43) Gorisch SM, Wachsmuth M, Toth KF, Lichter P, Rippe K, Histone acetylation increases chromatin accessibility. 118(Pt 24):5825-34 (2005).

44) Gräff J, Tsai LH, The potential of HDAC inhibitors as cognitive enhancers. *Annu Rev Pharmacol Toxicol*. **53**, 311-30 (2013).

45) Guan Z, Giustetto M, Lomvardas S,. Kim JH, Miniaci MC, Schwartz JH, Thanos D, Kandel ER, Integration of long-term-memory-related synaptic plasticity involves bidirectional regulation of gene expression and chromatin structure. *Cell*. **111**, 483-93 (2002).

46) Guo C, Chang CC, Wortham M, Chen LH, Kernagis DN, Qin X, Cho YW, Chi JT, Grant GA, McLendon RE, Yan H, Ge K, Papadopoulos N, Bigner DD, He Y. Global identification of MLL2-targeted loci reveals MLL2's role in diverse signaling pathways. *Proc Natl Acad Sci U S A*. **109**, 17603-8 (2012).

47) Gupta S, Kim SY, Artis S,. Molfese DL, Schumacher A, Sweatt JD, Paylor RE, Lubin FD, Histone methylation regulates memory formation. *J Neurosci.* **30**, 3589-99 (2010).

48) Guy J, Gan J, Selfridge J, Cobb S, Bird A, Reversal of neurological defects in a mouse model of Rett syndrome. *Science.* **315**, 1143-7 (2007).

49) Hargreaves DC, Crabtree GR, ATP-dependent chromatin remodeling: genetics, genomics and mechanisms. *Cell Res.* 21(3):396-420 (2011).

50) Hashim SA, VanItallie TB, Ketone body therapy: from the ketogenic diet to the oral admistration of ketone ester. *J Lipid Res*. **55**(9):1818-26 (2014).

51) Hasselbalch SG, Knudsen GM, Jakobsen J, Hageman LP, Holm S, Paulson OP. Blood-brain barrier permeability of glucose and ketone bodies during short-term starvation in humans. *American Journal of Physiology.* **268**:1161-6 (1995).

52) Henderson CH, Wijetunge L, Kinoshita MN, Shumway M, Hammond RS, Postma FR, Brynczka C, Rush R, Thomas A, Paylor R, Warren ST, Vanderklish PW, Kind PC, Carpenter RL, Bear MF, Healy AM, Reversal of

disease-related pathologies in the fragile X mouse model by selective activation of GABAB receptors with arbaclofen. *Sci Transl Med*. **4**, 152ra128 (2012).

53) Huang PH, Plass C, Chen CS. Effects of Histone Deacetylase Inhibitors on Modulating H3K4 Methylation Marks – A Novel Cross-Talk Mechanism between Histone-Modifying Enzymes. *Molecular and Cellular Pharmacology*. **3**:39-43. (2011)

54) Huber W, Carey VJ, Gentleman R, Anders S, Carlson M, Carvalho BS, Bravo HC, Davis S, Gatto L, Girke T, Gottardo R, Hahne F, Hansen KD, Irizarry RA, Lawrence M, Love MI, MacDonald J, Obenchain V, Oles AK, Pages H, Reyes A, Shannon P, Smyth GK, Tenenbaum D, Waldron L, Morgan M. Orchestrating high-throughput genomic analysis with Bioconductor. *Nat Methods*. **12**:115-21 (2015).

55) Hunter S, Jones P, Mitchell A, Apweiler R, Attwood TK, Bateman A, Bernard T, Binns D, Bork P, Burge S, de Castro E, Coggill P, Corbett M, Das U, Daugherty L, Duquenne L, Finn RD, Fraser M, Gough J, Haft D, Hulo N, Kahn D, Kelly E, Letunic L, Lonsdale D, Lopez R, Madera M, Maslen J, McAnulla C, McDowall J, McMenamin C, Mi H, Mutowo-Muellenet P, Mulder N, Natale D, Orengo C, Pesseat S, Punta M, Quinn AF , Rivoire C, Sangrador-Vegas A, Selengut JD, Sigrist CJ, Scheremetjew M, Tate J, Thimmajanarthanan M, Thomas PD, Wu CH, Yeats C, Yong SY, InterPro in 2011: new developments in the family and domain prediction database. *Nucleic Acids Res*. **40**, 306-12 (2012).

56) Jimenez-Sanchez G, Childs B, Valle D, Human disease genes. *Nature*. **409**:853-855 (2001).

57) Kasper LH, Lerach S, Wang J, Wu S, Jeevan T, Brindle PK, CBP/p300 double null cells reveal effect of coactivator level and diversity on CREB transactivation. *EMBO J*. **29**, 3660-72 (2010).

58) Kerimoglu C, Agis-Balboa RC, Kranz A, Stilling R, Bahari-Javan S, Benito-Garagorri E, Halder R, Burkhardt S, Stewart AF, Fischer A, Histone-methyltransferase MLL2 (KMT2B) is required for memory formation in mice. *J Neurosci.* **33**, 3452-64 (2013).

59) Kesner RP, An analysis of the dentate gyrus function. *Behav Brain Res*. **254**, 1-7 (2013).

60) Kim DH, Rhee JC, Yeo S, Shen R, Lee SK, Lee JW, Lee S. Crucial roles of mixed-lineage leukemia 3 and 4 as epigenetic switches of the hepatic circadian clock controlling bile acid homeostasis in mice. *Hepatology*. **61**:1012-1023 (2015).

61) Korzus E, Rosenfeld MG, Mayford M, CBP histone acetyltransferase activity is a critical component of memory consolidation. *Neuron*. **42**, 961-72 (2004).

62) Kung AL, Rebel VI, Bronson RT, Ch'ng LE, Sieff CA, Livingston DM, Yao TP. Gene dose-dependent control of hematopoiesis and hematologic tumor suppression by CBP. Genes & Development. **14**:272-7 (2000).

63) Kurdistani SK. Chromatin: a capacitor of acetate for integrated regulation of gene expression and cell physiology. *Current Opinion Genetics & Development*. **26**:53-8. (2014).

64) Langmead B, Salzberg SL, Fast gapped-read alignment with Bowtie 2. *Nat Methods*. **9**, 357-9 (2012).

65) Lederer D, Grisart B, Digilio MC, Benoit V, Crespin M, Ghariani SC, Maystadt I, Dallapiccola B, Verellen-Dumoulin C. Deletion of KDM6A, a histone demethylase interacting with MLL2, in three patients with Kabuki syndrome. *American Journal of Human Genetics* **90**:119–124. (2010).

66) Lee JE, Wang C, Xu S, Cho YW, Wang L, Fenx X, Baldridge A, Sartorelli V, Zhuang L, Peng W, Ge K, H3K4 mono- and di-methyltransferase MLL4 is required for enhancer activation during cell differentiation. *Elife*. **2**: e01503 (2013).

67) Lim S, Chesser AS, Grima JC, Rappold PM, Blum D, Przedborski S, Tieu K. D-b-hydroxybutyrate is protective in mouse models of Huntington's disease. *PLoS One.* **6**:e24620. (2011).

68) Loeys BL, Gerber EE, Riegert-Johnson D, Iqbal S, Whiteman P, McConnell V, Chillakuri CR, Macaya D, Coucke PJ, De Paepe A, Judge DP, Wigley F, Davis EC, Mardon HJ, Handford P, Keene DR, Sakai LY, Dietz HC, Mutations in fibrillin-1 cause congenital scleroderma: stiff skin syndrome. Sci Transl Med. **23**, 23ra20 (2010).

69) Lower KM, Turner G, Kerr BA, Mathews KD, Shaw MA, Gedeon AK, Schelley S, Hoyme HE, White SM, Delatycki MB, Lampe AK, Clayton-Smith J, Stewart H, van Ravenswaay CM, de Vries BB, Cox B, Grompe M, Ross S, Thomas P, Mulley JC, Gecz J, Mutations in PHF6 are associated with Borjeson-Forssman-Lehmann syndrome. *Nat Genet.* 32(4):661-5 (2002).

70) Lubitz S, Glaser S, Schaft J, Stewart AF, Anastassiadis, K Increased apoptosis and skewed differentiation in mouse embryonic stem cells lacking the histone methyltransferase Mll2. *Mol Biol Cell.* **18**, 2356-66 (2007).

71) Martinez-Canabal A, Akers KG, Josselyn SA, Frankland PW, Age-dependent effects of hippocampal neurogenesis suppression on spatial learning. *Hippocampus*. **23**, 66-74 (2013).

72) Matoulek M, Svododova S, Vetrovska, Stranska Z, Svacina S, Post-exercise changes of beta hydroxybutyrate as a predictor of weight changes. *Physiol Res.* **63** Suppl 2:S321-5 (2014).

73) Maulik PK, Mascarenhas MN, Mathers CD, Dua T, Saxena S, Prevalence of intellectual disability: a meta-analysis of population-based studies. *Res Dev Disabil.* **32**(2):419-36 (2011).

74) McCall MN, Uppal K, Jaffee HA, Zilliox MJ, Irizarry RA. The Gene Expression Barcode: leveraging public data repositories to begin cataloging the human and murine transcriptomes. *Nucleic Acids Research*. **39**:D1011-5 (2011).

75) McCall MN, Jaffee HA, Irizarry RA. 2012. fRMA ST: frozen robust multiarray analysis for Affymetrix Exon and Gene ST arrays. *Bioinformatics*. **28**:3153-4.

76) McCall MN, Jaffee HA, Zelisko SJ, Sinha N, Hooiveld G, Irizarry RA, Zilliox MJ. The Gene Expression Barcode 3.0: improved data processing and mining tools. *Nucleic Acids Research*. **42**:D938-43. (2014).

77) McCarthy DJ, Chen Y, Smyth GK, Differential expression analysis of multifactor RNA-Seq experiments with respect to biological variation. *Nucleic Acids Res*. **40**, 4288-97 (2012).

78) Meeran SM, Ahmed A, Tollefsbo TO, Epigenetic targets of bioactive dietary components for cancer prevention and therapy. *Clin Epigenetics.* **1**, 101-116. (2010).

79) Ming GL, Song H. Adult Neurogenesis in the Mammalian Brain: Significant Answers and Significant Questions. *Neuron*. **70**:687-702 (2011).

80) Miyake N, Mizuno S, Okamoto N, Ohashi H, Shiina M, Ogata K, Tsurusaki Y, Nakashima M, Saitsu H, Niikawa N, Matsumoto N. KDM6A point mutations cause Kabuki syndrome. *Human Mutation* **34**:108–110 (2013).

81) Morris AM, Churchwell JC, Kesner RP, Gilbert PE. Selective lesions of the dentate gyrus produce disruptions in place learning for adjacent spatial locations. *Neurobiol Learn Mem*. **97**, 326-31 (2012).

82) Munshi A, Tanaka T, Hobbs ML, Tucker SL, Richon VM, Meyn RE, Vorinostat, a histone deacetylase inhibitor, enhances the response of human tumor cells to ionizing radiation through prolongation of gamma-H2AX foci. *Mol Cancer Ther*. **5**,1967-74 (2006).

83) Nakamura S, Hisamura R, Shimoda S, Shibuya I, Tsubota K, Fasting mitigates immediate hypersensitivity: a pivotal role of endogenous D-beta-hydroxybutyrate. *Nutr Metab (Lond).* **11**:40 (2014).

84) Ng SB, Bigham AW, Buckingham KJ, Hannibal MC, McMillin MJ, Gildersleeve HI, Beck AE, Tabor HK, Cooper GM, Mefford HC, Lee C, Turner EH, Smith JD, Rieder MJ, Yoshiura K, Matsumoto N, Ohta T, Niikawa N, Nickerson DA, Bamshad MJ, Shendure J. Exome sequencing identifies MLL2 mutations as a cause of Kabuki syndrome. *Nature Genet*ics **42**:790–793. (2010).

85) Ordovas JM, Corella D. Nutritional genomics. *Annual Review of Genomics and Human Genetics*. **5**:71-118. (2004).

86) Petrij F, Giles RH, Dauwerse HG, Saris JJ, Hennekam RC, Masuno M, Tommerup N, van Ommen GJ, Goodman RH, Peters DJ, Rubenstein-Taybi syndrome caused by mutations in the transcriptional co-activator CBP. *Nature*. 376(6538):348-51 (1995).

87) Phiel CJ, Zhang F, Huang EY , Guenther MG, Lazar MA, Klein PS, Histone deacetylase is a direct target of valproic acid, a potent anticonvulsant, mood stabilizer, and teratogen. *J Biol Chem*. **276**, 36734-41 (2001).

88) Quinlan AR, Hall IM, BEDTools: a flexible suite of utilities for comparing genomic features. *Bioinformatics*. **26**, 841-2 (2010).

89) Remely M, Stefanska B, Lovrecic L, Magnet U, Haslberger AG, Nutriepigenomics: the role of nutrition in epigenetic control of human diseases. *Curr Opin Clin Nutr Metab Care.* **18**(4):328-33 (2015).

90) Rimoin DL, Hirschhorn K, A history of medical genetics in pediatrics. *Pediatr Res*. **56**(1): 150-9 (2004).

91) Robinson MD, McCarthy DJ, Smyth GK, edgeR: a Bioconductor package for differential expression analysis of digital gene expression data. *Bioinformatics*. **26**, 139-40 (2010).

92) Rossetti F, de Araujo Furtado M, Pak T, Bailey K, Shields M, Chanda S, Addis M, Robertson BD, Moffett M, Lumley LA, Yourick DL, Combined diazepam and HDAC inhibitor treatment protects against seizures and neuronal damage caused by soman exposure. *Neurotoxicology*. **33**(3):500-11 (2012).

93) Sengoku T, Yokoyama S, Structural basis for histone H3 Lys 27 demethylation by UTX/KDM6A. *Genes Dev*. 25(21):2266-77 (2011).

94) Shimazu T, Hirschey MD, Newman J, He W, Shirakawa K, Le Moan N, Grueter CA, Lim H, Saunders LR, Stevens RD, Newgard CB, Farese Jr. RV, de Cabo R, Ulrich S, Akassoglou K, Verdin E. Suppression of oxidative stress by beta-hydroxybutyrate, an endogenous histone deacetylase inhibitor. *Science*. **339**:211–214. (2013).

95) Shulz Y, Freese L, Manz J, Zoll B, Volter C, Brockmann K, Bogershausen N, Becker J, Wollnik B, Pauli S, CHARGE and Kabuki syndromes: a phenotypic and molecular link. *Hum Mol Genet.* **23**(16):4396-405 (2014).

96) Smyth GK. Linear models and empirical bayes methods for assessing differential expression in microarray experiments. *Statistical Applications in Genetics and Molecular Biology*. **3**:1-25. (2004).

97) Souslova EA, Belousov VV, Lock JG, Strömblad S, Kasparov S, Bolshakov AP, Pinelis VG, Labas YA, Lukyanov S, Mayr LM, Chudakov DM, Single fluorescent protein-based Ca2+ sensors with increased dynamic range. *BMC Biotechnol.* **7**, 37 (2007).

98) Sung YM, Lee T, Yoon H, Dibattista AM, Song JM, Sohn Y, Moffat EI, Turner RS, Jung M, Kim J, Hoe HS, Mercaptoacetamide-based class II HDAC inhibitor lowers Aβ levels and improves learning and memory in a mouse model of Alzheimer's disease. *Exp Neurol.* **239**:192-201 (2013).

99) Vecsey CG, Hawk JD, Lattal KM, Stein JM, Fabian SA, Attner MA, Cabrera SM, McDonough CM, Brindle PK, Abel T, Wood MA, Histone deacetylase inhibitors enhance memory and synaptic plasticity via CREB:CBP-dependent transcriptional activation. *J Neurosci.* **27**, 6128–6140 (2007).

100) Vermeulen M, Mulder KW, Denissov S, Pijnappel VW, van Schaik FM, Varier RA, Baltissen MP, Stunnenberg HG, Mann M, Timmers HT, Selective anchoring of TFIID to nucleosomes by trimethylation of histone H3 lysine 4. *Cell*. **131**, 58-69 (2007).

101) Wheless JW. History of the ketogenic diet. *Epilepsia*. **49**:3–5. (2008).

102) White H, Venkatesh B. 2011. Clinical review: Ketones and brain injury. *Critical Care.* **15**:219.

103) Williams SR, Aldred MA, Der Kaloustian VM, Halal F, Gowans G, McLeod DR, Zondag S, Toriello HV, Magenis RE, Elsea SH, Haploinsuffciency of HDAC4 causes brachydactyly mental retardation

syndrome, with brachydactyly type E, developmental delays, and behavioral problems. *Am J Hum Genet.* **87**(2):219-28 (2010).

104) Xu J, Andreassi M, Reversible histone methylation regulates brain gene expression and behavior. *Horm Behav*. **59**(3):383-92 (2011).

105) Yang X, Lay F, Han H, Jones PA, Targeting DNA methylation for epigenetic therapy. Trends Pharmacol Sci. **31**(11):536-46 (2010).

106) Yang P, Guo L, Duan ZJ, Tepper CG, Xue L, Chen X, Kung HJ, Gao AC, Zou JX, Chen HW, Histone methyltransferase NSD2/MMSET mediates constitutive NF-κB signaling for cancer cell proliferation, survival, and tumor growth via a feed-forward loop. *Mol Cell Biol*. **32**, 3121-31 (2012).

107) Zhang Y, Liu T, Meyer CA, Eeckhoute J, Johnson DS, Bernstein BE, Nusbaum C, Myers RM, Brown M, Li W, Liu XS, Model-based analysis of ChIP-Seq (MACS). *Genome Biol*. **9**, R137 (2008).

108) Zhang S, Suvannasankha A, Crean CD, White VL, Chen CS, Farag SS, The novel histone deacetylase inhibitor, AR-42, inhibits gp130/Stat3 pathway and induces apoptosis and cell cycle arrest in multiple myeloma cells. *Int J Cancer*. **129**, 204-13 (2011).

109) Zhao Q**,** Stafstrom CE, Fu DD, Hu Y, Holmes GL. Detrimental effects of the ketogenic diet on cognitive function in rats. *Pediatric Research*. **55**:498–506. (2004).

110) Zilliox MJ, Irizarry R. A gene expression bar code for microarray data. *Nature Methods*. **4**:911-913. (2007).

Permissions

THE AMERICAN ASSOCIATION FOR THE ADVANCEMENT OF SCIENCE LICENSE

TERMS AND CONDITIONS

Oct 23, 2015

This is a License Agreement between Joel Benjamin ("You") and The American Association for the Advancement of Science ("The American Association for the Advancement of Science") provided by Copyright Clearance Center ("CCC"). The license consists of your order details, the terms and conditions provided by The American Association for the Advancement of Science, and the payment terms and conditions.

All payments must be made in full to CCC. For payment instructions, please see information listed at the bottom of this form.

License Number

3734950349788

License date

Oct 23, 2015

Licensed content publisher

The American Association for the Advancement of Science

Licensed content publication

Science Translational Medicine

Licensed content title

Histone deacetylase inhibition rescues structural and functional brain deficits in a mouse model of Kabuki syndrome

Licensed content author

Hans T. Bjornsson,Joel S. Benjamin,Li Zhang,Jacqueline Weissman,Elizabeth E. Gerber,Yi-Chun Chen,Rebecca G. Vaurio,Michelle C. Potter,Kasper D. Hansen,Harry C. Dietz

Licensed content date

Oct 1, 2014

Volume number

6

Issue number

256

Type of Use

Thesis / Dissertation

Requestor type

Author of the AAAS published paper

Format

Print and electronic

Portion

Full Text

Order reference number

None

Title of your thesis / dissertation

Kabuki syndrome: Reversing Intellectual Disability by Promoting Open Chromatin

Expected completion date

Nov 2015

Estimated size(pages)

150

Total

0.00 USD

Terms and Conditions

American Association for the Advancement of Science TERMS AND CONDITIONS

Regarding your request, we are pleased to grant you non-exclusive, non-transferable permission, to republish the AAAS material identified above in your work identified above, subject to the terms and conditions herein. We must be contacted for permission for any uses other than those specifically identified in your request above.

The following credit line must be printed along with the AAAS material: "From [Full Reference Citation]. Reprinted with permission from AAAS."

All required credit lines and notices must be visible any time a user accesses any part of the AAAS material and must appear on any printed copies and authorized user might make.

This permission does not apply to figures / photos / artwork or any other content or materials included in your work that are credited to non-AAAS sources. If the requested material is sourced to or references non-AAAS sources, you must obtain authorization from that source as well before using that material. You agree to hold harmless and indemnify AAAS against any claims arising from your use of any content in your work that is credited to non-AAAS sources.

If the AAAS material covered by this permission was published in Science during the years 1974 - 1994, you must also obtain permission from the author, who may grant or withhold permission, and who may or may not charge a fee if permission is granted. See original article for author's address. This condition does not apply to news articles.

The AAAS material may not be modified or altered except that figures and tables may be modified with permission from the author. Author permission for any such changes must be secured prior to your use.

Whenever possible, we ask that electronic uses of the AAAS material permitted herein include a hyperlink to the original work on AAAS's website (hyperlink may be embedded in the reference citation).

AAAS material reproduced in your work identified herein must not account for more than 30% of the total contents of that work.

AAAS must publish the full paper prior to use of any text.

AAAS material must not imply any endorsement by the American Association for the Advancement of Science.

This permission is not valid for the use of the AAAS and/or Science logos.

AAAS makes no representations or warranties as to the accuracy of any information contained in the AAAS material covered by this permission, including any warranties of

merchantability or fitness for a particular purpose.

If permission fees for this use are waived, please note that AAAS reserves the right to charge for reproduction of this material in the future.

Permission is not valid unless payment is received within sixty (60) days of the issuance of this permission. If payment is not received within this time period then all rights granted herein shall be revoked and this permission will be considered null and void.

In the event of breach of any of the terms and conditions herein or any of CCC's Billing and Payment terms and conditions, all rights granted herein shall be revoked and this permission will be considered null and void.

AAAS reserves the right to terminate this permission and all rights granted herein at its discretion, for any purpose, at any time. In the event that AAAS elects to terminate this permission, you will have no further right to publish, publicly perform, publicly display, distribute or otherwise use any matter in which the AAAS content had been included, and all fees paid hereunder shall be fully refunded to you. Notification of termination will be sent to the contact information as supplied by you during the request process and termination shall be immediate upon sending the notice. Neither AAAS nor CCC shall be liable for any costs, expenses, or damages you may incur as a result of the termination of this permission, beyond the refund noted above.

This Permission may not be amended except by written document signed by both parties.

The terms above are applicable to all permissions granted for the use of AAAS material. Below you will find additional conditions that apply to your particular type of use.

FOR A THESIS OR DISSERTATION

If you are using figure(s)/table(s), permission is granted for use in print and electronic versions of your dissertation or thesis. A full text article may be used in print versions only of a dissertation or thesis.

Permission covers the distribution of your dissertation or thesis on demand by ProQuest / UMI, provided the AAAS material covered by this permission remains in situ.

If you are an Original Author on the AAAS article being reproduced, please refer to your License to Publish for rules on reproducing your paper in a dissertation or thesis.

FOR JOURNALS:

Permission covers both print and electronic versions of your journal article, however the AAAS material may not be used in any manner other than within the context of your article.

FOR BOOKS/TEXTBOOKS:

If this license is to reuse figures/tables, then permission is granted for non-exclusive world rights in all languages in both print and electronic formats (electronic formats are defined below).

If this license is to reuse a text excerpt or a full text article, then permission is granted for non-exclusive world rights in English only. You have the option of securing either print or electronic rights or both, but electronic rights are not automatically granted and do garner additional fees. Permission for translations of text excerpts or full text articles into other languages must be obtained separately.

Licenses granted for use of AAAS material in electronic format books/textbooks are valid only in cases where the electronic version is equivalent to or substitutes for the print version of the book/textbook. The AAAS material reproduced as permitted herein must remain in situ and must not be exploited separately (for example, if permission covers the use of a full text article, the article may not be offered for access or for purchase as a stand-alone unit), except in the case of permitted textbook companions as noted below.

You must include the following notice in any electronic versions, either adjacent to the reprinted AAAS material or in the terms and conditions for use of your electronic products: "Readers may view, browse, and/or download material for temporary copying purposes only, provided these uses are for noncommercial personal purposes. Except as provided by law, this material may not be further reproduced, distributed, transmitted, modified, adapted, performed, displayed, published, or sold in whole or in part, without prior written permission from the publisher."

If your book is an academic textbook, permission covers the following companions to your textbook, provided such companions are distributed only in conjunction with your textbook at no additional cost to the user:

- Password-protected website

- Instructor's image CD/DVD and/or PowerPoint resource

- Student CD/DVD

All companions must contain instructions to users that the AAAS material may be used for non-commercial, classroom purposes only. Any other uses require the prior written permission from AAAS.

If your license is for the use of AAAS Figures/Tables, then the electronic rights granted herein permit use of the Licensed Material in any Custom Databases that you distribute the electronic versions of your textbook through, so long as the Licensed Material remains within the context of a chapter of the title identified in your request and cannot be downloaded by a user as an independent image file.

Rights also extend to copies/files of your Work (as described above) that you are required to provide for use by the visually and/or print disabled in compliance with state and federal laws.

This permission only covers a single edition of your work as identified in your request.

FOR NEWSLETTERS:

Permission covers print and/or electronic versions, provided the AAAS material reproduced as permitted herein remains in situ and is not exploited separately (for example, if permission covers the use of a full text article, the article may not be offered for access or for purchase as a stand-alone unit)

FOR ANNUAL REPORTS:

Permission covers print and electronic versions provided the AAAS material reproduced as permitted herein remains in situ and is not exploited separately (for example, if permission covers the use of a full text article, the article may not be offered for access or for purchase as a stand-alone unit)

FOR PROMOTIONAL/MARKETING USES:

Permission covers the use of AAAS material in promotional or marketing pieces such as information packets, media kits, product slide kits, brochures, or flyers limited to a single print run. The AAAS Material may not be used in any manner which implies endorsement or promotion by the American Association for the Advancement of Science (AAAS) or Science of any product or service. AAAS does not permit the reproduction of its name, logo or text on promotional literature.

If permission to use a full text article is permitted, The Science article covered by this permission must not be altered in any way. No additional printing may be set onto an article copy other than the copyright credit line required above. Any alterations must be approved in advance and in writing by AAAS. This includes, but is not limited to, the placement of sponsorship identifiers, trademarks, logos, rubber stamping or self-adhesive stickers onto the article copies.

Additionally, article copies must be a freestanding part of any information package (i.e. media kit) into which they are inserted. They may not be physically attached to anything, such as an advertising insert, or have anything attached to them, such as a sample product. Article copies must be easily removable from any kits or informational packages in which they are used. The only exception is that article copies may be inserted into three-ring binders.

FOR CORPORATE INTERNAL USE:

The AAAS material covered by this permission may not be altered in any way. No additional printing may be set onto an article copy other than the required credit line. Any alterations must be approved in advance and in writing by AAAS. This includes, but is

not limited to the placement of sponsorship identifiers, trademarks, logos, rubber stamping or self-adhesive stickers onto article copies.

If you are making article copies, copies are restricted to the number indicated in your request and must be distributed only to internal employees for internal use.

If you are using AAAS Material in Presentation Slides, the required credit line must be visible on the slide where the AAAS material will be reprinted

If you are using AAAS Material on a CD, DVD, Flash Drive, or the World Wide Web, you must include the following notice in any electronic versions, either adjacent to the reprinted AAAS material or in the terms and conditions for use of your electronic products: "Readers may view, browse, and/or download material for temporary copying purposes only, provided these uses are for noncommercial personal purposes. Except as provided by law, this material may not be further reproduced, distributed, transmitted, modified, adapted, performed, displayed, published, or sold in whole or in part, without prior written permission from the publisher." Access to any such CD, DVD, Flash Drive or Web page must be restricted to your organization's employees only.

FOR CME COURSE and SCIENTIFIC SOCIETY MEETINGS:

Permission is restricted to the particular Course, Seminar, Conference, or Meeting indicated in your request. If this license covers a text excerpt or a Full Text Article, access to the reprinted AAAS material must be restricted to attendees of your event only (if you have been granted electronic rights for use of a full text article on your website, your website must be password protected, or access restricted so that only attendees can access the content on your site).

If you are using AAAS Material on a CD, DVD, Flash Drive, or the World Wide Web, you must include the following notice in any electronic versions, either adjacent to the reprinted AAAS material or in the terms and conditions for use of your electronic products: "Readers may view, browse, and/or download material for temporary copying purposes only, provided these uses are for noncommercial personal purposes. Except as provided by law, this material may not be further reproduced, distributed, transmitted, modified, adapted, performed, displayed, published, or sold in whole or in part, without prior written permission from the publisher."

FOR POLICY REPORTS:

These rights are granted only to non-profit organizations and/or government agencies. Permission covers print and electronic versions of a report, provided the required credit line appears in both versions and provided the AAAS material reproduced as permitted herein remains in situ and is not exploited separately.

FOR CLASSROOM PHOTOCOPIES:

Permission covers distribution in print copy format only. Article copies must be freestanding and not part of a course pack. They may not be physically attached to anything or have anything attached to them.

FOR COURSEPACKS OR COURSE WEBSITES:

These rights cover use of the AAAS material in one class at one institution. Permission is valid only for a single semester after which the AAAS material must be removed from the Electronic Course website, unless new permission is obtained for an additional semester. If the material is to be distributed online, access must be restricted to students and instructors enrolled in that particular course by some means of password or access control.

FOR WEBSITES:

You must include the following notice in any electronic versions, either adjacent to the reprinted AAAS material or in the terms and conditions for use of your electronic products: "Readers may view, browse, and/or download material for temporary copying purposes only, provided these uses are for noncommercial personal purposes. Except as provided by law, this material may not be further reproduced, distributed, transmitted, modified, adapted, performed, displayed, published, or sold in whole or in part, without prior written permission from the publisher."

Permissions for the use of Full Text articles on third party websites are granted on a case by case basis and only in cases where access to the AAAS Material is restricted by some means of password or access control. Alternately, an E-Print may be purchased through our reprints department (brocheleau@rockwaterinc.com).

REGARDING FULL TEXT ARTICLE USE ON THE WORLD WIDE WEB IF YOU ARE AN ‘ORIGINAL AUTHOR’ OF A SCIENCE PAPER

If you chose "Original Author" as the Requestor Type, you are warranting that you are one of authors listed on the License Agreement as a "Licensed content author" or that you are acting on that author's behalf to use the Licensed content in a new work that one of the authors listed on the License Agreement as a "Licensed content author" has written.

Original Authors may post the ‘Accepted Version’ of their full text article on their personal or on their University website and not on any other website. The ‘Accepted Version’ is the version of the paper accepted for publication by AAAS including changes resulting from peer review but prior to AAAS’s copy editing and production (in other words not the AAAS published version).

FOR MOVIES / FILM / TELEVISION:

Permission is granted to use, record, film, photograph, and/or tape the AAAS material in connection with your program/film and in any medium your program/film may be shown or heard, including but not limited to broadcast and cable television, radio, print, world wide web, and videocassette.

The required credit line should run in the program/film's end credits.

FOR MUSEUM EXHIBITIONS:

Permission is granted to use the AAAS material as part of a single exhibition for the duration of that exhibit. Permission for use of the material in promotional materials for the exhibit must be cleared separately with AAAS (please contact us at permissions@aaas.org).

FOR TRANSLATIONS:

Translation rights apply only to the language identified in your request summary above.

The following disclaimer must appear with your translation, on the first page of the article, after the credit line: "This translation is not an official translation by AAAS staff, nor is it endorsed by AAAS as accurate. In crucial matters, please refer to the official English-language version originally published by AAAS."

FOR USE ON A COVER:

Permission is granted to use the AAAS material on the cover of a journal issue, newsletter issue, book, textbook, or annual report in print and electronic formats provided the AAAS material reproduced as permitted herein remains in situ and is not exploited separately

By using the AAAS Material identified in your request, you agree to abide by all the terms and conditions herein.

Questions about these terms can be directed to the AAAS Permissions departmentpermissions@aaas.org.

Other Terms and Conditions:

v 2

Questions? customercare@copyright.com or +1-855-239-3415 (toll free in the US) or +1-978-646-2777.

Curriculum Vitae

Joel Benjamin B.S
Institute
Joelbenjamin882000@gmail.com
(831) 236-5896

Johns Hopkins Medical

733 North Broadway, MRB 426
Baltimore, MD 21205

Biographical Information:

Date of birth: 7/6/1988
City of birth: San Diego, CA

Education:

JHMI: Institute of Genetic Medicine **2010-2015**
Ph.D. Human Genetics

University of California, Santa Barbara **2006-2010**
B.S. Cell and Developmental Biology

Professional Activity:

Bjornsson Lab:
JHMI: Institute of Genetic Medicine **2012-2015**
Graduate student studying the pathophysiology of Kabuki syndrome and potential therapeutic interventions in Kabuki syndrome and related disorders

Previous Academic Work:

Cohn Lab:
JHMI: Institute of Genetic Medicine **2011-2012**
Graduate student studying congenital muscular dystrophy in Laminin alpha-2 deficient mice

Rice Lab:
UCSB: Department of Ecology, Evolution and Marine Biology **2008-2010**
Undergraduate research assistant studying sexually antagonistic co-evolution between male and female fruit flies in regards to seminal protein toxicity

Teaching Experience

Teaching assistant: Johns Hopkins University **2013**
Course: Advanced Topics in Human genetics

Additional Coursework:

49th Annual Short Course on
Medical and Experimental Mammalian Genetics **2011**
Jackson Laboratories

Eukaryotic Gene Expression **2012**
Cold Spring Harbor Laboratories

Professional Societies and Organizations:

JHMI Graduate student Association:
Human Genetics program representative **2014-2015**

American Society of Human Genetics **2012-2015**

Awards:

University of California Regents Scholar Award	**2006**
UCSB Deans List	**2007,2010**

Peer Reviewed Publications

Bjornsson HT*, **Benjamin JS***, Zhang L, Weissman J, Gerber EE, Chen YC, Vaurio RG, Potter MC, Hansen KD, Dietz HC. *Histone Deacetylase InhibitionRescues Structural and Functional Deficits In a Mouse Model of Kabuki Syndrome* Sci Transl Medicine 2014 Oct 1;6(256):256ra135. **2014**
***co-first authorship**

Benjamin JS, Pilarowski G, Carosso G, , Zhang, Hansen KD, Vernon HJ, Bjornsson HJ. *A ketogenic diet rescues epigenetic and neurogenesis defects in a mouse model of Kabuki syndrome*. In Preparation **2015**

Presentations and Posters:

Limb Specific Differences in Polyamine Related Genes in a Murine Model of Muscular Dystrophy Provide Potential Therapeutic Targets
American Society of Human Genetics (San Francisco) **2012**

A Mouse Model of Kabuki Syndrome Demonstrates Defective Hippocampal Neurogenesis Rescued by Treatment with AR-42, a Histone Deacetylase Inhibitor.
Bjornsson HT, **Benjamin JS,** Zhang L, Gerber EE, Chen Y, Potter MC, Dietz HC.
American Society of Human Genetics (Boston) **2013**

A Novel Mouse Model of Kabuki Syndrome Demonstrates a Hippocampal Neurogenesis Defect Attenuated with Histone Deacetylase Inhibition
NIH high risk high reward symposium (NIH Bethesda) **2013**

Histone Deacetylase Inhibition Recovers Neurological Dysfunction in a Mouse Model of Kabuki Syndrome
NIH high risk high reward symposium (NIH Bethesda) **2014**

A ketogenic Diet Rescues Hippocampal Memory Defects In a Mouse Model of Kabuki syndrome
American Society of Human Genetics (Baltimore) **2015**

References:

Dr. Hans Bjornsson
McKusick-Nathans Institue of Genetic Medicine
Johns Hopkins University School of Medicine
733 N. Broadway, MRB 415
Baltimore, MD 21205
E-mail: hbjorns1@jhmi.edu

Dr. Ronald Cohn
The Hospital for Sick Children

Phone: (416) 813-7654 Ext. 228780
Fax: (416) 813-5345
e-mail: ronald.cohn@sickkids.ca

Dr. David Valle
Henry J. Knott Professor and Director of the Institute of Genetic Medicine
Professor, Departments of Pediatrics
Ophthalmology and Molecular Biology & Genetics
Johns Hopkins University School of Medicine
Institute of Genetic Medicine
733 N Broadway
Broadway Research Building, 519
Baltimore, MD 21287
Phone: 410-955-4260
Fax: 410-955-7397
E-mail: dvalle@jhmi.edu